Low Tranverse Momentum Scattering

Ann. Rev. Nucl. Science

23, 219 – 313 (1973)

Reprinted from
ANNUAL REVIEW OF NUCLEAR SCIENCE
Volume 23, 1973

PRODUCTION MECHANISMS OF TWO-TO-TWO SCATTERING PROCESSES AT INTERMEDIATE ENERGIES

Geoffrey C. Fox[1]
C. C. Lauritsen Laboratory of High Energy Physics, California Institute of Technology, Pasadena, California

C. Quigg[2]
Institute for Theoretical Physics, State University of New York, Stony Brook, Long Island, New York

Dedicated to Bruno Renner

CONTENTS

[1] Work supported by the US Atomic Energy Commission under Contract AT(11-1)-68.
[2] Research supported in part by the National Science Foundation under Grant No. GP-32998X.

1 INTRODUCTION

Together with hadron spectroscopy, the study of two-body reactions has until very recent times been the goal of most experiments on the high energy collisions of elementary particles, and the source of most of our understanding of strong interaction dynamics. However, we must confess to some embarrassment at finding ourselves charged with the task of summarizing briefly the status of a vast subject which is experiencing a prolonged and painful adolescence. In a few pages, it is difficult to convey accurately the sense of exasperation now felt by many workers in the field without giving short shrift to the concepts which form, we feel sure, a sturdy foundation (1) for a future theory of two-body collisions, and, indeed, of hadronic interactions in general. It is all too easy, when bewailing the lack of dramatic progress in the theory of high energy processes, to overlook the steady accumulation of insights that make up our present incomplete understanding of two-body reactions. We therefore feel fortunate to be able to refer to the article by Chiu (2) in the preceding volume of *Ann. Rev. Nucl. Sci.* in which the principal successes of two-body phenomenology have been recounted. Although we shall mention the underlying ideas in the next section, we will for the most part assume familiarity with the contents of Chiu's chapter. In addition, we are able to direct the reader to numerous reviews (3–13) that explore in depth the successful applications of these ideas. Likewise, the failures of the present-day Regge phenomenology (which occur in quantitative detail and not, we stress, in gross structure) have been the subject of other reviews (14–22), and we shall not dwell on them at length here. Instead we will concentrate on the experimental systematics and the gems of theoretical insight that organize them into a pattern which will be the basis of future deeper understanding.

For the rest of the introduction, we first continue on a spiritual level and explain the obstacles facing the development of the subject. Then we define the problem and finally present the details of our article.

1A Impasse

There are three basic points to be made. Firstly, in some respects the failures of our Regge-based phenomenology are indeed due to weakness of the theory. Here we have in mind the lack of any technique for computing Regge pole residues or the contributions of Regge cuts to scattering amplitudes.

Secondly, it is likely that in many instances the absence of experimental systematics is due to the existence of small effects which are often irrelevant and simply serve to obscure the simplicity of the principal two-body reaction mechanisms. We need not go far afield to find a dramatic (and well-understood) example: In the case of elastic πd scattering, a deep dip in the dominant contribution to the differential cross section is completely camouflaged (23) by a contribution from transitions between the s-wave and d-wave components of the deuteron wave function although the deuteron is only 7% d-wave.

Thirdly, for a large number of former aficionados of two-body reactions, the appeal has gone out of model building because there are not enough data of detailed enough nature to select among many "plausible" but unconvincing alternative theoretical schemes. Thus the belief is widespread that it is about as pointless at this time to concoct a model for two-body collisions as it is to build another theory of CP violation. There is the difference in degree that models for high energy collisions can be refuted by experiment within a time short on the scale of a physicist's productive years, whereas models for CP violation apparently cannot! In both cases, some new clue is needed to point the way to a "convincing" model.

It is the demise of explicit models that has led to the current vogue for "amplitude analysis," by which is meant the experimental determination of individual scattering amplitudes, rather than the mere measurement of incoherent sums of absolute squares of amplitudes as they occur in cross sections. It is disconcerting that we have come to this, and Sonderegger (24) has spoken poignantly of amplitude analysis "which must be the ultimate aspiration of the experimenter, but which has in fact become the last resort of theorists."

Lest the reader despair, we remember that the intuition gleaned from two-body collisions is the basis (25–27) for virtually all our expectations for the multiparticle production experiments that become more common as the eager physicist gains access to higher energy accelerators. For instance, the rise of a Regge phenomenology of inclusive reactions (28, 29) following Mueller's discovery of the Generalized Optical Theorem (30) serves as a reminder of the utility of our basic theoretical structure for organizing vast amounts of experimental information. The same ideas employed (with semiquantitative success) in two-body studies are providing for the first time a framework for the understanding and appreciation of multiparticle production. Even here, we must expect eventually to encounter the same difficulties that now confound the analysis of two-body reactions.

1B The Subject

Let us now say a few words about the scope of our problem. The partition of the total cross section into elastic scattering, inelastic two-body and quasi two-body

channels, and "true" multiparticle production is summarized in Table 1 for three energy regimes. We will use the notation

$$a+b \to a+b \qquad 1.1.$$

to denote elastic scattering:

$$\begin{array}{l} a+b \to c+d \\ \qquad\quad \big\lfloor\!\!\big\rfloor \hookrightarrow (\gamma\delta\ldots) \\ \qquad\quad \big\lfloor\!\!\big\rfloor \hookrightarrow (\alpha\beta\ldots) \end{array} \qquad 1.2.$$

to indicate production of the (possibly unstable) particles c and d (where $\alpha\beta\gamma\delta\ldots$ are the products of subsequent decays of c and d):

$$a+b \to 1+2+3+\ldots+n \qquad 1.3.$$

to specify n-particle production; and

$$a+b \to c+\text{anything} \qquad 1.4.$$

to represent a single-particle inclusive reaction. Our attention will be confined

Table 1 Composition of the total cross section

Scattering Process	Fraction of Total Cross Section: Low Energy	~2 GeV c	High Energy	Observables
Total Cross Section	1	1	1	σ_{tot} (essentially constant at high energy).
Elastic Scattering	>0.5	0.15–0.20	0.15–0.20	$d\sigma/dt$ (essentially constant at high energy); polarization parameters P, R, A.
Two (Stable) Particle Inelastic Channels	<0.5	0.10–0.15	→0	$d\sigma/dt$ (falls like 1/beam momentum at high energy); polarization parameters P, R, A.
Two (Unstable) Particle Inelastic Channels: Single or Double Resonance Production	0	0.70–0.75	<0.20	$d\sigma/dt$ (falls with incident momentum for most channels); decay angular distributions.
Genuine Multiparticle Channels	0	0	0.60–0.80	Production cross section; differential cross section as a function of $3n-4$ kinematic variables.

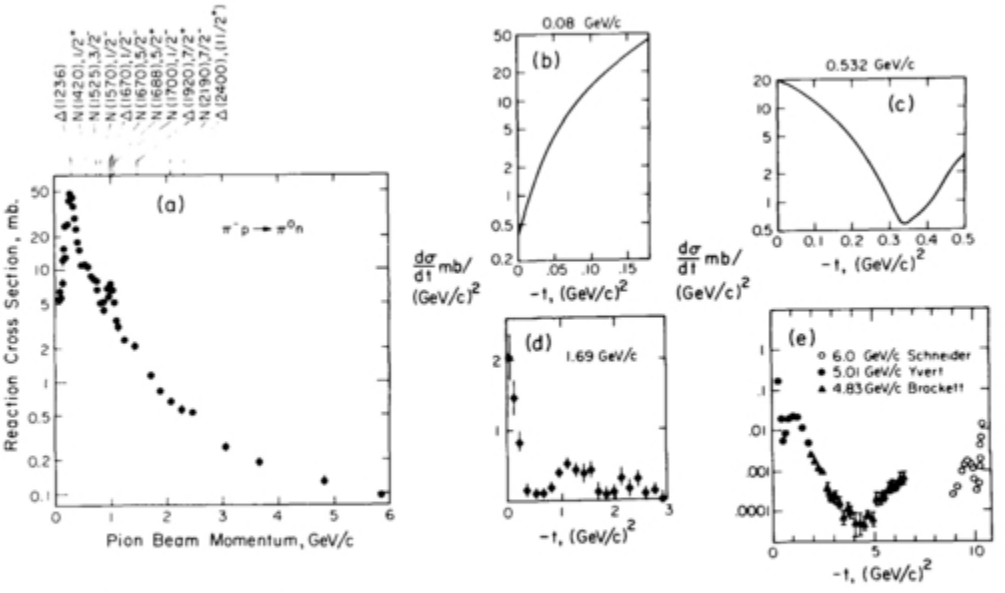

Figure 1 Integrated reaction cross section (297) and differential cross section (118, 206, 298, 300) for $\pi^- p \to \pi^0 n$ at various laboratory momenta.

mainly to reactions 1.1 and 1.2, which are classified further (according to the properties of the final-state particles) in section 5.

Figure 1 summarizes the evolution of the differential cross section for the charge-exchange reaction $\pi^- p \to \pi^0 n$ as the beam momentum is increased from threshold through the resonance region to the intermediate-energy regime. The qualitative features are common to nearly all two-body reactions. (Exceptions to this generalization are explained in section 2.) From the obligatory s-wave angular distribution at threshold, the cross section turns into a nearly background-free p-wave distribution in the neighborhood of the isolated $P_{33}[\Delta(1236)]$ resonance, becomes more complicated at momenta of a few GeV/c where several resonances overlap, and finally assumes a stable shape at momenta above 3 GeV/c where the reaction takes place through many partial waves. The production angular distribution is typified by a forward "peripheral" peak and a backward peak much smaller in magnitude. It is the theoretical description of these peripheral peaks for incident momenta in the range from approximately 3 GeV/c to 30 GeV/c that forms the subject of this article. We shall refer to this range as the "intermediate-energy regime," in anticipation of different systematics at still higher energies.

1C The Article

In the next section, we continue on a descriptive note and summarize the qualitative features of peripheral and Regge ideas. We shine a tarnished sun on the many dusty and discarded Regge models; dawn breaks and points the way to future sections; reflection adds perspective to past articles (2). The third section details dull formalism: We attack the sloppy and inconsistent conventions that make the study of resonance reactions unnecessarily hard. This brief polemic is supplemented by a separate preprint that lists and relates all experimental observables (polarizations, density matrix elements). Section 4 is a critical review of the many amplitude analyses of πN and hypercharge exchange reactions. The former are qualitatively similar while the latter are all found wanting. We examine the evidence for "peripheral" imaginary parts and find the evidence much less certain than often assumed. In particular, the so-called dual absorption model (31) is in some difficulties (32, 33).

Section 5 lists all known experimental systematics of forward scattering while section 6 outlines the pearls of theoretical wisdom that organize these results. We also suggest some fruitful areas for experimental investigation and finally conclude in section 7 with dreams for the future. The nonspecialist should probably omit the rather technical sections 3–5 on a first perusal.

2 SELF-EVIDENT TRUTHS AND THEIR EXTRAPOLATIONS

2A Validity of the Peripheral Exchange Picture

In our introductory remarks, we have touched upon the outstanding characteristic of differential cross sections for two-body reactions: They are *peripheral*, i.e. sharply peaked about the forward or backward directions. This feature may be appreciated in terms of a geometrical picture in which the relative angular momentum l of the

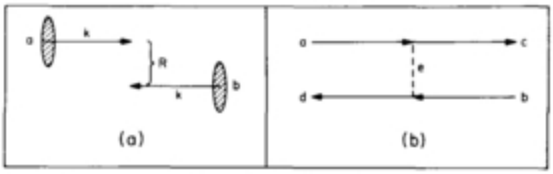

Figure 2 Complementary views of two-body reactions: (*a*) geometrical picture; (*b*) peripheral exchange picture.

incoming particles dictates the partial waves through which the reaction takes place (Figure 2*a*) and, in turn, the shape of the production angular distribution as $d\sigma/d\Omega_{cm} \sim [P_l(\cos\theta_{cm})]^2$. From the shape of peripheral peaks, one may roughly "measure" l and, therefore, knowing the cm momentum k of the colliding particles, deduce a semiclassical interaction radius R from the connection $l \approx kR$. This sort of reasoning typically implies an interaction radius of about 1 fm. This is large or comparable to hadron Compton wavelengths (1.4 fm for pions, 0.2 fm for nucleons), which may be expected to define a scale, and fully consistent with the range of nuclear forces (35).

While the geometrical picture provides a fount of intuition not only for two-body reactions (in which context we shall revisit it), but as well for more complicated hadron-hadron collisions (36), the keystone of the theory of two-body reactions is the peripheral exchange picture. The long apparent range of interaction makes it natural to associate scattering with the exchange (Figure 2*b*) of the least massive particle carrying the requisite quantum numbers. This natural association is also correct: Without important exception, all occurrences or nonoccurrences of peripheral peaks in two-body reactions can be understood in terms of the quantum numbers of the known [SU(3) multiplets of] mesons and baryons. The detailed verification of this hypothesis ranks as the outstanding achievement in the development of two-body phenomenology (37, 38).

To make concrete the implications of the peripheral exchange picture, let us introduce two-body kinematics and consider some specific cases. The scattering of spinless particles $1+2 \to 3+4$, represented in Figure 3, is described by a quantum mechanical amplitude $A(s,t)$, which is an analytic function of Mandelstam's energy variables

$$s = (p_1 + p_2)^2 \qquad 2.1.$$

$$t = (p_1 - p_3)^2 \qquad 2.2.$$

$$u = (p_1 - p_4)^2 \qquad 2.3.$$

where p_i is the four-momentum of particle i. In the usual experimental situation with particle 1 incident on particle 2 at rest,

$$s = m_1^2 + m_2^2 + 2m_2(p_{1,\text{lab}}^2 + m_1^2)^{\frac{1}{2}} \to 2m_2 p_{1,\text{lab}} \qquad 2.4.$$

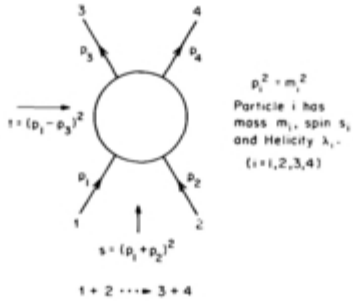

Figure 3 Labeling of particles for a two-body to two-body collision. The momenta are labeled p_i, masses m_i, particle spins s_i, and helicities λ_i.

at high energies. The squared momentum transfer is related to the cm scattering angle through

$$\cos\theta_s = \left[2st + s^2 - s\sum_{i=1}^{4} m_i^2 + (m_1^2 - m_2^2)(m_3^2 - m_4^2)\right] \Big/ S_{12}S_{34} \to 1 + 2t/s \qquad 2.5.$$

at high energies. Here we use

$$S_{ij} = [s - (m_i + m_j)^2]^{\frac{1}{2}}[s - (m_i - m_j)^2]^{\frac{1}{2}} \qquad 2.6.$$

The principle of crossing (e.g. 3, 5) relates the six reactions

$$1 + 2 \leftrightarrow 3 + 4 \quad [s\text{-channel}] \qquad 2.7.$$

$$1 + \bar{3} \leftrightarrow \bar{2} + 4 \quad [t\text{-channel}] \qquad 2.8.$$

$$1 + \bar{4} \leftrightarrow 3 + \bar{2} \quad [u\text{-channel}] \qquad 2.9.$$

to the same function $A(s,t)$ (in the spinless case). Because $s + t + u = m_1^2 + m_2^2 + m_3^2 + m_4^2$, where m_i is the mass of particle i, it is convenient to display the Mandelstam variables in triangular coordinates, as we have done in Figure 4 for the reactions

$$s\colon\ K^- p \to \pi^- \Sigma^+ \qquad 2.10.$$

$$t\colon\ \bar{p}\Sigma^+ \to \pi^- K^+ \qquad 2.11.$$

$$u\colon\ \pi^- p \to K^+ \Sigma^- \qquad 2.12.$$

In the s- and u-channels, resonance formation is prominent at low energies; the resonances masses are indicated as lines of constant s or u. In contrast, no known resonances have the quantum numbers of the t-channel. Beyond the resonance

region energies, forces for the scattering processes are provided by the available exchange particles. The absence of t-channel resonances thus implies the absence of forward peaks in the s- and u-channel reactions. On the other hand, the s-channel resonances are available as peripheral exchanges for backward scattering in the u-channel, and vice versa. The unmeasurable t-channel reaction has the u-channel

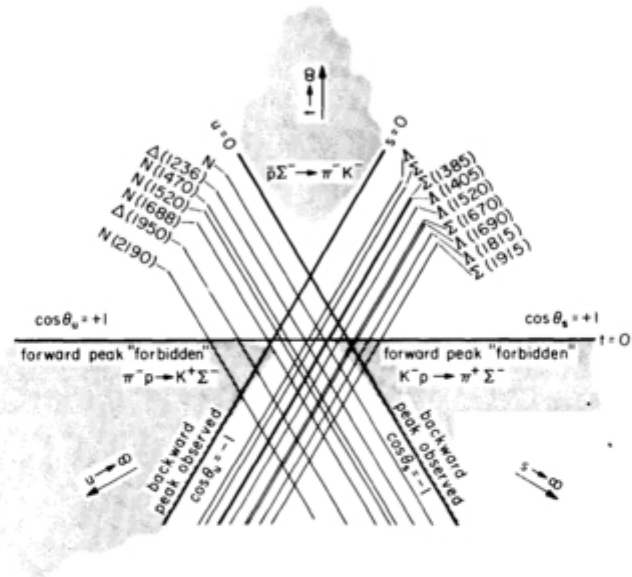

Figure 4 Mandelstam plot for the reactions $K^- p \to \pi^+ \Sigma^-$, $\pi^- p \to K^+ \Sigma^-$, and $p\bar{\Sigma}^- \to \pi^- K^-$, showing the correspondence between crossed-channel resonances and peripheral peaks in differential cross sections. Physical regions for the s-, t-, and u-channels are shaded.

resonances to drive forward scattering and the s-channel resonances to drive backward scattering.

More generally, it is a spectroscopic fact of life that all mesons fit into SU(3) singlets and octets, and all baryons fit into singlets, octets, and decimets, as prescribed by the elementary quark model (34, 39). The implied restriction on resonance quantum numbers allows one to predict occurrences of peripheral peaks. Some illustrative cases are collected in Table 2. [Other similar tabulations

Table 2 Correspondence between peripheral peaks and nearby poles

Reaction	*t*-channel quantum nos.			nearby poles[a]	peak?[b]	*u*-channel quantum nos.			nearby poles	peak?
	$\|Q_t\|$	I_t	Y_t			$\|Q_u\|$	I_u	Y_u		
$\bar{p}p \to \bar{p}p$	0	0, 1	0	[$\not P$], f, ρ, ω, A_2	↘	2	1	2	—	0
$pp \to pp$	0	0, 1	0	[$\not P$], f, ρ, ω, A_2	↘	forward-backward symmetric				↘
$\pi^- p \to \pi^- p$	0	0, 1	0	[$\not P$], f, ρ	↘	2	3/2	1	Δ	↘
$\pi^+ p \to \pi^+ p$	0	0, 1	0	[$\not P$], f, ρ	↘	0	1/2, 3/2	1	N, Δ	↘
$K^- p \to K^- p$	0	0, 1	0	[$\not P$], f, ρ, ω, A_2	↘	2	1	2	—	0
$K^+ p \to K^+ p$	0	0, 1	0	[$\not P$], f, ρ, ω, A_2	↘	0	0, 1	0	Λ, Σ	↘
$\pi^- p \to \pi^0 n$	1	1	0	ρ	↘	1	1/2, 3/2	1	N, Δ	↘
$\pi^- p \to K^+ \Sigma^-$	2	3/2	−1	–	0	0	0, 1	0	Λ, Σ	↘
$\pi^- p \to \eta^0 n$	1	1	0	A_2	↘	1	1/2	1	N	↘
$\pi^+ p \to \omega^0 \Delta^{++}$	1	1	0	B, ρ	↘	1	1/2	1	N	↘
$\pi^+ p \to \rho^0 \Delta^{++}$	1	1	0	π, A_2	↘	1	1/2, 3/2	1	N, Δ	↘
$\bar{p}p \to \bar{\Sigma}^+ \Sigma^+$	0	1/2, 3/2	1	K, K^*, K^{**}	↘	2	3/2	1	—	0
$\bar{p}p \to \bar{\Sigma}^+ \Sigma^+$	2	3/2	1		0	0	1/2, 3/2	1	—	0
$K^- p \to \pi^- \Sigma^+$	0	1/2, 3/2	−1	K^*, K^{**}	↘	2	3/2	1	Δ	↘
$K^- p \to \phi\Lambda$	1	1/2	−1	K^*, K^{**}	↘	1	1/2	1	N	↘[c]

[a] $\not P$ denotes Pomeron Exchange (sections 5A–C).

[b] The "exotic" reactions which have no particle to exchange, do, in fact, have a *small* peripheral peak. Section 5M considers this more carefully.

[c] Suppressed by the quark-model selection rule $N\bar{N} \not\to \phi$. See e.g. (34) and section 5M.

are given in (3) and (37).] The remainder of our review is devoted to attempts to extend this framework to a quantitative theory of peripheral cross sections.[3]

2B *The Regge Pole Framework*

To the known SU(3) multiplets of resonances correspond families of Regge trajectories which obey a linear relation between particle spins (α) and masses squared:

$$\alpha(m^2) = \alpha_0 + \alpha' m^2 \qquad 2.13.$$

The slope parameter α' is universal (for all Regge trajectories) and equal to (0.85 1) $(\text{GeV}/c)^{-2}$. The interpretation of this universality is one of the appealing results of dual resonance models (41). For dynamical reasons which either imply or are implied by the absence of exotic[4] states, the forces which build the hadron spectrum are exchange degenerate (42), so a particle occurs for each integer value of spin along a meson trajectory. A familiar example of this feature of the spectrum is the well-established set of $I = 1$ natural parity mesons ρ, A_2, g which occur at spins 1, 2, 3 on the trajectory $\alpha(m^2) \approx \frac{1}{2} + m^2$.

Let us now discuss in the Regge pole language the features we have already noticed in Figure 1. At low energies for the reaction $\pi^- p \to \pi^0 n$, the reaction cross section is characterized by the excitation of states on (for example) the Δ trajectory (Figure 5*a*). In the t-channel, there occur the states $\rho, g \ldots$ appearing on the ρ trajectory, which mediate forward scattering at high energies (Figure 5*b*) and give rise to the characteristic $s^{\alpha(0)}$ behavior of the near-forward scattering amplitude. Similarly, backward scattering proceeds at high energies (Figure 5*c*) by exchange of the u-channel trajectories, such as the nucleon trajectory, which generate the $s^{\alpha(u)}$ behavior of the near-backward scattering amplitude. For charge exchange, which is quite typical in this respect, the backward peak is an order of magnitude smaller than the forward peak. The study of the transition region, exemplified by Figure 1*d*, has led in recent years to a detailed understanding of the interplay of direct-channel resonances and crossed channel Regge trajectories. The beautiful work of Dolen, Horn & Schmid (43) showed conclusively that the direct-channel (resonance) and crossed-channel (Regge pole) descriptions are complementary. Thus the resonances cooperate to build up the high energy Regge behavior, whereas the Regge pole description is valid in an average sense, even in the resonance region

[3] An analogy may help the reader who is not a high energy physicist to understand the present state of our art. If one had invented nonrelativistic quantum mechanics, quantized the radiation field, and discovered that the fine structure constant is small, he could correctly enumerate allowed and forbidden transitions between atomic states but would be unable to compute every rate precisely. In two-body scattering, the peripheral exchange picture and the quark model for the resonance spectrum allow one to catalog allowed and forbidden peaks, but do not confer the ability to compute cross sections precisely. We do not know why the quark model works, but neither does quantum electrodynamics explain the size of α. Our goal, however, is to explain scattering and spectrum (i.e. everything) at once (40).

[4] By exotic states, we mean mesons with quantum numbers not given by quark-antiquark pairs or baryons with quantum numbers not given by three quark states.

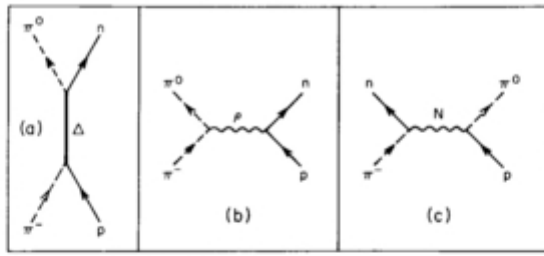

Figure 5 (*a*) Low energy pion-nucleon charge exchange is characterized by the production of direct-channel nucleon resonances among which are the $\Delta(1236)$, $\Delta(1950)$, and $\Delta(2420)$ lying on the Δ trajectory. (Compare Figure 1*a*.) (*b*) The high energy forward peak shown in Figure 1*c*, is driven by t-channel exchange of the ρ trajectory. (*c*) The high energy backward peak, also shown in Figure 1*c*, is driven by u-channel exchange of several baryon trajectories, among them the nucleon trajectory.

below 2 GeV/c. The equivalence of the two modes of description is known as duality and is further discussed in sections 4C and 4D. The remarkable cooperation between resonances, which leads to familiar high energy features, is illustrated in Figure 6 for the πN scattering amplitudes corresponding to isovector exchange in the t-channel. The first zeros of the Legendre functions associated with direct channel resonance contributions to the spinflip amplitude (dominant in πN charge exchange) all occur near $t = -0.6$ $(\text{GeV/c})^2$, where the pronounced dip appears (see Figure 1*e*) in the high energy cross section, while the first zeros associated with the nonflip amplitude are gathered near $t = -0.2$ $(\text{GeV/c})^2$, where the crossover between $\pi^- p$ and $\pi^+ p$ cross sections takes place (see Figure 7).

The mutual constraints among s-channel, t-channel, and u-channel trajectories are embodied in the dual resonance model given by Veneziano's inspired guess (44), wherein zero-width resonances appear as poles on the real axis. The Veneziano model therefore gives a caricature of the dual behavior of hadrons which cannot be quantitatively reliable. Gdorico (45) has advocated the viewpoint that even when the transition is made from the dual resonance model idealization to real world situations, artifacts of the simple structure of the Veneziano amplitude remain. As one example, Figure 8 shows that the differential cross section for $K^- p \to \bar{K}^0 n$ exhibits structure at fixed u in the low energy ($\lesssim 2$-*GeV/c*) regime of the kind suggested by the Veneziano formula. Successes of this sort have led others (8, 46) to support the contention that *qualitative* lessons are indeed to be learned from dual resonance model amplitudes. Another implication of the dual resonance model is that $1\ \alpha'$ sets the scale for hadronic phenomena both for the mass spectrum and for scattering dynamics. This suggests that for $s \gtrsim 10$ GeV^2 we are in the (asymptotic) Regge pole regime. It now seems that there are complications (Regge cuts?) which become dominant only at much higher energies, perhaps for

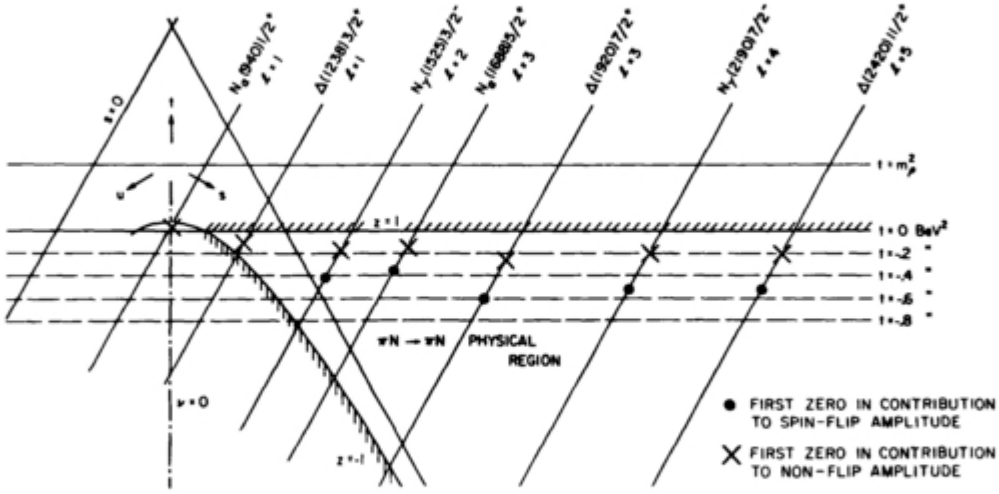

Figure 6 First zeros of the prominent resonances on the Mandelstam plot for the πN problem [from 143].

$s \gtrsim 100\ \text{GeV}^2$. If this be so, the study of two-body reactions at the National Accelerator Laboratory may provide many surprises.

In the intermediate energy regime, we may confront the distinctive predictions

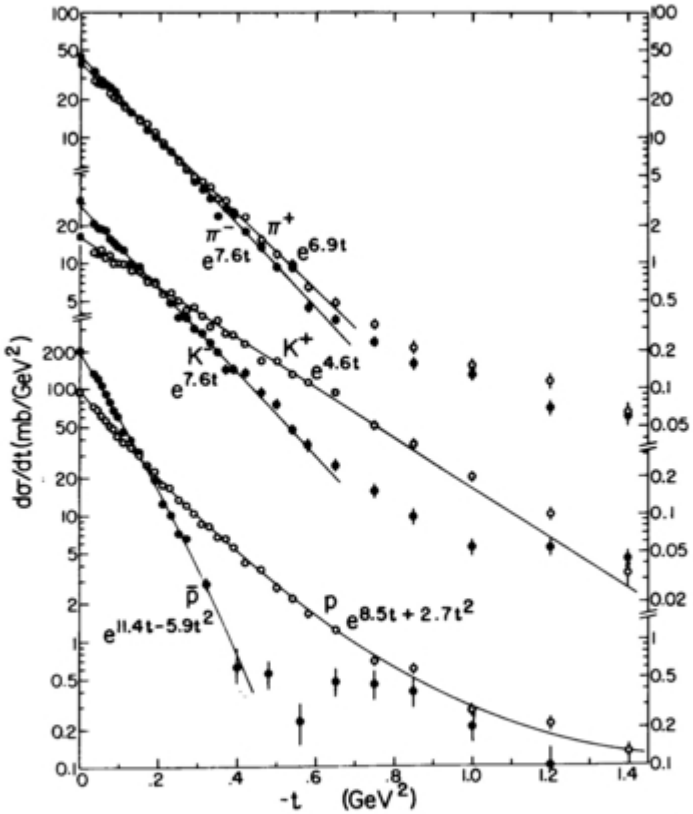

Figure 7 Differential cross sections for the scattering of six different particles from protons at a laboratory momentum of 5 GeV/c [from t103i]. The crossover which occurs in $\pi^+ p$ scattering near $t = -0.2\ (\text{GeV/c})^2$ is ascribed to the vanishing of the imaginary part of the nonflip ρ-exchange amplitude.

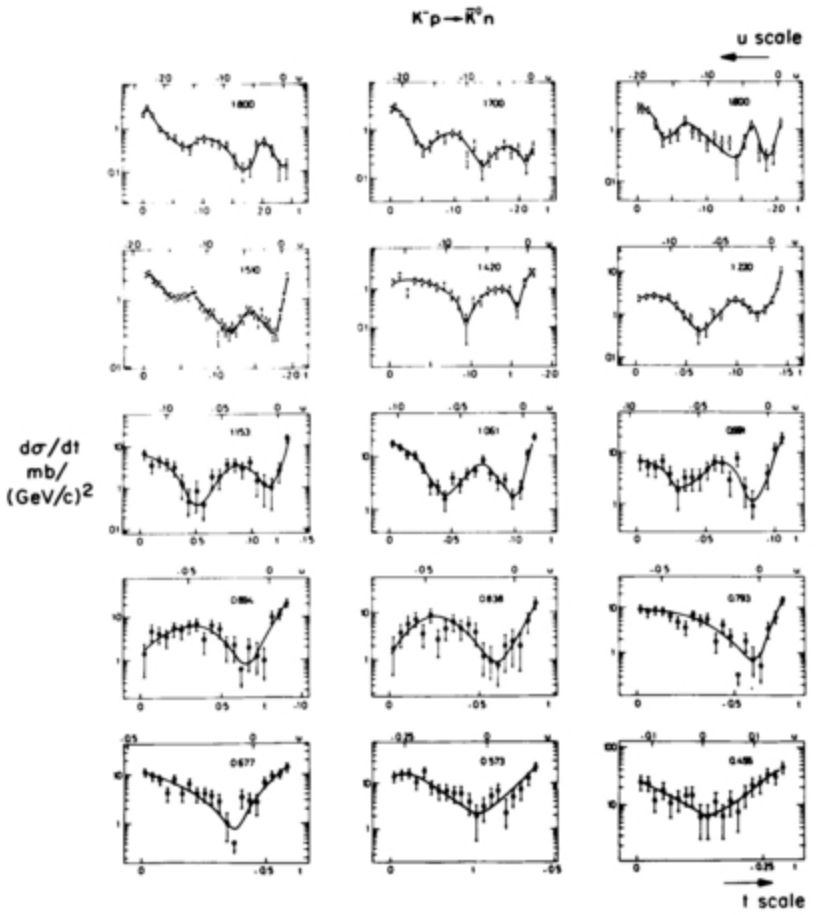

Figure 8 $K^- p \to \bar{K}^0 n$ angular distributions between 0.45 and 1.8 GeV c plotted vs t and u (the beam momentum is indicated in each frame). The solid lines are hand-drawn to guide the eye. The figure shows three dips at constant positions of $u \approx -0.1$, -0.7, and -1.7 (GeV/c)^2 [from (45)].

of Regge theory with experiment. As a typical Regge pole amplitude, let us consider that for πN charge exchange:

$$A(s,t) = g_{\pi\pi}(t) g_{N\bar{N}}(t) \Gamma\left(1 - \alpha_\rho(t)\right)\left(e^{-i\pi\alpha_\rho(t)} - 1\right)(\alpha' s)^{\alpha_\rho(t)} \qquad 2.14.$$

which displays the basic properties of interest. The most characteristic of these is "shrinkage." Recalling that $d\sigma/dt \propto s^{-2}|A|^2$, and using the linear trajectory $\alpha(t) = \alpha_0 + \alpha' t$ (2.13), we have the prediction

$$\frac{d\sigma}{dt}(t) \Big/ \frac{d\sigma}{dt}(0) = (\text{Function of } t) \times \exp(2\alpha' t \log s) \qquad 2.15.$$

of a forward peak which becomes more sharply peaked ("shrinks") as the primary energy is increased. One way of exhibiting shrinkage is by fitting the experimental cross sections to the form

$$\frac{d\sigma}{dt}(s,t) = (\text{Function of } t) \cdot (\alpha' s)^{2\alpha_{\text{effective}}(t) - 2} \qquad 2.16.$$

If the reaction is dominated by the exchange of a single Regge pole, the effective trajectory inferred from the scattering data will match the trajectory determined by the resonance spectrum. For πN charge exchange, this is indeed the case (2).

The second prediction of exchange-degenerate Regge theory is of the occurrence of zeros in the scattering amplitude (hence in the cross section) at wrong signature nonsense points (47), e.g. at $\alpha_\rho = 0$ in the case of πN charge exchange. Again this provides a successful explanation for the dip in $d\sigma/dt$ at $t \approx -0.6$ (GeV/c)^2 [cf. Figure 1*e*]. Another consequence of the exchange degeneracy of meson trajectories is the prediction that vector and tensor exchange amplitudes should be 90° out of phase so that pairs of reactions such as

$$K^- p \to \bar{K}^0 n \qquad 2.17a.$$

$$K^- n \to K^0 p \qquad 2.17b.$$

for which the corresponding amplitudes are

$$\text{Vector} + \text{Tensor} \qquad 2.18a.$$

$$-\text{Vector} + \text{Tensor} \qquad 2.18b.$$

should have equal cross sections. Such line-reversal relations are well enough satisfied that systematics of the *breaking* of exchange degeneracy have been cataloged.

A final prediction of Regge theory is that Regge pole residues should factorize. For example, the ρ-exchange contributions to the reactions $\pi^- \pi^0 \to \pi^0 \pi^-$, $\pi^- p \to \pi^0 n$, and $np \to pn$ will be in the ratios

$$\left[g_{\pi\pi}(t)\right]^2 : g_{\pi\pi}(t) g_{N\bar{N}}(t) : \left[g_{N\bar{N}}(t)\right]^2 \qquad 2.19.$$

(where we have suppressed helicity indices). Factorization has been tested extensively, especially for the Pomeranchuk singularity (48, 49) in both two-body and inclusive reactions, but never (for lack of precise data) in situations which provide very

stringent tests. Since factorization is derivable from S-matrix axioms in the case of isolated Regge poles, any test probes the nature of the J-plane singularities.

2C *Some Contemporary Models*

Although we shall avoid in this paper detailed quantitative confrontations of particular models with experimental results, it will be helpful to have in mind some of the divergent viewpoints represented by contending theories.

THE DUAL ABSORPTION MODEL That the examination of scattering amplitudes in the impact parameter plane leads to important insights into reaction mechanisms has been stressed in modern times by Ross, Henyey & Kane (50). Their original discussions of the systematics of s-channel helicity amplitudes and the b-plane interpretation of those systematics did not, however, make contact with the concurrent developments in the field of duality. A synthesis of the Michigan school's s-channel-impact parameter view with the predictive power of duality was proposed by Harari (31) who named his scheme the dual absorption model. The idea is a throwback with additional sophistication to the old "ring model" (51). Harari guessed that the imaginary parts of scattering amplitudes (in nonexotic channels) were built up, through duality, by resonances concentrated on a peripheral ring of radius $R \approx 1$ fm, and should therefore be given by the amplitudes for Fraunhofer diffraction from an illuminated ring, which are proportional to $J_n[R(-t)^{\frac{1}{2}}]$, where n is the net s-channel helicity flip. We examine the evidence for this idea in section 4F.

COMPLEX REGGE POLES[5] A general result of multiperipheral models is that the collision of J-plane singularities gives rise to complex conjugate Regge poles on unphysical sheets which may be approximated by a pair of first-sheet poles over a limited energy range. It has been hoped that complex poles might provide a compact parameterization for "input" Regge poles and the associated Pomeron-Reggeon branch cuts.

EFFECTIVE ABSORPTION MODELS[6] In an effort to retain the intuitive appeal of the absorption recipe for Regge cuts while circumventing the embarrassments of line-reversal inequalities and πN charge exchange polarization, a number of authors (33, 54–60) have replaced the conventional elastic rescattering amplitude with an effective rescattering amplitude constructed to reproduce the observable quantities and without any a priori motivation. Apparently there is little predictive power in such an approach, although it might be hoped that one could understand how amplitudes get to be as they are. It is too early to judge (84) even the interpolative value of such models but it has already been pointed out that they all violate finite energy sum rules (61) so even their pedagogical value is to be doubted. It may be expected that the effective absorption models take into account Reggeon-Reggeon cuts as well as Reggeon-Pomeron cuts, but here again duality constraints

[5] A compact review is given by Roy (52).
[6] For a brief review, see Tran Thanh Van (53).

raise doubts. Finkelstein (62) and Worden (63) have obtained selection rules for Reggeon-Reggeon cuts which suppress the contributions to KN charge exchange and πN charge exchange, where their effects would have been particularly welcome. Although these arguments can always be breached or ignored, we are coming to believe that a pertubative approach to Regge cuts may be futile. The confrontation between experiments now in progress[7] on double charge exchange reactions and the Reggeon-Reggeon cut predictions of Michael (64) and Quigg (65) may provide a final verdict.

THE STRONG CENTRAL ABSORPTION PRESCRIPTION One modified absorption scheme that has a possibility of being derivable from physical arguments, and not merely adjusted to agree with data, is the strong central absorption prescription (SCAP) advocated by Chiu (2), which is similar in effect (though not in motivation) to the $\pi N \to \rho N$ model of Williams (66), whose generalization to the arbitrary π-exchange process has come to be called the Poor Man's Absorption Model (67). Arguments drawing on the statistical model for particle production support the ancient absorptive peripheral model lore (68) that small impact parameter collisions do not contribute appreciably to production of two-body final states. The original proposal (2) disagrees with experiment. However, the so-called weak SCAP hypothesis that complete central absorption occurs in and only in reactions described by planar duality diagrams (69, 70), e.g. $K^- p \to \bar{K}^0 n$, $\pi^- p \to K^- \Sigma^+$, does appear consistent [(71) and section 4F] but of curtailed predictive power. To sharpen the distinction between models, we remember that Harari (31) postulates peripheral behavior for all imaginary parts and all spin amplitudes, whereas Chiu (2, 71) postulates peripheral behavior for both real and imaginary parts in the nonflip amplitude of a subset of reactions.

3 DEFINITIONS AND CONVENTIONS

In this section we introduce the constructs needed to extract and present in organized fashion the experimental data on two-body scattering. First, we introduce the scattering amplitudes with which the processes are described theoretically. Then we express the experimental observables in terms of amplitudes for the simplest (realizable) case of $0^- \tfrac{1}{2}^+ \to 0^- \tfrac{1}{2}^+$ scattering. The two final subsections, which are devoted to definitions and observables for resonance production reactions, may be skipped by the casual reader. The observables are uncomplicated in principle but have been made to appear arcane by a host of different conventional axes and phases used in the literature. To the problem of extracting a resonance cross section from the observed bump on background in the mass spectrum of its decay products, however, there is no absolutely correct solution. The practical necessity of comparing different experiments in any case calls for a uniform procedure (72). To this end we describe in the final subsection some of the methods used previously

[7] J. Guillaud, Orsay, Private communication. D. Mayer, Ann Arbor, Private communication.

and support a reasonable standard technique, the universal adoption of which would bring about consistently defined and hence more useful data.

3A *Amplitudes for* $0^-\frac{1}{2}^+ \to 0^-\frac{1}{2}^+$ *Scattering*

The scattering of spinless particles, to which we alluded in section 2A, though theoretically trouble free, is not of practical importance for the simplest laboratory reactions (e.g. $\pi N \to \pi N$) involve two spin-$\frac{1}{2}$ particles. To describe reactions of interest, we must add spin labels to our amplitudes; for every choice of a spin basis, we obtain a distinct set of amplitudes. We need only mention here s-channel and t-channel helicity amplitudes ($H_s^{\lambda_1\lambda_2\to\lambda_3\lambda_4}$ and $H_t^{\lambda_1\lambda_3\to\lambda_2\lambda_4}$, respectively), which are the usual Jacob-Wick (73) amplitudes for reactions 2.7 and 2.8. The spin axes appropriate to particle 3 are shown in Figure 9. These sets of amplitudes are related

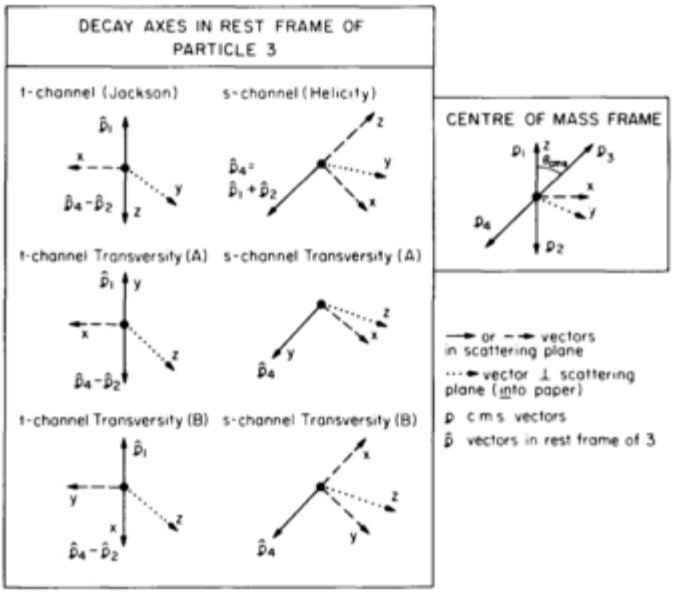

Figure 9 Some coordinate systems used to describe the spin-states and momenta for $1+2\to 3+4$. Indicated are the overall center mass frame and six of the more common frames used to define spin-states and decay angles of particle 3. There are analogous sets of six axes defined in the rest frames for the other three particles (1, 2, and 4) in the reaction.

by a rotation (of the spin axes)—called the Trueman-Wick crossing relation (74)—whose exact form need not concern us here.

In the simple but important special case of meson-baryon elastic and (hyper)-charge-exchange scattering, particles 1 and 3, the mesons, have spin-parity 0^- and particles 2 and 4, the baryons, have spin-parity $\frac{1}{2}^+$. There are consequently two independent amplitudes which we choose as the s-channel helicity nonflip amplitude N and helicity flip amplitude F:[8]

$$\begin{aligned} N &= H_s^{+\to+} = H_s^{-\to-} \\ F &= H_s^{+\to-} = -H_s^{-\to+} \end{aligned} \tag{3.1.}$$

The experimental observables are

$$\mathrm{d}\sigma/\mathrm{d}t = K\{|N|^2 + |F|^2\} \tag{3.2.}$$

$$\sigma_{\text{tot}} = K' \operatorname{Im} N(s, t=0) \tag{3.3.}$$

$$P\,\mathrm{d}\sigma/\mathrm{d}t = 2K \operatorname{Im}(NF^*) \tag{3.4.}$$

$$\hat{R}\,\mathrm{d}\sigma/\mathrm{d}t = 2K \operatorname{Re}(NF^*) \tag{3.5.}$$

$$\hat{A}\,\mathrm{d}\sigma/\mathrm{d}t = K\{|N|^2 - |F|^2\} \tag{3.6.}$$

where we have defined the kinematic factors

$$K = 0.3893\,[\mathrm{mb}/(\mathrm{GeV})^2]/64\pi m_2^2 P_{\text{lab}}^2 \tag{3.7.}$$

and

$$K' = 0.3893\,[\mathrm{mb}/(\mathrm{GeV})^2]/2m_2 P_{\text{lab}} \tag{3.8.}$$

The differential cross section $\mathrm{d}\sigma/\mathrm{d}t$ and total cross section σ_{tot} off an unpolarized target require no discussion. The polarization P is related to the asymmetry in the scattering off a polarized target; $\hat{R}$ and $\hat{A}$ are in general linearly related to, and asymptotically become equal to, the Wolfenstein (75) parameters R and A which are the nonzero components of polarization of the final baryon scattered off a polarized target. The observables 3.2–3.4 and 3.5, 3.6 are then listed in ascending order of measurement difficulty. In particular, $\hat{R}$ and $\hat{A}$ have only been measured (85) in elastic scattering, for which the cross section is large. In the immediate future, we can anticipate $\hat{R}$ and $\hat{A}$ measurements in associated production reactions leading to self-analyzing (76) final-state hyperons (Λ^0, Σ^-).

3B Density Matrix Elements and Decay Angular Distributions

If the produced particles are unstable, the spin structure of the scattering amplitudes may be deduced from the angular distributions of their decay products (77–82). For instance, for particle 3 a ρ^0 meson decaying into $\pi^+\pi^-$, the angular distribution of π^+ momenta in the ρ^0 rest frame, is given by

$$\begin{aligned} W(\theta, \phi) = (1/4\pi)\{&1 + \tfrac{1}{2}(1 - 3\rho^{00})(1 - 3\cos^2\theta) \\ &- 3[\rho^{1,-1}\sin^2\theta\cos 2\phi + \sqrt{2}\,\mathrm{Re}\,\rho^{10}\sin 2\theta\cos\phi]\} \end{aligned} \tag{3.9.}$$

[8] We designate $\pm\frac{1}{2}$ by $\pm$.

The spherical polar angles (θ, ϕ) specify the direction of the π^+ momentum $\vec{q}$ in the ρ^0 rest frame with respect to a specified coordinate system. The form 3.9 is valid for any orientation of the coordinate axes; each choice leads to a particular set of density matrix elements which are expressible in terms of corresponding scattering amplitudes. Referring $\vec{q}$ to the t-channel ("Jackson") frame, we obtain*

$$\rho_t^{mm'} \, d\sigma/dt = [(-1)^{m-m'} K/(2s_1+1)(2s_2+1)] \sum_{\lambda_1 \lambda_2 \lambda_3 \lambda_4} H_t^{\lambda_1 \lambda_2, m-\lambda_3, \lambda_4} [H_t^{\lambda_1 \lambda_2, m'-\lambda_3, \lambda_4}]^* \tag{3.10}$$

in terms of t-channel helicity amplitudes. Alternatively, referring $\vec{q}$ to the s-channel ("helicity") frame, we have

$$\rho_s^{mm'} \, d\sigma/dt = [K/(2s_1+1)(2s_2+1)] \sum_{\lambda_1 \lambda_2 \lambda_3 \lambda_4} H_s^{\lambda_1 \lambda_2, m-\lambda_3, \lambda_4} [H_s^{\lambda_1 \lambda_2, m'-\lambda_3, \lambda_4}]^* \tag{3.11}$$

In either case,

$$d\sigma/dt = [K/(2s_1+1)(2s_2+1)] \sum_{\lambda_1 \lambda_2 \lambda_3 \lambda_4} |H^{\lambda_1 \lambda_2 \lambda_3 \lambda_4}|^2 \tag{3.12}$$

The formulae pertaining to the decay of particle 4 are entirely analogous. Observe, however, that in equation 3.9 the element ρ^{10} changes sign if the conventional y-direction is reversed. Although there is universal agreement to choose the normal to the production plane ($\hat{y}$) along $\vec{p}_1 \times \vec{p}_3$ for analysis of particle 3, no such consensus exists in the case of particle 4. We endorse the same definition in both situations: $\hat{y} = \vec{p}_1 \times \vec{p}_3 = \vec{p}_2 \times \vec{p}_4$. Many experimental reports now leave the choice of the normal to the production plane as a conundrum for the reader, and occasionally incorrect expressions for the connection between density matrix elements and decay angular distributions in complicated cases occur in the literature. With the low-statistics data now extant such inconsistency is merely annoying, but in the coming era of multiparticle spectrometers continued casualness will lead to significant wasted effort. To ameliorate the situation, we have prepared a compendium of guaranteed formulae for relations analogous to equations 3.9–3.12 which we will supply on request.

Figure 9 also depicts the so-called transversity frame (83) for which the quantization axis is normal to the production plane. There are even two variants (marked A and B in Figure 9) of the transversity axes! Uniformity being desirable, we recommend the adoption of variant A which is related by a rotation through $\pi/2$ about the x-axis to the longitudinal frame pictured above it. Finally, for completeness, let us mention that the angular distributions are frequently described in terms of statistical tensors $T_{m'}^{j_1 j_2}$, $T_{m'm}^{j_1 j_2}$, which are related to the density matrix elements in (80).

To illustrate the importance of density matrix element information, we note from equation 3.10 that $\rho^{00} \, d\sigma/dt$ only receives contributions from amplitudes with $\lambda_3 = 0$. As Gottfried & Jackson (78) proved, this fact allows the separation of $d\sigma/dt$ into the contributions from natural- and unnatural-parity exchange mechanisms. Taking for definiteness the reaction $\pi N \to \rho N$, we recall that $\rho^{1m1} \, d\sigma/dt$

* The phase $(-1)^{m-m'}$ is a consequence of the "particle 2" convention of (73).

is given in terms of unnatural parity (π, A_1) exchanges and that to leading order in s the combinations $(\rho^{11} \pm \rho^{1,-1})\mathrm{d}\sigma/\mathrm{d}t$ correspond respectively to natural parity (A_2) and unnatural parity (π, A_1) exchanges.

3C *Extraction of Resonance Cross Sections*

It is very well to discuss a resonance reaction such as $\pi^- p \to \rho^0 n$, but in fact, all we can measure is the three-body final state, $\pi^- p \to \pi^- \pi^- n$ wherein, as shown in Figure 10, the presence of the ρ^0 resonance is evidenced by a bump in the $\pi^+\pi^-$ mass spectrum. The observed spectrum consists of both resonance and background contributions which must be disentangled. Many ingenious techniques have been devised for making the separation. The common feature of the methods is the parameterization of the cross section as

$$\sigma = \alpha^2 |T_R(m_{\pi\pi})|^2 + \beta^2 |T_B(m_{\pi\pi})|^2 \qquad 3.13.$$

where the resonant amplitude T_R is a (modified) Breit-Wigner form (79, 86) and the incoherent background amplitude T_B is a smooth (usually polynomial) function of $m_{\pi\pi}$. The parameter α and hence the resonance production cross section is determined by fitting equation 3.13 to the data.

The basic method may be refined in many ways, for example, by the introduction of t-cuts or exponential t-dependences, by mass conjugation (87, 88), by the inclusion of many resonances in different subchannels of the final state (89), by the imposition

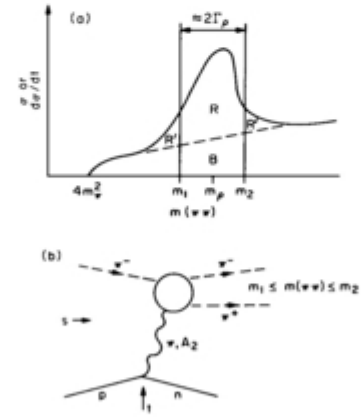

Figure 10 (*a*) Various ways (72) of defining a resonance cross section using a mass-cut $m_1 \leq m(\pi\pi) \leq m_2$ with possible background (B) and resonances tail correction (R'). (*b*) A Regge-pole exchange diagram for mass-cut data: m_1, m_2 are held fixed as $s \to \infty$.

of longitudinal phase space cuts, and ultimately by examination of prism plot displays (90) and of detailed partial-wave analyses (91, 92). Unfortunately, none of these techniques is free from ambiguity because the problem is inevitably "ill-posed." Therefore the fact that data from virtually every experiment are treated in a distinct way presents a decided obstacle to the comparison of resonance data from different sources. This is a more serious problem than the different choice of axes for density matrix elements; the latter may be corrected, a posteriori, by the user as the different axes are related by well-defined kinematic rotations.[10]

There are yet more ways (72) of defining cross sections as when an experiment contains only a few events, the fit methods are no longer applicable and it is usual to make a simple mass-cut, taking all data with $m_1 \leqslant m(\pi\pi) \leqslant m_2$; there are no universally adopted values of m_1, m_2 commonly used are $m_1 \approx m_R - \Gamma, m_2 \approx m_R + \Gamma$ where the resonance has mass m_R and width Γ. This choice is the regions $R + B$ on Figure 10*a*; also used are "background subtraction" (R only) or "background subtraction + correction for resonance tails" ($R + R'$ only). The latter two resonance definitions are subject to the same arbitrariness and lack of uniformity as the fit methods. If universal values of m_1 and m_2 were agreed on, the simple mass-cut ($R + B$) would allow a *uniform* definition of a "resonance" cross section. It would not be a faithful representation of a theoretical single resonance cross section; however, this is of no great import because any theory of, say $\pi N \to \rho N$, should also be able to describe $\pi N \to (\pi\pi)N$ where the $\pi\pi$ system in a fixed mass-cut has both a $J^P = 1^-$ resonant ρ and a big $J^P = 0^+$ background amplitude. In particular, Regge pole exchanges with their characteristic energy dependence should describe such mass-cut data (Figure 10*b*). We therefore urge that in the future all resonance results be quoted for a simple mass-cut. The more complicated fit methods should *also* be used and are indeed vital for many applications [e.g. extraction of pure $I = 0$ exchange by forming $\sigma(\pi^- p \to \rho^- p) + \sigma(\pi^- p \to \rho^0 p) - \sigma(\pi^- p \to \rho^0 n)$].

We should also warn the reader against the confusing practice of finding the overall production cross section by a fit method. Then, as each t bin contains but a few events, it is common to define $d\sigma/dt$ by a mass-cut but renormalize by a t-independent factor λ so that

$$\lambda \int_{-\infty}^{0} dt \, d\sigma/dt \Big|_{\text{mass-cut}} = \sigma_{\text{prod}} \Big|_{\text{fit}} \tag{3.14}$$

Again this leads to lack of uniformity and it would be helpful if the unrenormalized $d\sigma/dt_{\text{mass-cut}}$ were always given as well.

There are also many techniques (87, 92) developed for finding density matrix elements in the presence of background. We can mention the use of control regions on either side of the resonance, mass conjugation, or more generally maximum likelihood fits to the data with competing resonances removed. It appears that there is less difference in the various methods than for the overall cross section. However,

[10] All that is lost is an accurate evaluation of the errors as the full error matrix is rarely given for the density matrix elements only the usual diagonal elements giving the separate error in each observable.

a different approach will be necessary with the high-statistics data now becoming available. For instance, the quark model predicts the vanishing of a number of statistical tensors. The predictions are roughly satisfied by existing data, within quite large errors. It is not known whether deviations indicate failures of the model for "pure" resonance production or confusion due to background. In future analyses the complete ($\geq$3-body) final state should be parameterized in a fashion consistent with all the common theoretical constraints upon resonance and background production, and the parameterization confronted with the original data sample of four-momenta. The popular procedure of "model-independent" extraction of the resonance signal carries an uncontrolled systematic error of about $10^{\circ}_{\circ}$, which cannot significantly be reduced.

4 PHENOMENOLOGICAL WEAPONS

In this section, we discuss methods of extracting from experimental data information on the s, t, spin, and partial-wave dependence of amplitudes underlying the observables. Such an approach has the considerable advantage that amplitude structure can be compared directly with theoretical expectations, and provides precise tests of (for instance) the distinct zero patterns for different amplitudes suggested by the absorption model (10, 11, 16, 93). In contrast, in making brute force fits of models to experimental observables (which are bilinear in the amplitudes), one may find comparable fits with many different sets of amplitudes, or may have a successful parameterization for one amplitude obscured by the poor description of another.

This powerful amplitude approach is unfortunately rarely applicable; it requires a complete set of observables and at present these are only available in πN elastic scattering. In other cases, we can try to use it but we must (partially) commit the sin of the model fit and introduce extra and probably wrong assumptions.

4.4 *Amplitude Analysis of πN Elastic Scattering*

Pion nucleon elastic and charge exchange scattering can be described in terms of four complex amplitudes. These are the nonflip N and spinflip F amplitudes corresponding to two possible isospin states which we take to be the usual $I = 0$ and 1 t-channel exchanges. (These are normalized to be conventional + and $-\pi N$ isospin states respectively.)

The amplitudes of the three measurable reactions are:

$$H(\pi^- p \to \pi^- p) = H(I = 0) + H(I = 1)$$
$$H(\pi^+ p \to \pi^+ p) = H(I = 0) - H(I = 1)$$
$$H(\pi^- p \to \pi^0 n) = -\sqrt{2}H(I = 1)$$

where the above holds separately for H as N or F the two spin amplitudes.

At 6 GeV c, a complete set of measurements exists for $-t \lesssim 0.5$ (GeV/c)^2 and, using the notation of section 2 for polarization observables, these are P, R, and $d\sigma/dt$ for $\pi^+ p \to \pi^+ p$, and P plus $d\sigma/dt$ for $\pi^- p \to \pi^0 n$. A is also known for

$\pi^- p \to \pi^- p$ but, in fact, this only gives sign information as its magnitude is known to greater accuracy from the relation $P^2 + R^2 + A^2 = 1$. The eight experimental observables are (one) more than enough to determine the four complex amplitudes $N(I = 0, 1)$, $F(I = 0, 1)$ within the usual unobservable overall phase.

Four amplitude analyses of this data have been performed recently[11] (94–97) and we summarize their results in Figures 11 and 12. We have recast all analyses in the same units [i.e. so that $d\sigma/dt = \frac{1}{4}|N|^2 + |F|^2$; mb (GeV c)^2] and have chosen the overall phase in the same way for each analysis. Thus $N(I = 0)$ is prescribed to have the same phase as given by the Barger-Phillips (98) Regge pole fit to all high energy πN data. This fit was constrained by finite energy (FESR) and continuous moment (CMSR) sum rules and so its amplitude structure ought to be reliable. In fact, its value for small $-t \lesssim 0.2$ (GeV c)^2) for the $I = 0$ phase is confirmed by dispersion theory calculations (99, 100). However, at large $-t$ there is no such supportive information and the basic FESR CMSR input is less reliable; correspondingly the curves in Figures 11 and 12 may require rotation by the common (t-dependent) unobservable phase for $-t \gtrsim 0.2$ (GeV c)^2.

The three early analyses [marked HM (94), Kelly (95), and Saclay (96) in the figures] were based on essentially the same data set. The ANL group (97) substituted their own new measurements (101) of $\pi^- p \to \pi^0 n$ polarization, which gave values considerably smaller than those of the CERN data (102) used by the other groups (see Figure 13). They also made use of the beautiful new data on $\pi^+ p$ elastic scattering (103) that we have already displayed in Figure 7, which, because of the precise determination of relative normalization, specify rather well the small difference between the $\pi^+ p$ cross sections near the forward direction.

HM and Saclay use similar methods: the data points are interpolated to the same t values and the amplitudes are determined separately for each t: Saclay uses many more t values than HM. ANL and Kelly both parameterize the amplitudes as a function of t and fit the data at the measured positions. Further, Kelly parameterizes all eight quantities [Re, Im N, $F(I = 0, 1)$] while, in recognition of the unknown overall phase, ANL fixes $\mathrm{Re}\, N(I = 0) = 0$. The former seems best in principle as one should parameterize the true amplitudes and not those subject to an arbitrary rotation. However, the overall phase should still be poorly determined and the implementation in (95) must be wrong as this uncertainty was not reflected in the quoted error analysis. The difference between ANL and Kelly techniques is illustrated in Figure 11*d* for the small $\mathrm{Re}\, F(I = 0)$ amplitude. The zero at $t \approx -0.15$ (GeV c)^2 in the ANL solution was not present in their original "$\mathrm{Re}\, F(I = 0)$" but is produced by the rotation to the Barger-Phillips overall phase. Clearly the smoothness assumption implicit in the ANL Kelly method is not reliable for small amplitudes.

While we are discussing the general technique, it is worth noting that the qualitative similarity in the four analyses plotted in Figures 11 and 12 suggests that there is little point in repeating them without attempting to estimate the

[11] See also B. Wicklund, Private communication and Report at XVI International Conference on High-Energy Physics (Batavia, 1972).

possible overall phase rotation for $-t \gtrsim 0.2$ (GeV/c)^2. The latter can only be constrained through dispersion relations (or their relative FESR/CSMR), which can transmit to high energies the phase information contained in low energy unitarity. Some attempt in this direction has been made by Pietarinen (104, 105) but although his analysis technique may be impeccable, the results are not presented in a useful form. Similar sentiments have been expressed by Lovelace (106) who also has a useful review of parameterization techniques.

Concurrently with theoretical refinements, further experimental data are needed. A Monte Carlo simulation study to determine the most useful new measurements is described by Fox (107).

4B *Lessons from the πN Amplitude Analyses*

First we define the partial wave amplitudes

$$f_{n,F} = 1/(32\pi\sqrt{s}k)\int_0^\infty N, F(s,t)J_n(b\sqrt{-t})d(-t) \qquad 4.1.$$

$n = (0, 1)$ for (*N*onflip, spin*F*lip) amplitude

Here we have put k equal to the cms momentum and defined $b = l/k$ as the impact parameter discussed qualitatively at the beginning of section 2. N, F are normalized as in equation 3.2 and f is normalized so that it would be $e^{i\delta}\sin\delta$ for a

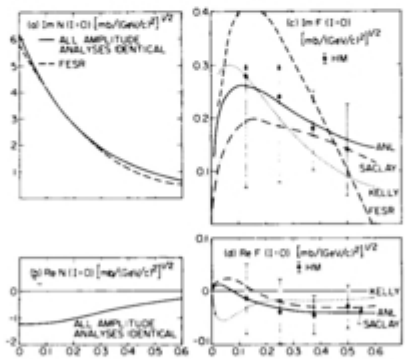

Figure 11 Results of πN amplitude analyses at 6 GeV/c for the $I = 0$ t-channel exchange. N and F refer to s-channel nonflip and spinflip amplitudes respectively (section 3A). The four analyses come from References 97 (ANL), 94 (HM), 95 (Kelly), and 96 (Saclay). The crude finite energy sum rule estimate of the imaginary parts (marked FESR) are described in section 4C. For clarity, we omit the error estimates on all except the HM analysis.

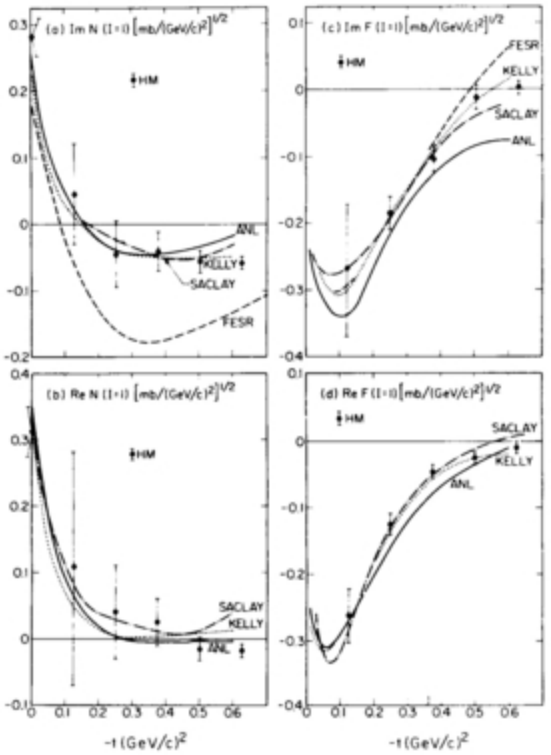

Figure 12 Results of πN amplitude analyses at 6 GeV c for $I = 1$ t-channel exchange. Designations are the same as in Figure 11.

channel of definite s-channel isospin and spin. For instance, $f_5(h = 0) = i\,2$ corresponds to complete s-wave absorption.

In Figure 14, we present the results of Kelly (95) who used equation 4.1 to partial wave decompose his amplitudes. This work has a nice treatment of errors but suffers from the disadvantage of an incorrect overall phase, which differs by $\sim 20^\circ$ from the Barger-Phillips value shown in Figures 11 and 12; so the reader should make allowance for this extra error in interpreting Figure 14. Similar partial wave analyses are presented in (108 HM solution) and (109 Barger-Phillips fit).

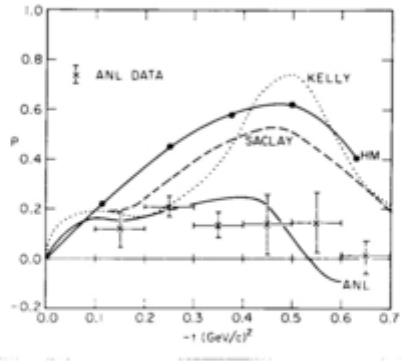

Figure 13 Comparison of the four 6-GeV/c πN amplitude analyses with the new 5-GeV/c $\pi^- p \to \pi^0 n$ polarization data from (101). The analyses are designated as in Figure 11. We do not show the CERN $\pi^+ p \to \pi^0 n$ polarization data (102) which are similar to three analyses (HM, Kelly, Saclay) based upon them.

We can make the following (by now trite) observations from our figures:

(*a*) Im $N(I = 0)$ dominates its approximate e^{2t} dependence translates into a Gaussian in Figure 14*a* concentrated at small impact parameter b.

(*b*) The reduced ratio $|F/N_{\perp} - t|$ for $I = 0$ is 0.17 ± 0.02 at 6 GeV/c and 0.14 ± 0.03 at 16 GeV/c (96), both for the t range $0.2 \lesssim -t \lesssim 0.5$ (GeV/c)^2. The corresponding ratio for t-channel amplitudes is much larger at 0.8. Correspondingly s-channel helicity conservation ($F_+ = 0$) is reasonably satisfied[12] while t-channel helicity conservation is ruled out (110, 111).

(*c*) The similar phase of N and $F(I = 0)$ indicates that Pomeron and P' have similar spin structure; in particular, the latter must also satisfy s-channel helicity conservation. The similarity between P and P' couplings was already indicated by the near-mirror symmetry of the polarization in $\pi^+ p$ elastic scattering.

(*d*) Turning to $I = 1$, we find spinflip dominance. The current analyses do not extend far enough in t to confirm it, but the spinflip amplitudes are very near the Regge predictions: Re F proportional to $\alpha_\rho^2(t)$ with a double zero at $t \approx -0.6$ (GeV/c)^2 and Im F proportional to α_ρ (compare equation 2.14).

(*e*) On the other hand, Im N quite contrary to the Regge zero at -0.6 has a zero at -0.15 (GeV/c)^2, to achieve the crossover (again, see Figure 7). Re N is also intriguing if it vanishes at all for $-t \lesssim 0.5$ (GeV/c)^2, its zero lies at larger $-t$ than the zero of Im N. In any case, its very small size for $-t \gtrsim 0.2$ (GeV/c)^2 is suggestive as an artifact of the Regge double zero at $\alpha_\rho = 0$. In the b-plane, Im f_+ and Im f_ϕ both peak at $b \approx 1$ F while the real parts are more central. This observation was part of the phenomenological basis of the dual absorption model (section 2) and we will return to it in section 4F.

[12] However, this does contradict (119), which suggested that $F_+ \to 0$ as $s \to \infty$.

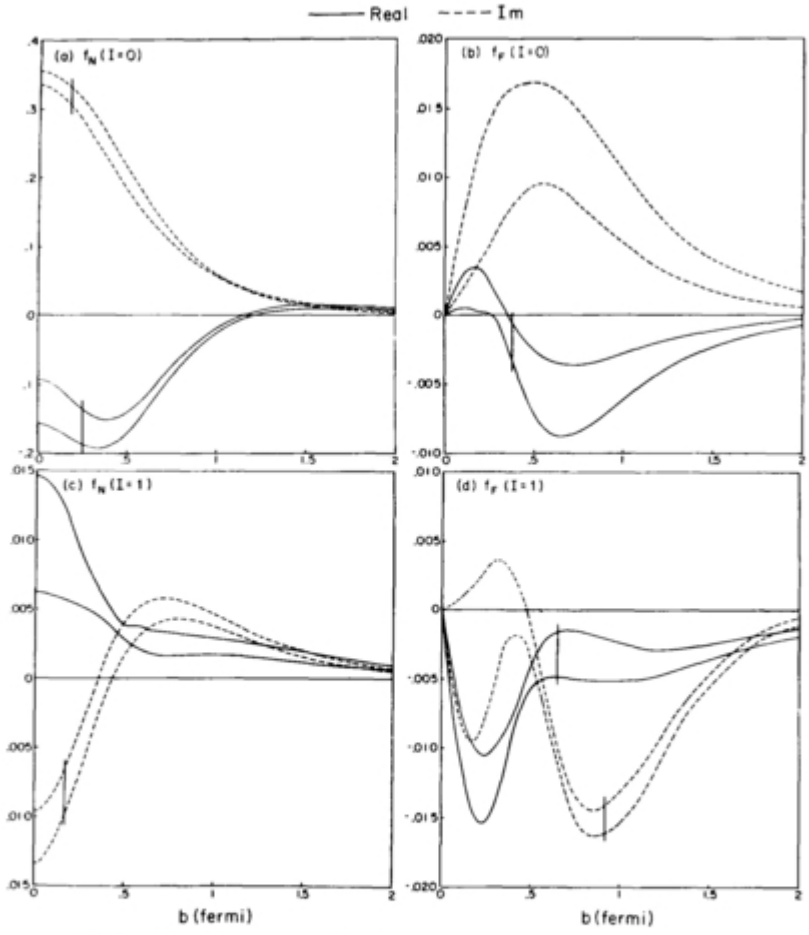

Figure 14 Partial wave (impact parameter) analysis of the πN amplitudes of Figures 11, 12 from the Keily analysis (95). The curves represent statistical error bounds. However, for impact parameters smaller than the values indicated by vertical bars, systematic uncertainty from the unknown large $-t$ behavior of the amplitudes is larger than the indicated errors.

(*f*) Both Re and Im $N(I=1)$ have a rapid variation away from $t=0$ which is confirmed by dispersion relations (112, 113). In the b-plane, this corresponds (10, 11, 108) to a tail at large impact parameter which can be calculated quite rigorously from 2π exchange (114, 115).

4C *Finite Energy and Continuous Moment Sum Rules*

If we assume Regge asymptotic behavior at fixed t

$$\text{Im}\, T \sim \sum_{i=1}^{m} r_i \nu^{\alpha_i(0)} \qquad 4.2.$$

where $\nu = (s-u)/2$, then analyticity implies the finite energy sum rule (FESR) (43)

$$\int_0^{\nu_c} d\nu\, \nu^n\, \text{Im}\, T = \sum_{i=1}^{m} r_i (\nu_c^{\alpha_i+n+1}/\alpha_i+n+1) \qquad 4.3.$$

In equation 4.3, n is any even (odd) integer for an invariant amplitude T that is odd (even) under crossing $\nu \to -\nu$. Choosing ν_c so that the left-hand side of equation 4.3 can be evaluated from low energy phase shifts, the right-hand side gives useful constraints on the residues r_i of the Regge poles assumed to dominate the high energy amplitude. Typical of the qualitative utility of finite energy sum rules are the curves marked FESR in Figures 11 and 12. These come from evaluating equation 4.3 using the old CERN phase shift solution[13] (116) up to $s = 4.8\ (\text{GeV/c})^2$ and $\alpha(I=0) = 0.8$, $\alpha(I=1) = 0.58 + t$. This gives one an effective r_i for each amplitude which can be used in equation 4.2 to estimate Im T at 6 GeV/c. It is clear from the figures that the FESR curves, and hence low energy data plus analyticity, have predicted all the qualitative features of the 6-GeV/c amplitudes. FESRs have the great advantage that they directly predict individual amplitudes but the disadvantage that they can never be exact, as the Regge asymptotic expansion will always be an approximation at 2 GeV/c.

Similar constraints on the real part, and indeed on arbitrary mixtures of real and imaginary parts, may be found by replacing Im T by Im $\{(\nu^2-\nu_0^2)^\epsilon T\}$ in equations 4.2 and 4.3 (any real ν_0, ϵ). The resultant relations are called continuous moment sum rules (CMSRs).

As we have already mentioned, Barger & Phillips (98) fitted all available πN high energy data in a Regge pole model constrained by FESRs and CMSRs. Although some of their poles (P'', ρ') are frankly phenomenological and surely no true asymptotic property of the πN amplitudes, the success of their fit is very striking. (It essentially *predicted* the amplitudes shown in Figures 11 and 12.) Their model has enjoyed much greater longevity and utility than many fits which, at the time, seemed to have greater theoretical motivation. Still the fact that their success was a triumph more for analyticity than for Regge poles does mean that it is only useful for interpolating and interpreting medium energy ($P_{\text{lab}} \lesssim 10$ GeV/c) data; deviations are inevitable and present at higher energies (120).

[13] The errors—especially in the small amplitude with many cancellations Im $N(I=1)$—are quite large. FESR calculations using more recent analyses (117, 118) were not available.

Finite energy sum rules have also proved useful in photoproduction (121–123) and KN scattering (124), but the low energy phase shifts (and hence data) must be improved before the results are uniformly convincing.

4D Duality

In deriving equation 4.3, one only assumes the Regge approximation 4.2 as an average from $\nu = \nu_c$ to ∞. There are some more speculative uses of low energy data to deduce results on the high energy amplitude, which essentially assume that equation 4.2 is valid at $\nu = \nu_c$, and so one is allowed to equate high and low energy amplitudes. As ν_c is lowered, one must average the low energy data over a few hundred MeV (a typical resonance width) to avoid local resonance oscillations. This is usually justified by the totally abused word "duality" or the fine sounding "semi-local duality." It should be stressed that these deductions are even less quantitative than FESRs; and, in particular, they are often wrong (125) in the Veneziano model which is the basis of the current theoretical formulation of duality. Nevertheless, such duality analyses are useful because they allow much more explicit deductions than FESRs. To believe them, one must at least ask that a given deduction be both independent of ν_c and insensitive to the trivial ambiguities of the extrapolation of high energy asymptotic expansions to low values of s.

Typical of a reasonable use of duality is the identification (126, 127) of the resonance contribution to low energy scattering with the Regge (P', ω, ρ, A_2,...) "pole" contribution and the remaining background with the Pomeron term. This was, for instance, used by Harari & Zarmi (128) to discuss helicity conservation and deduce results in qualitative agreement with those found in section 4C from the high energy amplitude analyses. Fukugita & Inami (129) have tried to use this idea to discuss the partial wave structure of Im $N(P')$. We know (sections 2 and 4B) that there is solid evidence that Im $N(\omega, \rho)$ has a peak at impact parameter $b \simeq 1$ fm. EXD would predict a similar feature for Im $N(P', A_2)$, but it turns out there is no direct evidence for this (see section 4F). However, plots of the partial wave amplitudes (Figure 15*a*) for KN and Figure 16 for πN) do show a peak at $b \approx 1$ fm for the direct channel resonance component: "duality" then implies such a peak for Im $N(P')$. This is not conclusive, for at small impact parameter it is difficult to tell (broad) resonances from background and the Pomeron part (identified with the background) may be concealing a relatively large P' contribution at low b. We can test whether P' and ρ have the same impact parameter structure by asking if

$$\begin{aligned}&\left[\text{Im } f_\nu(P' : b = 1 \text{ fm})/\text{Im } f_\nu(\rho : b = 1 \text{ fm})\right]\\ &\quad = \left[\text{Im } N(P' : t = 0)/\text{Im } N(\rho : t = 0)\right] \qquad 4.4.\end{aligned}$$

The right-hand side of this is well determined by total cross-section data; the left-hand side is consistent with equation 4.4, but data fluctuations make it impossible to be quantitative.[14] Better is to use equation 4.4 with ρ replaced by ω so the right-hand side is 1. Then if Im $f_\nu(P') <$ Im $f_\nu(\omega)$ at $b = 1$ fm (as we shall later

[14] M. L. Griss, Private communication (1973).

suggest), the decomposition $\bar{K}N(I_t = 0) = P + P' + \omega$, $KN(I_t = 0) = P + P' - \omega$ would suggest a depression of the KN partial wave amplitude at $b \gtrsim 1$ fm. The relevant data are shown in Figures 15*b–d*. There is no real evidence for the suggested suppression and the small size of both the KN and $\bar{K}N$ background

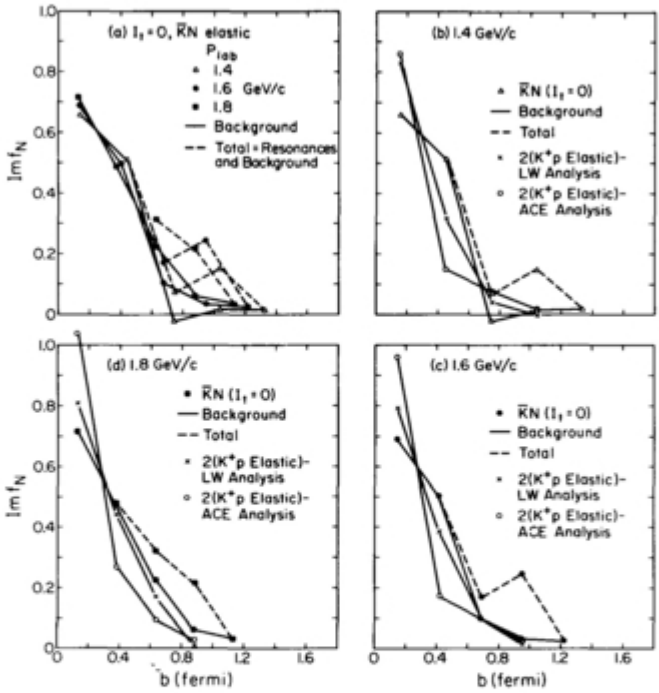

Figure 15 Partial wave structure of KN and $\bar{K}N$ scattering. (*a*) Background and resonance contributions to $\bar{K}N(I_t = 0)$ partial wave amplitude Im f_N—normalized as in equation 4.1—at various lab momenta. The figure is adapted from (129) and the data are from (301). The $I_t = 0$ isospin amplitude is normalized so that halving it gives its contribution to say $K^- p \to K^- p$. (*b*)–(*d*) Comparison of the same $\bar{K}N$ amplitude as in (*a*) with twice $K^+ p$ amplitude from (302) (marked LW, plotted is solution IA) and (303) (marked ACE). $K^+ n$ data are not available so we were forced to use $2(K^+ p)$ to estimate $I_t = 0$ for KN scattering.

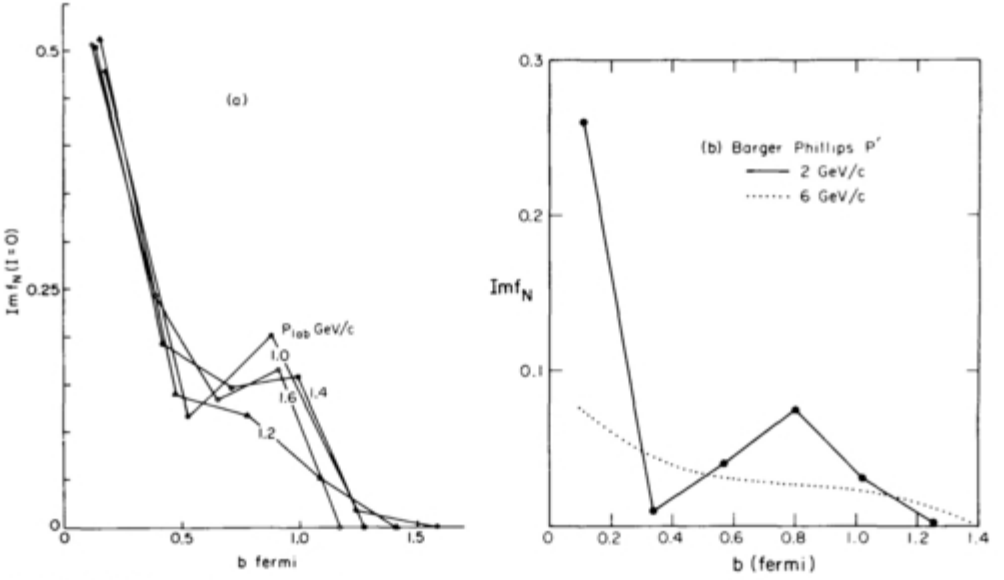

Figure 16 (*a*) Plot [adapted from (129)] of the partial wave decomposition normalized as in equation 4.1 for Im $N(I = 0)$ in πN scattering at various lab momenta. The data come from (304). The curves unlike those in Figure 15 are not separated into resonance and background terms. Had they been, the peak at $b \approx 0.8$ fm would be found to correspond to resonance contributions. (*b*) Partial wave analysis at 2 and 6 GeV/c (P. R. Stevens, Private communication) for the P' contribution to Barger and Phillips Regge pole fit to πN data (98).

amplitudes at $b \approx 1$ fm give equality there of $\mathrm{Im}\, f_V(P')$ and $\mathrm{Im}\, f_V(\omega)$ to within 20%.

One must use duality to make such arguments because the small size of the P' and ω at higher energies washes out the pronounced 1-fm peak. Furthermore, there is the difficulty that we are not seeing a true asymptotic effect at $1 \to 2$ GeV/c and the partial wave structure changes with energy. This is illustrated by the Barger-Phillips πN fit where the P' has a peak at $b \approx 1$ fm at 2 GeV/c but this disappears at 6 GeV/c (Figure 16*b*).

4E *Amplitude Analyses of Hypercharge Exchange Reactions*

Consider the reactions $\pi N \to K(\Lambda, \Sigma)$, $\bar{K}N \to \pi(\Lambda, \Sigma)$ where for definiteness we shall usually choose the hyperon to be Λ.[15] $\pi^- p \to K^0\Lambda$ and $K^- n \to \pi^-\Lambda$ can be described in terms of amplitudes of definite symmetry under crossing as

$$\begin{aligned} H(\pi^- p \to K^0\Lambda) &= H_T + H_V \\ H(K^- n \to \pi^-\Lambda) &= H_T - H_V \end{aligned} \qquad 4.5.$$

where in the simple Regge pole approximation H_V corresponds to K^* and H_T to K^{**} exchange. Invoking SU(3) and EXD, one can easily prove (130–135) that $\mathrm{Im}\, H_T = \mathrm{Im}\, H_V$ and so $H(K^- n \to \pi^-\Lambda)$ is purely real. In fact, $\pi^- p \to K^0\Lambda$ and $K^- n \to \pi^-\Lambda$ should have (*a*) equal cross sections and (*b*) zero polarization if EXD were true and (*c*) equal but opposite values of $P\, d\sigma/dt$ if described by two Regge pole K^* and K^{**} exchange. Predictions (*a*), (*b*), and (*c*) are all false for $P_{\mathrm{lab}} \lesssim 5$ GeV/c while at higher energies we can only say with conviction that (*b*) remains false. (Polarization in $\pi^+ p \to K^+\Sigma^+$ is energy independent (136) and nonzero up to 14 GeV/c.) These deviations from simple Regge theory are not unexpected; it is a simple consequence of SU(3) which is confirmed by the data that these reactions have a large nonflip amplitude, and Figure 12 showed that Regge theory failed for such an amplitude.

Now our two reactions are determined by eight quantities Re, $\mathrm{Im}\, N$, $F_{V,T}$ of which six are in principle determinable (each reaction has an unobservable overall phase). At the present time, only four observables have been measured, namely the polarization P and $d\sigma/dt$ for each reaction. Any amplitude analysis must therefore make additional assumptions. Now the results[16] of three analyses (132, 134, 135) are shown in Figure 17. There is not only little resemblance between the amplitudes from different analyses but even worse; each analysis predicts a large difference between $\mathrm{Im}\, N_V$ and $\mathrm{Im}\, N_T$ at $t = 0$. This is surprising because the flat total cross sections for $K^+ n$ and $K^+ p$ show that $\mathrm{Im}\, N_V = \mathrm{Im}\, N_T$ for both $V = \omega$, $T = P'$, and the pair $V = \rho$, $T = A_2$ exchange. The error in this assertion may be made quantitative by comparing at 5 GeV/c, the difference between $K^+ p$ and $K^- p$ total cross sections (measures $P' + \omega + A_2 + \rho$) to that between $K^+ p$ and its "flat" Pomeron value at 20 GeV/c (measures $P' - \omega + A_2 - \rho$). This procedure indicates at most a 10% breaking of exchange degeneracy.

[15] The Σ data are superior but FESR analysis has only been applied to the Λ reactions.

[16] We actually replotted the results of (132) to correspond to a conventional K^*, K^{**} Regge trajectory $\alpha(t) = 0.32 + 0.82t$.

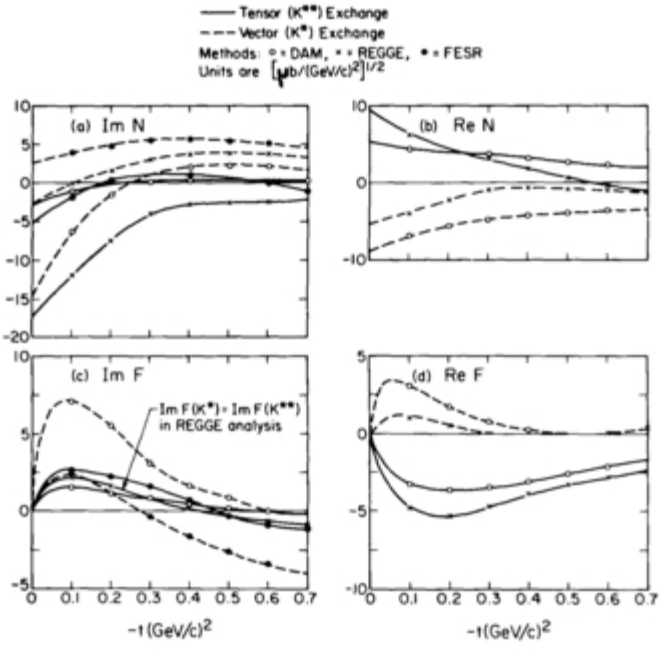

Figure 17 Results of amplitude analyses of $\pi^- p \to K^0\Lambda$ and $K^- n \to \pi^- \Lambda$ at 4 GeV c. The curves marked DAM, REGGE, and FESR come from (135, 134, 132, respectively). For the latter, we only take the imaginary part predictions. The amplitudes are split up into Vector (V) and Tensor (T) contributions in accordance with equation 4.5.

Further, using the quark model suggestion (34) that ϕ and f' exchange decouple (justified by the small cross sections for $\pi^- p \to \phi n, f'n$), we establish that V and T exchange have the same F D value at the $N\bar{N}$ vertex. Then it is an immediate consequence of SU(3) that $\mathrm{Im}\, N_V = \mathrm{Im}\, N_T$ at $t = 0$ in our reactions and deviations should only be typical SU(3) breaking say 20% not the factor of five differences in Figure 17. This argument is strengthened by the fact that one gets a similar F/D ratio from the ratio of Λ to Σ reactions (131, 133–135) as one does from the above σ_{tot} argument. It is thus important to see whether one can find a set of amplitudes satisfying the constraint $\mathrm{Im}\, N_V \approx \mathrm{Im}\, N_T$ at $t = 0$. Here we merely detail the assumptions in the current work and indicate where they may be unreliable.

(*a*) The curves marked DAM (dual absorption model) in Figure 17 come from

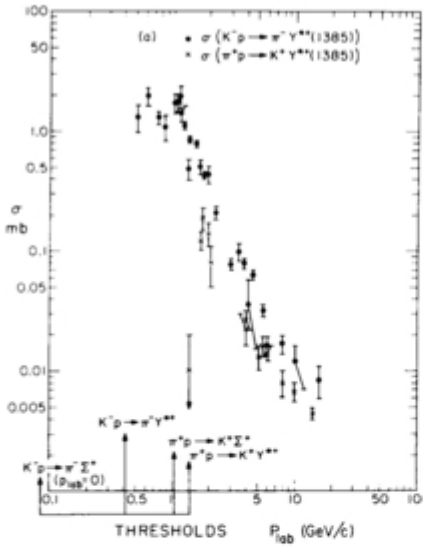

Figure 18 (*a*) Comparison of reaction cross sections for $K^- p \to \pi^- Y^{*+}(1385)$ and $\pi^+ p \to K^+ Y^{*+}(1385)$. The data were taken from (272, 297, 305, 306).

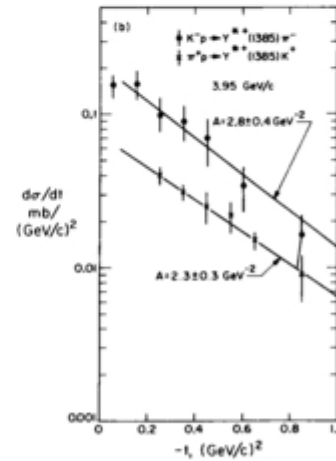

(*b*) Comparison (272) of differential cross section vs t for our two reactions at the same energy.

assuming that "imaginary parts are peripheral" while real parts are parameterized rather generally (135). In practice, this means $\mathrm{Im}\,N_1$, $\mathrm{Im}\,N_2$ and $\mathrm{Im}\,F_1$, $\mathrm{Im}\,F_2$ vanish together. Perhaps the bad results ($N_1 \approx 6N_2$) could be overcome by just a small relaxation in this basic assumption. On the other hand, we will discuss in section 4F some evidence that the dual absorption model idea may itself be badly violated.

(*b*) The curves marked REGGE come from the assumption that the spinflip amplitudes are in perfect agreement with Regge theory (134). This is motivated by the nice agreement illustrated in Figure 12*c*, *d* of the ρ, A_2 spinflip amplitudes with Regge theory. However, it then predicts equal cross sections for spinflip K^*, K^{**} exchange processes a suggestion violated by a factor of 2 by $\pi^- p \to K^- Y^{*++}_{1385}$ and $K^- p \to \pi^- Y^{*+}_{1385}$ at intermediate energies (137). This is demonstrated in Figure 18 which also marks the reaction thresholds. Naively one can interpret the suppression of $K^- Y^{*++}$ compared with $\pi^- Y^{*+}$ as a consequence of the higher threshold for the former reaction. This may be true, but one would get exactly the same threshold suppression of $K^- \Sigma^+$ vs $\pi^- \Sigma^+$ and can only deem 4 GeV/*c* too low an energy for asymptotic Regge assumptions.

Analyses using the above assumption have been presented in both (134) and (71).

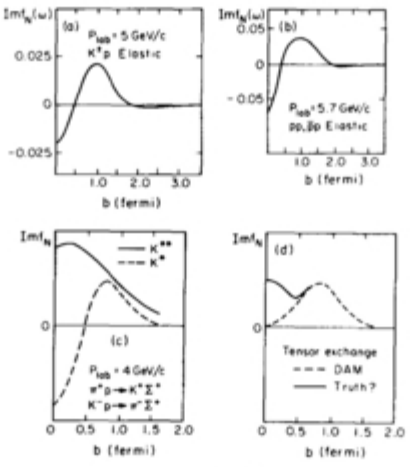

Figure 19 Some partial wave profiles for Im N (imaginary part of nonflip amplitude). (*a*), (*b*) ω exchange from (139). (*c*) K^*, K^{**} exchange from (71). (*d*) Two possible tensor (P', A_2, K^{**}) profiles. That marked DAM is postulated by the dual absorptive model (31); that marked "truth" is suggested by the evidence discussed in section 4F. (*a*), (*b*) are normalized as in equation 4.1; (*c*), (*d*) are unnormalized.

For clarity, we only give curves from the former, although to play no favorites, in Figure 19 we take the partial wave analysis from (71).

(c) The curves marked FESR come from finite energy sum rule calculations of the type described in the last subsection (132). The good qualitative results in πN scattering suggest that the difficulties with this analysis are due to the poor quality of the low energy data on hypercharge exchange.

4F *Is Tensor Exchange Peripheral?*

It is well established that the imaginary parts of vector exchange amplitudes are "peripheral"; in the b-plane this corresponds to a large partial wave amplitude near $b = 1$ fm, and in the t-plane to a zero in Im N near $t = -0.2$ (GeV/c)^2. This was illustrated in Figures 12a and 14c for ρ exchange while for ω exchange it follows from the crossovers in $K^{\pm}p$ and in $^1\bar{p}^1p$ scattering (see Figure 7). The latter allow estimation of Im $N(\omega)$ by (138, 139)[17]

$$\begin{aligned} \text{Im } N(\omega) &= \left[\mathrm{d}\sigma/\mathrm{d}t(K^- p) - \mathrm{d}\sigma/\mathrm{d}t(K^+ p)\right]/4\sqrt{\mathrm{d}\sigma/\mathrm{d}t(K^+ p)} \\ \text{or} \quad &= \left[\mathrm{d}\sigma/\mathrm{d}t(\bar{p}p) - \mathrm{d}\sigma/\mathrm{d}t(pp)\right]/4\sqrt{\mathrm{d}\sigma/\mathrm{d}t(pp)} \end{aligned} \qquad 4.6.$$

Expression 4.6 was partial wave analyzed in (139) and typical results[18] are shown in Figure 19a, b. In both KN and NN scattering ω exchange has the characteristic peak at 1 fm; note, however, that these figures and Figure 14c all show a significant negative peak at $b = 0$.

Now EXD would suggest that tensor exchange (P', A_2, K^{**}) has a similar partial wave profile, and this is indeed postulated in the dual absorption model. Nevertheless, there is no direct evidence for it and several papers have claimed that tensor exchange is nonperipheral (32, 33, 60). Let us discuss the pros and cons here.

(a) Typical of a "nonperipheral" tensor exchange is the solid line in Figure 19c. Note that the partial wave amplitude is still big at $b = 1$ fm; there is, however, a positive contribution at $b = 0$ and translated into the t-plane this moves the magic -0.2 zero out to ≈ -0.6 (GeV/c)^2. On the other hand, the dotted line in Figure 19c, or in fact all our examples of vector exchange, has a negative contribution at small b which is destructive in the t-plane and moves the -0.2 zero in. The latter still looks "peripheral" in the t-plane even though its partial wave amplitude at $b = 0$ is no smaller in magnitude than the so-called "nonperipheral" tensor exchange. So the first point to emphasize is that by a uniform terminology, both vector and tensor exchanges appear nonperipheral in Figures 14c and 19. For vector exchange, the negative excursion at small b has been seen in essentially all analyses;[19] but one must admit it is sensitive to the large t behavior of the amplitude, and a common bias in the treatment of this could have produced a universally

[17] To be precise, this is really $\omega + \rho$, but the latter is only a 25% contaminant.

[18] Actually (139) uses $\frac{1}{2}[\mathrm{d}\sigma/\mathrm{d}t(K^+ p) + \mathrm{d}\sigma/\mathrm{d}t(K^- p)]$ rather than $\mathrm{d}\sigma/\mathrm{d}t(K^+ p)$ in denominator of equation 4.6. We will not debate the correct choice here.

[19] See (139) or Figure 9 of (16) for similar effects in $\bar{N}N$ scattering.

false conclusion. For tensor exchange, we will discuss whether the amplitude is positive at small b and the t-zero moved out; we follow convention and use the abused term "nonperipheral" for this situation.

(*b*) The study of P' exchange in πN, KN, and NN elastic scattering is complicated by the ubiquity of the Pomeron. As we showed in section 4D, low energy data suggest unlike Figure 19*c* but consistent with either curve in 19*d* a *peak* in the P' partial wave spectrum at $b \gtrsim 1$ fm. However, these duality arguments can never be precise. For instance, the possible central component under discussion (i.e. the area between the dotted and solid curves in Figure 19*d*) will only contribute some 20% of the amplitude at $t = 0$. So even the best verified consequence of duality the equality of the 1-fm peaks in P' and ω amplitude to within 20% cannot settle the argument.

We should also note that the P' residue found by Harari & Zarmi (128) from resonance dominance of FESR was "nonperipheral."

(*c*) One can try to distinguish P' and Pomeron on the basis of their different energy dependence in $\pi^- p$ elastic scattering. If one assumes a flat Pomeron, the P' has no zero near $t = 0$; if one assumes a Pomeron with slope $\gtrsim 0.7$, the P' has the peripheral -0.2 (GeV c)^2 zero. This was pointed out many years ago (125, 140), forgotten (141), and then rediscovered (32, 142). Anyhow, the first assumption is suggested by $\gamma p \to \phi p$, the second by *some* models[20] of pp and $K^+ p$ scattering. A choice is impossible at present.

(*d*) If one assumes a $t = -0.2$ (GeV c)^2 zero in Im $N(4_2)$ and a central Re $N(4_2)$ [i.e. Re N either has no zero or the zero occurs at $-t > 0.2$ (GeV c)^2], then negative polarization is predicted (16) in $\pi^- p \to \eta^0 n$ at $t \simeq -0.2$ (GeV c)^2. The data are meager (102, 144, 145) but they suggest positive polarization. Although there seems no compelling reason for the second assumption, better polarization data for $\pi^- p \to \eta^0 n$, $K^- p \to \bar{K}^0 n$ and $K^+ n \to K^0 p$ would be very helpful in pinning down the elusive tensor exchange.

(*e*) Modified absorption models (33, 60), using a large negative real to imaginary ratio in the absorbing amplitude, successfully fitted the ρ exchange amplitudes in Figure 12. They automatically predict less absorption for tensor exchange and produce partial wave profiles similar to the solid lines in Figure 19*c*, *d*.

(*f*) The amplitude analyses (71, 134) of hypercharge exchange reactions using a pure Regge spinflip amplitude produce a "nonperipheral" K^{**} exchange (see Figures 17*a* and 19*c*). Although we have expressed grave doubts about their validity, it appears that this particular conclusion is not sensitive to deficiencies in the analysis. The essential point is that the data show large (up to factors of 2) violations of line reversal symmetry with the "real" reaction ($K^- n \to \pi^- \Lambda$, $K^- p \to \pi^- \Sigma^+$) being larger than the "moving phase" reaction ($\pi^- p \to K^0 \Lambda$, $\pi^+ p \to K^+ \Sigma^+$) for $-t \lesssim 0.4$ (GeV c)^2 (see Figure 20E1). In this region the spinflip amplitude is too small to explain the breaking. The flip amplitude can be estimated from isospin bounds (134), SU(3), and KN charge exchange (71) or the quark model

[20] The good fits of (143) found a Pomeron of low slope (0.3) could describe pp scattering up to ISR energies.

and $\pi N \to KY^*$, $\bar{K}N \to \pi Y^*$. So, simply consider a nonflip amplitude and write its real and imaginary parts for vector and tensor as Re, Im V, T respectively. Then, taking Σ reactions, we can write

$$\begin{aligned} d\sigma/dt(K^- p \to \pi^- \Sigma^+) &= \text{"Real"} = (\text{Re}\, T + \text{Re}\, V)^2 + (\text{Im}\, T - \text{Im}\, V)^2 \\ d\sigma\ dt(\pi^+ p \to K^+ \Sigma^+) &= \text{"Moving"} = (\text{Re}\, T - \text{Re}\, V)^2 + (\text{Im}\, T + \text{Im}\, V)^2 \end{aligned} \qquad 4.7.$$

where we have chosen signs *unconventionally* so that all four amplitudes are positive at $t = 0$. Then it is easy to see that for *any* given ordering of zeros for the four amplitudes, we can predict the ratio of the two reactions at the zeros. Writing $x < y$ to denote that amplitude x vanishes before y, we force $\text{Im}\, V < \text{Re}\, V$ from πN amplitude analysis and $\text{Im}\, V < \text{Im}\, T$ from the sign of $K^- p \to \pi^- \Sigma^+$ polarization. (This is almost certainly implied by the negative excursion in vector amplitudes at $b = 0$.) Then there are eight possible zero orderings summarized in Table 3. Only two of these (Nos. 2, 8) predict $K^- p \to \pi^- \Sigma^+$ (real reaction) to be larger than $\pi^+ p \to K^+ \Sigma^+$ (moving) at all zeros and these are the "nonperipheral" $\text{Im}\, T$ model of the effective absorption approach (33, 60). Options 1, 3, 5, and 6 have a possibly peripheral $\text{Im}\, T$ but option 3 is ruled out at once by line reversal systematics; the remainder all predict the moving reaction to be come larger than the real at the third zero. For sensible zero positions, this is marginally consistent with the data while for 1, the line reversal data definitely imply a nonperipheral $\text{Im}\, T$: $\pi^+ p \to K^+ \Sigma^+$ favors 5 over 6 but, in fact, both of these predict the apparently wrong sign for the $\pi N \to \eta N$ polarization. Thus there is no satisfactory solution with a peripheral tensor exchange and current data clearly favor a nonperipheral $\text{Im}\, N(K^{**})$. Better data at higher energies are of obvious importance to test the hypothesis that the line reversal breaking is an asymptotic effect.

We have summarized a lot of rather questionable information. It appears to us that

Table 3 Possible zero orderings for real and imaginary parts of vector V and tensor T nonflip amplitudes

		Larger Reaction R = Real, M = Moving				Is Tensor Exchange Peripheral?
		Zero No.				
	Zero Ordering	1	2	3	4	
1	$\text{Im}\, V < \text{Re}\, T < \text{Im}\, T < \text{Re}\, V$	R	R	M	M	Maybe
2	$\text{Im}\, V < \text{Re}\, T < \text{Re}\, V < \text{Im}\, T$	R	R	R	R	No
3	$\text{Re}\, T < \text{Im}\, V < \text{Im}\, T < \text{Re}\, V$	M	M	M	M	Maybe
4	$\text{Re}\, T < \text{Im}\, V < \text{Re}\, V < \text{Im}\, T$	M	M	R	R	No
5	$\text{Im}\, V < \text{Im}\, T < \text{Re}\, T < \text{Re}\, V$	R	R	M	M	Maybe
6	$\text{Im}\, V < \text{Im}\, T < \text{Re}\, V < \text{Re}\, T$	R	R	M	M	Maybe
7	$\text{Im}\, V < \text{Re}\, V < \text{Im}\, T < \text{Re}\, T$	R	R	M	M	No
8	$\text{Im}\, V < \text{Re}\, V < \text{Re}\, T < \text{Im}\, T$	R	R	R	R	No

a nonperipheral Im N is suggested for both vector and tensor exchange. These amplitudes appear to have opposite signs at small impact parameters so as to cancel in moving phase reactions this is the content of the weak SCAP hypothesis of Chiu (71).

5 REACTIONLAND

Here we briefly document some of the important theoretical and phenomenological features that have been discovered in *meson* exchange processes. We stress particularly characteristics that appear to be common to several different reactions. We do not cover backward scattering because our current theoretical and experimental knowledge is too fragmentary to make such a compilation of ideas useful. The reactions discussed in sections 5A 5M are listed with illustrative pictures in Figures 20A–20M respectively. The latter are organized by exchanged quantum numbers, labeled A1 to M5, and list possible exchanges in ρ, A_2, π, and B nonets. For clarity, we omit possible exchanges of the A_1 nonet and its EXD partners; the evidence for the presence of these exchanges is detailed in section 5L(*iii*). Further we only record Pomeron exchange when it obeys vacuum selection rules including the so-called Gribov-Morrison rule (146) which says the value of τP, signature × parity, is unchanged by diffraction. The experiment evidence against this is discussed in section 5I(*ii*). In section 6, we bring together some of the theoretical points raised in the following subsections.

Although all the reactions listed in Figure 20 have been measured somewhere, sometime, it is obviously impractical to give the original references here. The reader is referred to the many review articles and compilations some of which we have cited.

5A *Elastic Reactions*

(*i*) Total cross sections for reactions A1–5 measure Im $N(s,0)$: the imaginary part of the nonflip amplitude at $t = 0$ (cf. equation 3.3).

(*a*) All can be fitted from $p_{\text{Lab}} = 5$ to 30 GeV c as $\sigma_{\text{tot}} = a + bs^{-\frac{1}{2}}$ (see Figures 20A1, A2) where a is Pomeron and b is secondary (P', ω, ρ, A_2) Regge trajectory exchange (120). The value of a shows the Pomeron is an SU(3) singlet with around $20\%_{\text{oct}}$ octet admixture. The measurement of b for reactions A1, A2 allows extraction of the D/F ratio for $B\bar{B}$ coupling of V and T mesons. This turns out to be $D/F \simeq -0.2$ (Figure 21*a*) in reasonable agreement with the quark model prediction $D/F = 0$ (147–149). In Figure 21*a*, we calculate D/F from comparison of ρ and ω exchanges by the formula

$$D/F = 1 - 2[\sigma_{\text{tot}}(K^- n) - \sigma_{\text{tot}}(K^+ n)] / [\sigma_{\text{tot}}(K^- p) - \sigma_{\text{tot}}(K^+ p)] \qquad 5.1.$$

One can also test the validity of SU(3) by comparing ρ exchange contributions to KN and πN; the ratio R should be 1 if SU(3) is exact where

$$R = \frac{[\sigma_{\text{tot}}(K^- p) - \sigma_{\text{tot}}(K^+ p) - \sigma_{\text{tot}}(K^- n) + \sigma_{\text{tot}}(K^+ n)]}{[\sigma_{\text{tot}}(\pi^- p) - \sigma_{\text{tot}}(\pi^+ p)]} \qquad 5.2.$$

	Reaction	Exchanges
A1	$\pi^+p \to \pi^+p$ $\pi^-n \to \pi^-n$ $\pi^-p \to \pi^-p$ $\pi^+n \to \pi^+n$	$\mathbb{P}$, ρ', ρ
A2	$K^+p \to K^+p$ $K^+n \to K^+n$ $K^-p \to K^-p$ $K^-n \to K^-n$	$\mathbb{P}$, P',ω, A_2, ρ
A3	$pp \to pp$ $pn \to pn$ $nn \to nn$ $\bar{p}p \to \bar{p}p$ $\bar{p}n \to \bar{p}n$	$\mathbb{P}$, P',ω A_2, ρ π, B η, h
A4	$\bar{\Lambda}p \to \bar{\Lambda}p$ $\bar{\Lambda}n \to \bar{\Lambda}n$ $\bar{\Lambda}p \to \bar{\Lambda}p$ $\bar{\Lambda}n \to \bar{\Lambda}n$ $\Sigma^+p \to \Sigma^+p$ $\Sigma^-p \to \Sigma^-p$ $\Sigma^-n \to \Sigma^-n$	$\mathbb{P}$, P',ω A_2,ρ π,B η,h
A5	$\gamma p \to \gamma p [\sigma_{tot}(\gamma p)]$ $\gamma n \to \gamma n [\sigma_{tot}(\gamma n)]$	$\mathbb{P}$ P',A_2 π,η

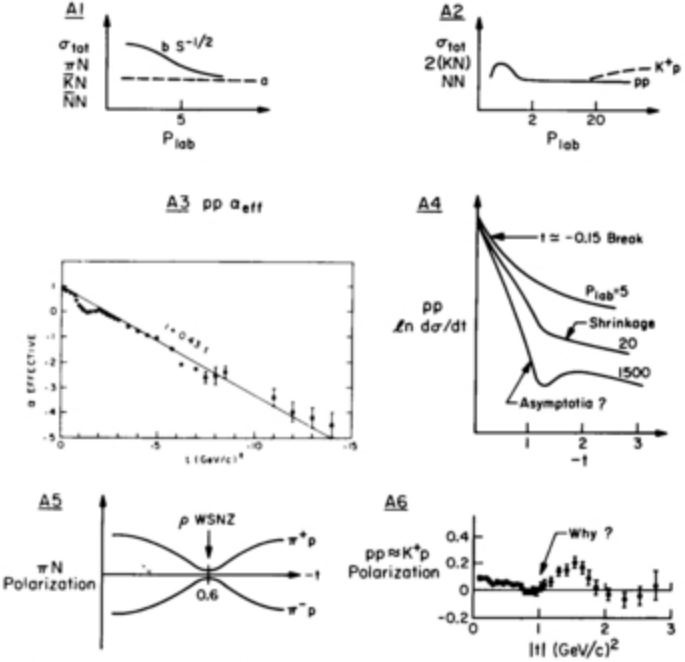

Figure 20A Elastic reactions: (*A1, A2*) Sketch of total cross sections. (*A3*) $\alpha_{eff}(t)$ for pp elastic scattering for $8 < P_{lab} < 30$ GeV/c (162). (*A4*) Sketch of pp differential cross sections. (*A5*) Sketch of $\pi^- p$ elastic polarizations. (*A6*) pp polarization (176).

The data in Figure 21*b* are not very conclusive either way; it would be nice to improve them.

The experimentally observed value $h \approx 0$ for K^+p and pp implies EXD for P', ω and ρ, A_2. The error in this is at most 10% (section 4E) in KN but is as high as 25% in NN scattering (120).

(*b*) The comparison of reactions A5 with A1 and A2 successfully checks vector dominance plus quark model ideas of the similarity of $(\rho, \omega, \phi)N$ scattering to πN scattering (150).

(*c*) The comparison of reactions A3 with A1 and A2 (120, 148, 149, 151) checks to 20% the quark prediction $a(NN) = 3\ 2a(\pi N)$ (Figure 21*d*); further the comparison checks ω universality ($\omega \to NN = 3\ (\omega \to K\bar{K})$ amazingly well[21] (Figure 21*c*). ρ universality ($\rho \to NN = \rho \to K\bar{K}$) is not as easy to check due to poor neutron data. (Anyhow it is implied by ω universality plus $D\ F = 0$.)

(*d*) Reactions A4 [latest data (152–154); theory (155)] allow a test of singlet Pomeron plus SU(3) and factorization for secondary trajectories. ($D\ F \approx -0.2$ plus data on A3 reactions implies A4.)

(*e*) The rise in the K^+p total cross section (156) at Serpukhov energies (above 20 GeV/c) and the contrast with the otherwise similar pp total cross section, which does not rise (if at all) until ISR energies (156a), is not understood.

(*f*) Also the difference between the π^-p and π^+p total cross sections (pure ρ exchange) falls surprisingly slowly with energy (151). It violates (157) unsubtracted dispersion relations when compared to the Serpukhov (158) $\pi^-p \to \pi^0 n$ data (reactions D1).

(*ii*) Coulomb interference measurements give Re $N(s, 0)$ and allow tests of dispersion relations and Regge phase. [See, for instance, (159) for πp, (160) for pp.] The former are particularly impressive in a recent Compton scattering ($\gamma p \to \gamma p$) measurement (161). Here interference with the known Bethe-Heitler amplitude in principle allows measurement of the real part away from $t = 0$.

(*iii*) Striking features of the elastic differential cross sections are (12):

(*a*) pp, K^+p $d\sigma/dt$ shrink up to 30 GeV/c. As EXD says secondary trajectories should be real and not interfere with Pomeron, these should be our best glimpse of the pure Pomeron. The effective slope, found for the Pomeron this way (Figure 20A3) varies between 0.5 and 1 depending on reaction and energy range used (32, 162).

(*b*) pp elastic $d\sigma$ dt develops a break at p_{Lab} of 20 GeV c for $t \approx -1.2$ (GeV c)^2. This break becomes a dip at ISR energies.[22] The shrinkage, mentioned in (*a*), definitely slows down and may have essentially stopped for smaller [e.g. $-t \lesssim 2$ (GeV/c)^2] momentum transfer (Figure 20A4). This behavior implies that the *effective* Pomeron slope mentioned in (*a*) gets smaller, the higher the energy of the data; it follows that values calculated from $p_{Lab} \lesssim 30$ GeV c are of little fundamental significance.

[21] A check of universality at nonzero t-values is contained in (139).

[22] Rumor which will be fact by the time this paper is published.

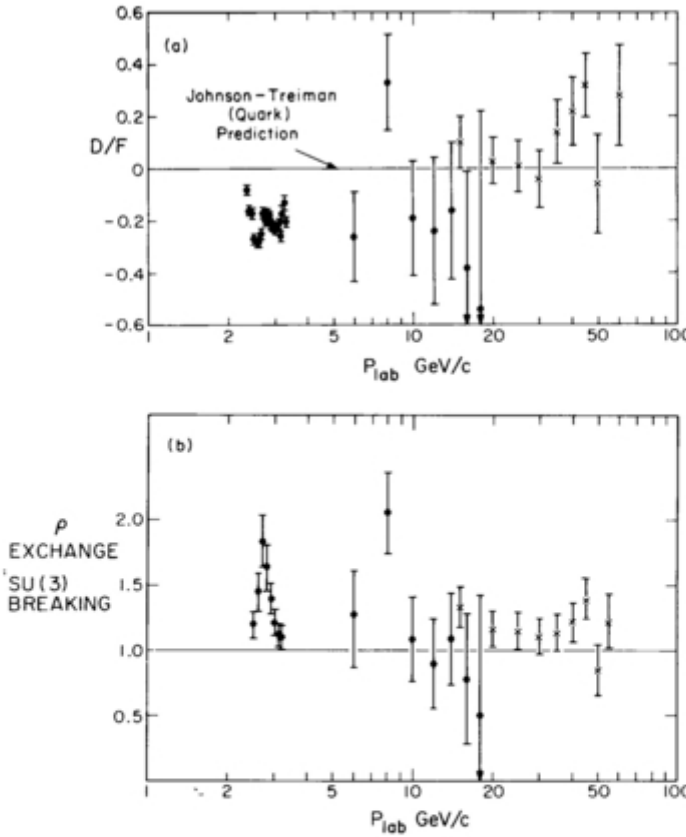

The dip and entire shape of $d\sigma/dt$ is nicely predicted by the Chou-Yang model (163–165).

(c) There is also a change in slope for pp $d\sigma/dt$ at ISR energies for $t \approx -0.15$ $(\text{GeV}/c)^2$ [i.e. in $d\sigma/dt \propto e^{At}$, A goes from 10.5 for $t < -0.15$ to 12.5 for $t > -0.15$ $(\text{GeV}\ c)^2$]. This same effect is almost certainly present at lower energies (166). If there is a similar structure in πp scattering it occurs at smaller $-t$

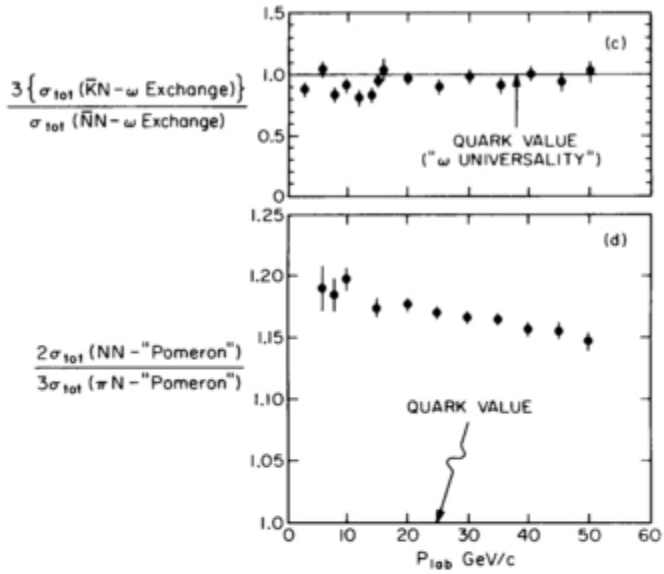

Figure 21 (above and facing) (*a*) The D/F ratio for vector meson (ρ, ω) exchange in the nonflip amplitude at $t = 0$. It is calculated at each energy from total cross sections using equations 5.1 and as explained in section 5E(*ii*), a conventional interpretation of SU(3) suggests we should use the lower energy value $D/F \simeq -0.2$ as our best estimate. The data are from (308, 309) and (151); the figure is adapted from the latter reference where the low energy points are incorrectly plotted. (*b*) The ratio R defined in equation 5.2 which should be 1 if SU(3) is exact. The data are from (308, 311) and (151) and the figure is adapted from the latter reference. (*c*) 3 × (ratio of ω contributions to $\bar{K}N$ and $\bar{N}N$ scattering) which should be 1 if ω universality holds. The data are from (308, 312, 313, and 151), while the graph is taken from latter reference. (*d*) 2/3 of (ratio of Pomeron and P' contributions to NN and πN scattering) which should be 1 in quark model. The data are from (309, 311, 313, 314, and 151) while the graph is taken from latter reference.

(167, 168); an exact analysis is confused by uncertainties in experimental normalization (169).

Theoretically this slope change or curvature is given automatically by the Chou-Yang model. Alternately it may be due to the singularity at $t = 4m_\pi^2$ which must be present in the pp amplitude (170, 171).

(*d*) There is the notorious crossover between particle and antiparticle $d\sigma/dt$

(i.e. $\pi^- p$ vs $\pi^+ p$, $K^- p$ vs $K^+ p$, $\bar{p}p$ vs pp elastic) for $-t = 0.1$ to 0.2 (GeV/c)^2. This implies a zero in this t range for Im $N(s,t)$ of ρ and ω exchange, which disagrees with the Regge prediction of a zero at α_ρ or $\alpha_\omega = 0$. [$t \approx -0.5$ (GeV/c)^2.] These data on the other hand are splendid successes for absorption models (sections 2B, 4F, and Figure 7).

(*e*) $\pi^+ p$ dσ dt do not shrink for $p_{lab} \lesssim 40$ GeV/c and $-t \lesssim 1$ (GeV/c)^2 (168); this can be understood in two ways. First (32, 125, 141, 142), interference of an "effective" Pomeron with slope 0.5 to 1 [as needed in pp or $K^+ p$—see (*a*)] with a P' exchange whose imaginary part changes sign at $t \approx -0.2$ (GeV/c)^2 [i.e. P' has peripheral zero required by EXD duality and seen in (*d*) for ω/ρ exchange]. The second explanation is more natural but perhaps less consistent with other data; in this, the "effective" Pomeron has little slope and the P' has no structure in its t-dependence (cf. "peripheral" P' discussion in section 4F).

(*ii*) The larger $-t$ dσ dt data exhibit:

(*a*) A dip at $t \approx -3$ (GeV/c)^2 in $\pi^+ p$; is this related to $t \approx -1.4$ dip in pp ISR data?

(*b*) All differential cross sections shrink very fast for $p_{lab} \lesssim 30$ GeV/c and $-t > 1$ (GeV/c)^2. The shrinkage disappears for pp at ISR energies and a similar fate no doubt awaits the other reactions (207) [cf. (*iiib*)].

(*c*) At $\cos\theta_{cm} = 0$, the shrinkage is translated into a fast fall of dσ/dt with s. In agreement with theoretical prejudice, the fall can be fitted (162, 172–174) to s^{-n} with n lying between 7 and 12 for $\gamma p \to \pi p$, $\pi p \to \pi p$, and $pp \to pp$.

The origin of the shrinkage plus the transition from models for 90° scattering to small t(exchange) models is not understood. In particular, for $p_{lab} \lesssim 5$ GeV/c and, say, $1 < -t < 3$ (GeV/c)^2, the elastic shrinkage is similar to that in a host of quantum number exchange ($\pi^- p \to \pi^0 n$, $\pi^+ p \to K^+ \Sigma^+$, $\pi^- p \to p\pi^- \ldots$) reactions (9, 16) and fittable in a Regge model.

(*d*) The $K^+ p$ dσ/dt can be fitted to large $-t$ with a simple exponential form, e.g. at 5 GeV/c, this form fits up to $t = -2$ (GeV/c)^2. In particular, the break occurs at larger $-t$ than in otherwise similar pp elastic scattering; this can be interpreted in an absorption model as smaller multiple scattering in $K^+ p$ than in pp. However, it is then difficult to understand the earlier rise in σ_{tot} for $K^+ p$ than for pp.

(*e*) The polarization (Figures 20A5, A6) is sensitive to the spinflip amplitude of the Regge V, T exchange. The data for $-t \lesssim 1$ (GeV/c)^2 are in beautiful agreement with simple pole theory (15, 16, 175) in $\pi^+ p$, $K^+ p$, pp, and $\bar{p}p$ scattering. The pp polarization exhibits some rather surprising energy dependence (it falls a little too fast) and has ill-understood (141) structure at $t \approx -1$ (GeV/c)^2 (176). There are also difficulties in explaining the energy dependence of the (small) $I = 0$ spin-flip exchange amplitude demanded by the $\pi^+ p$ polarization data (177). Somebody should measure the pn polarization and check the theoretical prediction that it is equal and opposite to pp.

(*f*) Comparison of $\pi^- n \to \pi^- n$ with $\pi^+ p \to \pi^+ p$, or $\Lambda n \to \Lambda n$ with $\Lambda p \to \Lambda p$ allows

an unambiguous check of the Glauber technique for extracting neutron cross sections from deuterium data.

(*iii*) Reaction A5 with real photons demonstrated the similarity of real photon and hadron data (150). The inelastic electron data from SLAC measure off shell photon total cross sections, i.e. $\sigma_{\gamma^* p}[\gamma^*(q^2)p, n]$, for (large) spacelike q^2 and the similarity disappears. (Scaling and point-like behavior sets in.) However, a Regge analysis is still possible for large "ν q^2" and successful (178). In particular, roughly the same D/F ratio is applicable.[23]

It would be nice to measure $d\sigma/dt$ for $\gamma p \to \gamma p$ and $\gamma n \to \gamma n$ (real photons). A crossover at $t \simeq -0.2$ (GeV/c)^2 would directly indicate (179) a peripheral zero in Im $N(A_2)$ [cf. (*iiic*) and section 4F].

5B *Diffraction Dissociation*

General reviews may be found in (13, 180, 181).

(*i*) Reaction B contains nonelastic processes whose quantum numbers allow vacuum (Pomeron) exchange (Figure 20B1). Their cross sections are roughly energy independent (Figure 20B2); although inelastic processes fall a little faster than elastic, the former still fall much slower than the typical $p_{\text{lab}}^{-1.5 \to -2.5}$ of a quantum number exchange reactions (e.g. $\pi^- p \to K^+ \Sigma^-$, $\pi^- p \to \pi^0 n$).

(*ii*) It is not clear if bumps seen in reactions B1–B5 are true resonances. A_1, A_3, Q, L, and N^* (1400) are almost certainly mainly some sort of kinematic enhancement typified by Deck model (182, 183 Figure 20B3). In each case, one expects a real resonance roughly at the mass of the bump; however, the parameters of the bump are wrong and in the case of A_1, A_3, no resonant phase variation is found (92, Figure 20B4). N^*(1400) appears at different masses in πN and $\pi\pi N$ decays (expected in Deck model), but this is a general feature of multichannel resonance decays (86) and need not be evidence against a resonance interpretation. It is not known if "diffractively" produced $N^*(\simeq 1700)$ is $5/2^+$ $N^*(1688)$, $5/2^-$ $N^*(1680)$, or just a kinematic bump! The former seems most reasonable (184, 185), but the A_2 data [see (*iv*)] might suggest the $5/2^-$ possibility.

(*iii*) There is theoretical (duality plus zero triple Pomeron coupling) and experimental evidence that background under "resonances" in $\pi N \to \pi N^*$ decreases with incident energy (186). This does not seem consistent with $\pi N \to (A_1, A_2, A_3)N$ data (92) while Einhorn et al (187) point out complications in the theory.

(*iv*) The A_2 is seen in the same ($\pi^+ \pi^+ \pi^- p$) final state as A_1 and A_3; the A_2 has the right (mass, width, phase) properties to be identified with a resonance but energy dependence of data (92) implies $\pi N \to A_2 N$ (reaction H) is Pomeron exchange (Figure 20B2) contradicting the Gribov-Morrison rule (146).

(*v*) The cross sections for $\pi N \to \pi N^*$, $NN \to NN^*$, and $KN \to KN^*$ allow tests of Pomeron factorization (48). As reviewed in (13), the current data are consistent with this idea but the energy dependence difficulty [cf. (*ii*)] and the uncertain identification

[23] E. D. Bloom, Private communication. D/F can be calculated from the proton–neutron ratio.

	Reaction	Exchanges
B1	$\pi^+ p \to A_1^+ p$ $\pi^- p \to A_1^- p$ $\pi^+ p \to A_3^+ p$ $\pi^- p \to A_3^- p$	$\mathbb{P}$ P', ρ η, B
B2	$\pi^+ p \to \pi^+ N^{*+}$ (many) $\pi^- p \to \pi^- N^{*+}$ (many) $\pi^- n \to \pi^- N^{*0}$ (many)	$\mathbb{P}$ P', ρ
B3	$K^+ p \to Q^+ p$ $K^0 p \to Q^0 p$ $K^- p \to Q^- p$ $\bar{K}^0 p \to \bar{Q}^0 p$ $K^+ p \to L^+ p$ $K^- p \to L^- p$	$\mathbb{P}$ P', ω A_2, f π, B η, h
B4	$K^+ p \to K^+ N^{*+}$ (many) $K^+ n \to K^+ N^{*0}$ (many) $K^- p \to K^- N^{*+}$ (many)	$\mathbb{P}$ P', ω A_2, ρ
B5	$pp \to p N^{*+}$ (many) $pn \to p N^{*0}$ (many) $\bar{p}p \to \bar{p} N^{*+}$ (many) $\bar{p}n \to N^{*-}$(many) n $\bar{p}n \to \bar{p} N^{*0}$ (many)	$\mathbb{P}$ P', ω A_2, ρ π, B η, h
B6	$\gamma p \to \rho p$ $\gamma p \to \rho' p$ $\gamma p \to \omega p$ $\gamma p \to \phi p$	$\mathbb{P}$ P', A_2 π, η $\mathbb{P}$

Figure 20B (above and facing page) Diffraction dissociation: (*B1*) Typical Pomeron exchange reactions. Elastic, single, and double dissociation. (*B2*) Energy dependence (in roughly $5 \lesssim P_{lab} \lesssim 20$ GeV/c) of elastic and diffraction dissociation reactions [adapted from (131)]. (*B3*) Deck model. (*B4*) Mass dependence of cross section and relative $1^+(A_1)$ and 0^- (background) s-wave phases for $\pi^- p \to A_1^- p$ at 40 GeV/c (92). (*B5*) Ratio of $\gamma p \to \gamma N^*(1688)$ to $\gamma p \to \gamma p$ for $\gamma = p$ (symbolized ●), $\pi(\times)$ and electron (Δ) (189). (*B6*) t-dependence of $\pi^- p \to A_{1,3} p$ at 40 GeV/c (92).

of bumps with resonances confuses the interpretation. [Note that a Deck bump would factorize and this model would explain results in Tables II and III of (131)]. The reported failure for double diffraction processes (188) merely indicates large non-Pomeron components in high multiplicity states around 20 GeV/c.

Figure 20B5 shows that factorization works as a function of t for $N^*(1688)$ production (189).

(*vi*) More than one theoretical model predicts a zero at $t = 0$ for $d\sigma/dt$ of N^*

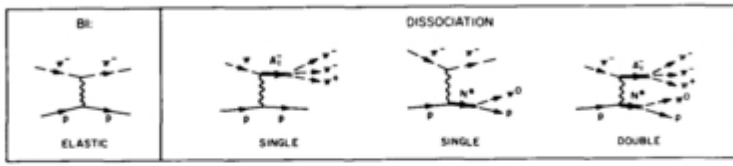

B2: $\sigma \propto P_{lab}^{-n}$ FITS

Reaction	n
$K^0 p \to Q^0 p$	0.59 ± 0.16
$K^+ p \to Q^+ p$	0.60 ± 0.05
$\pi^- p \to A_1^- p$	0.41 ± 0.11
$\pi^- p \to A_2^- p$	0.57 ± 0.08
$\pi^+ p \to A_2^+ p$	0.8 ± 0.3
$K^+ p \to K^+ p$	0.09 ± 0.03
$K^- p \to K^- p$	0.39 ± 0.04
$\pi^- p \to \pi^- p$	0.22 ± 0.11
$\pi^+ p \to \pi^+ p$	0.28 ± 0.05
$pp \to pp$	0.2 ± 0.07

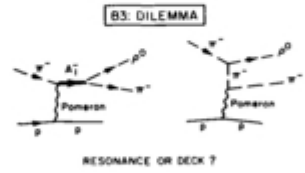

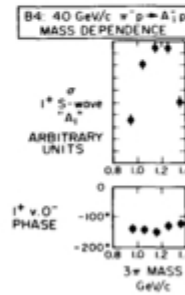

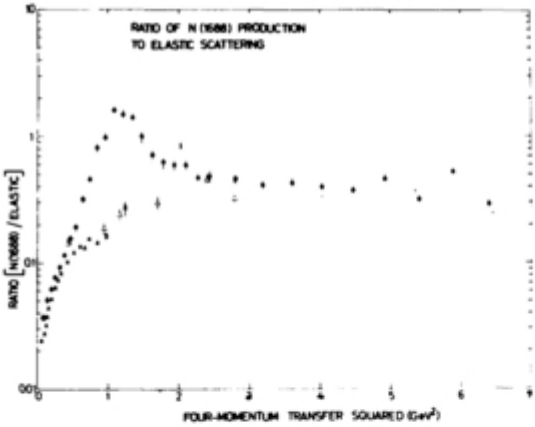

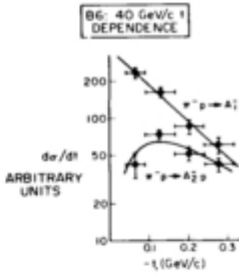

production. This is consistent with but not proved by the current data. Thus $d\sigma\ dt$ is very sharp for $KN \to QN$, $\pi N \to A_1 N$, and $NN \to NN^*(1400)$ (Figure 20B6); however perhaps the Q, A_1 and $N^*(1400)$ are not resonances. $NN \to NN^*(1688)$ shows a flat $(e^{3t}1)d\sigma\ dt$; taking a simple mass-cut to define the N^* (1688) shows no $t = 0$ zero. However, a Breit-Wigner fit to the mass spectrum

shows a decrease in signal/background as $t \to 0$ (189) and suggests a zero in the true resonance component.

The similarity in $eN \to eN^*$ and $NN \to NN^*$ after scaling by the elastic cross section, in Figure 20B5, supports models that make Pomeron couplings proportional to those of the photon (190).

(*vii*) $d\sigma/dt$ for $K^0 p \to Q^0 p$ vs $\bar{K}^0 p \to \bar{Q}^0 p$ show (191) a similar crossover at $t \approx -0.2$ (GeV/c)^2 to that in $K^+ p \to K^+ p$ vs $K^- p \to K^- p$. This suggests the universality and hence importance of such particle antiparticle crossovers. Secondly, the fact that $\bar{Q}^0 p$ is bigger at $t = 0$ than $Q^0 p$ contradicts the Deck model (showing it is a typical and not the only background amplitude).

A similar crossover is seen in $\pi^- p \to A_1^- p$ vs $\pi^+ p \to A_1^+ p$ but now the values at $t = 0$ are consistent with the Deck model (13).

(*viii*) The reactions in B6 are less confusing.

(*a*) The decay of the ρ shows s-channel helicity conservation (110) in agreement with πN elastic and Compton scattering. This helicity conservation was *not* seen in B1–B5 where t-channel helicity conservation is preferred (13).

(*b*) $\gamma p \to \phi p$ is useful as one expects zero coupling for secondary Regge (P') trajectories (as ϕ is purely strange quarks). This reaction is perfect for examining the Pomeron amplitude. The current data (13, 192) support a flat Pomeron (i.e. no shrinkage). Attempts to correlate this with the flat Pomeron observed for pp scattering at ISR are dubious because all $\gamma N \to VN$ reactions have t-dependences similar to elastic scattering in the $p_{\text{lab}} \lesssim 30$ GeV/c regime where the Pomeron is observed to shrink.

(*c*) $\gamma p \to \omega p$ also has sizable π exchange (see reactions G12).

(*d*) It is not known whether the ρ' observed (193) in $\gamma p \to \rho' p$ is a true resonance state or a kinematic enhancement of the type that plagued reactions (B1–B5).

5C *Elastic Deuteron and Nuclear Reactions*

(*i*) We do not list the analogous reactions with nuclear targets. Neither the deuteron (23) (see also reactions K) or nuclear (194–197) processes has added much to our understanding of elementary particle theory. Their isolation of $I = 0$ exchange is, in practice, achieved also in the reactions of groups A and B.

(*ii*) Current data confirm (23) Glauber theory with interesting additional contributions (198, Figure 20C1) from inelastic states at high energy ($\gtrsim 10$ GeV/c). The latter affects extraction of neutron cross sections from data on deuteron targets.

There is also evidence for D-wave in the deuteron which obscures a multiple scattering dip (23, 199, Figure 20C2). The deuteron is strongly polarized at the t-value of the dip.

(*iii*) There is the d^* [$N\Delta(1234)$ state analogous to d as np state] which is an amusing example of quantum mechanics. We do not list associated reactions (e.g. $\pi d \to \rho d^*$) as their properties follow (in principle) straightforwardly from subreactions obtained by writing d and d^* in terms of their constituents. Typical is (200) which finds the curious sharing of decay π^- between decays of L and d^* in $K^- d \to K^- \pi^- \pi^+ d$; a similar effect is seen in the "constituent" reactions $K^+ p \to K^+ \pi^- \pi^+ p$.

	Reaction	Exchanges
C1	$\pi^+d \to \pi^+d$ $\pi^-d \to \pi^-d$	$I\!P, P'$
	$K^+d \to K^+d$ $K^-d \to K^-d$	$I\!P$ P', ω
	$pd \to pd$ $nd \to nd$ $\bar{p}d \to \bar{p}d$	$I\!P$ P', ω η, h
	$\Sigma^-d \to \Sigma^-d$	
C2	$K^+d \to Q^+d$ $K^-d \to Q^-d$	$I\!P$ P', ω η, h
	$K^+d \to L^+d$ $K^-d \to L^-d$	
C3	$\gamma d \to \rho d$	$I\!P, P', \eta$
	$\gamma d \to \omega d$	
	$\gamma d \to \phi d$	$I\!P$

C1 : Glauber corrections

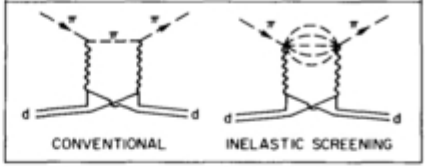

C2 : π d elastic scattering

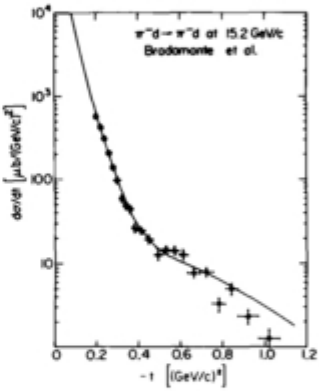

C3 : A_{eff} A from photon nucleus total cross sections

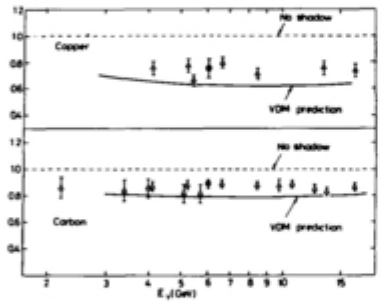

Figure 20C Elastic and diffractive deuteron and nuclear reactions: (*C1*) Diagrams calculated in Glauber theory including Gribov's addition of inelastic contributions (198). (*C2*) Differential cross sections for π d elastic scattering at 15.2 GeV c, measured by the CERN-Trieste High Energy Group (307). The prominent features are the sharp forward peak, due mostly to single scattering, and a shallower slope at larger values of $|t|$, due to double scattering. The curve is a Glauber theory calculation by Sidhu & Quigg (199). (*C3*) Comparison of photon nucleus total cross section data with vector dominance (VDM) and point photon ("No Shadow") predictions (202).

(*iv*) The A (atomic number) dependence of γ Nucleus $\to (\rho, \omega, \phi)$ Nucleus lies between A^1(Volume) and $A^{2/3}$(Surface). This indicates that γ has both point-like and hadronic (vector-dominance) features (201). Typical is Figure 20C3, taken from (202), which analyzes data in terms of A_{eff} (201).

Electroproduction (virtual photon) data off nuclei would be important for clarifying point-like nature of the photon at large q^2.

(*ii*) The reactions listed in C2 are similar to B3 [indicating that, say, structure on Q region (200) is indeed attributable to diffractive $I = 0$ production]. Data (203) on n Carbon $\rightarrow (N^{*0} \rightarrow p\pi^-)$ Carbon shows a $p\pi^-$ decay angular distribution which differs from that in reactions B2, B4, B5 (184, 185). It is presumably some nuclear effect but no explanation has appeared in the literature.

(*iii*) If you believe the relevant theory (204), coherent nuclear reactions $xA \rightarrow yA$ allow extraction of the yN total cross section. Sensible values are obtained for $\sigma_{tot}(\phi p, \eta p,$ etc.), but it is no longer thought that the $\pi A \rightarrow (3\pi)A$ data, which find $\sigma_{tot}[(3\pi)p] \approx \sigma_{tot}(\pi N)$, imply a resonant (A_1) 3π system.

5D $I = 0, 1$ Natural Parity Exchange

(*i*) The simplest of these reactions are D3. According to the quark model they are pure spinflip [this is tested by beautiful $K^+p \rightarrow K^0\Delta^{++}$ data (205) at 2.25 GeV/c which show $d\sigma\ dt$ (Figure 20D2) dipping to 1/10 its maximum value at $t = 0$]. This model also predicts the Stodolsky-Sakurai decay distributions $\rho_{33} = 3/8$, $\rho_{3-1} = -3/8$, and $\rho_{31} = 0$, which agree well with data even at low incident energy (Figure 20D3). Current folklore (section 4) believes ρ, A_2 spinflip amplitudes should agree well with simple pole theory. This indeed holds for shape (WSNZ) and energy dependence of $d\sigma\ dt$ for D3 reactions. There is, however, definite evidence for failure of EXD [line-reversal see (*iii*)].

The picture is slightly muddied theoretically as the quark model naturally predicts a pure t-channel spinflip amplitude while folklore prefers s-channel spinflip as the perfect Regge amplitude. Rotation of the quark amplitude to the s-channel would give some non-Regge nonflip and double flip amplitudes. The effect is quite small and existing data are much too poor to test for its presence.

(*ii*) Reactions D1 are dominantly spinflip but $d\sigma/dt$ (Figure 20D1) shows a flattening near $t = 0$ corresponding to a small nonflip amplitude. The latter is isolated relatively exactly by the amplitude analyses and is definitely non-Regge (section 4). $d\sigma\ dt$ is dominated by the spinflip amplitude and shows Regge energy dependence up to $-t \simeq 3$ (GeV/c)^2 (206) [cf. (207) which finds similar energy dependence for πp elastic]. The ρ, A_2 WSNZs at $-t = 0.6$ and 1.5 are seen but not the second ρ WSNZ at $-t \approx 2.5$ (GeV/c)^2 (206).

The quark model relates the spinflip amplitudes in reactions D1 and D3. This relation fails by factor of 1.5 to 2 in cross section the Δ^{++} cross section is too big (208).

The polarization in $\pi^- p \rightarrow \pi^0 n$ first indicated the failure of pure Regge theory. This polarization was, however, correctly predicted at small $-t$ by absorption models (which correctly moved the zero of Im N from $\alpha_\rho = 0$ to smaller $-t$). The lack of a negative spike at $t \simeq -0.6$ (GeV/c)^2 then destroyed the old absorption model (which *in*correctly moved the zero of Re N to smaller $-t$ than Im N). There is some controversy at present about the exact experimental values (101, 102, Figure 13).

The sign of the $\pi^- p \to \eta^0 n$ polarization at $-t \approx 0.2$ (GeV c)^2 is an important test of models (section 4F); current data are poor (102, 144, 145).

(*iii*) This same marvelous Regge natural parity spinflip amplitude seen in reactions D1 and D3 can also be isolated in $K^+ p \to K^{*+} p$ (reactions G5), $\pi^+ p \to \rho^+ p$ (G1), and $\pi^+ p \to A_2^+ p$ (I1). For these last reactions, we extract our amplitude using $(\rho_{11} + \rho_{1\,-1})d\sigma/dt$ while polarized photon data isolate it in $\vec{\gamma} p \to \pi^0 p$ and $\vec{\gamma} n \to \pi^0 n$ (reactions I3). The amplitude always has the same phenomenological properties: universal shape, WSNZ where expected, shrinkage (not tested always) and line reversal breaking systematics [see (*iv*)]. The same amplitude also contributes to innumerable other processes but its exact isolation is not possible; for instance, it gives observed polarization in $\vec{\gamma} p \to \pi^+ n$ (reaction H3) and has the usual line reversal breaking in $\pi^- p \to K^{*0}(890)\Lambda$ vs $K^- p \to \omega\Lambda$ [section 5L(*iv*)].

(*iv*) In spite of its many Regge beauties, this wondrous spinflip amplitude exhibits strong violation (209) of the expected line reversal symmetry [e.g. $d\sigma/dt(K^+ n \to K^0 p) = d\sigma/dt(K^- p \to \bar{K}^0 n)$]. Always the "real" ($K^+ n \to K^0 p$, $K^- p \to K^{*-} p$) is larger than the "moving phase" ($K^- p \to \bar{K}^0 n$, $K^- p \to K^{*0} p$) reaction. For $K^+ n \to K^0 p$ the deviation is only present below 5 GeV c; for $K^- p \to K^0 \Delta^-$ vs $K^- n \to K^0 \Delta^-$ or $K^- p \to \pi^- Y^{*+}(1385)$ vs $\pi^+ p \to K^+ Y^{*-}(1385)$ (reactions E4) current data suggest the effect persists to higher energy (Figures 20D4 and 18).

Examination of $d\sigma/dt$ reveals that $K^- p \to \bar{K}^0 n$ and $K^- n \to \bar{K}^0 \Delta^-$ have a break at $t \approx -0.6$ (GeV c) (reminiscent of multiple scattering), but $K^+ n \to K^0 p$ and $K^+ p \to K^0 \Delta^{++}$ are quite smooth here.

We might as well note here that $K^+ n \to K^{*+} n$ and $K^- n \to K^{*-} n$ do *not* show any line reversal breaking (210); this is believed to be because the spinflip amplitude is reduced in size as ρ and ω contribute with opposite signs; the observed $(\rho_{11} + \rho_{1\,-1})d\sigma/dt$ is contaminated with double flip and nonflip amplitudes. For similar reasons, the difference (211) between $K^+ p \to K^{*+} p$ and $K^- p \to K^{*-} p$ becomes more pronounced if one extracts the pure natural parity exchange contribution.[24]

(*v*) The reaction D2, $K_L^0 p \to K_S^0 p$, is important because it is dominantly nonflip which amplitude disagrees with Regge theory. Current data (212) show a break at $t \approx -0.2$ (GeV c)^2 [corresponding to zero in $\mathrm{Im}\,N(\omega)$] and rapid shrinkage of $d\sigma/dt$ at larger $-t$ (even though Regge has wrong zero structure!). Detailed polarization (it should be negative at small $-t$) and $d\sigma/dt$ studies of this reaction will be rewarding.

(*vi*) The small $I = 0$ exchange polarization in $\pi^+ p \to \pi^+ p$ indicates that the f^0 (and hence by EXD ω) s-channel spinflip coupling is small. This implies an s-channel spinflip D/F value of 3 for V, T exchange. The quark model predicts $D/F = 3/2$ in the t-channel (16). Rotation of $\rho \to N\bar{N}$ s-channel spinflip coupling plus nonflip couplings from σ_{tot} shows this is consistent with current data.

(*vii*) It will be important to see whether there is a ρ exchange dip in $\pi^+ p \to \pi^0 \Delta(1940)$ or more generally in $\pi^+ p \to \pi^0$(fast)$(\pi^+ p)$ (reactions D4). The former and, for instance,

[24] B. Musgrave, Private communication.

$K^+p \to K^0\Delta(1940)$ are good places to look for possible decay symmetries analogous to Stodolsky-Sakurai for the $\Delta(1234)$. The ρ photon analogy (213) predicts a decay similar to that in photoproduction $\gamma N \to \Delta(1940) \to \pi N$.

(*viii*) Comparison of $\pi^+p \to \eta\Delta^{++}$ and $\pi^+p \to \eta'\Delta^{++}$ provides a direct measure of $\eta - \eta'$ mixing *if* one ignores the "disconnected quark graph" coupling. This gives (214, 215) a mixing angle of -30° to -40° in disagreement with -10° expected for the favored quadratic mass formula. However, this large value should be disregarded as the analysis reported in section 5E(*iii*) renders the quark assumption invalid (216).

	Reaction	Exchanges
D1	$\pi^-p \to \pi^0 n$ $\pi^+n \to \pi^0 p$	ρ
	$\pi^-p \to \eta n$ $\pi^+n \to \eta p$ $\pi^-p \to \eta' n$ $\pi^+n \to \eta' p$	A_2
	$K^+n \to K^0 p$ $K^0p \to K^+n$ $K^-p \to \bar{K}^0 n$	A_2, ρ
D2	$K_L^0 p \to K_S^0 p$	ρ, ω
D3	$\pi^+p \to \pi^0\Delta^{++}$ $\pi^+n \to \pi^+\Delta^0$ $\pi^+p \to \pi^+\Delta^+$ $\pi^-p \to \pi^-\Delta^+$ $\pi^-p \to \pi^0\Delta^0$	ρ
	$\pi^+p \to \eta\Delta^{++}$ $\pi^+p \to \eta'\Delta^{++}$	A_2
	$K^-n \to \bar{K}^0\Delta^-$ $\bar{K}^0p \to K^-\Delta^{++}$ $K^-n \to K^-\Delta^0$ $K^-p \to K^-\Delta^+$ $K^-p \to \bar{K}^0\Delta^0$	ρ, A_2
	$K^+p \to K^0\Delta^{++}$ $K^+p \to K^+\Delta^+$ $K^+n \to K^0\Delta^+$ $K^+n \to K^+\Delta^0$	
D4	$\pi^-p \to \pi^0 N^{*0}$ (many) $\pi^+p \to \pi^0 N^{*++}(I=3/2)$	ρ
	$K^+p \to K^0 N^{*++}(I=3/2)$ $K^+n \to K^0 N^{*+}$ (many) $K^-p \to \bar{K}^0 N^{*0}$ (many)	ρ, A_2

Figure 20D $I = 0, 1$ nondiffractive natural parity exchange: (*D1*) Typical differential cross sections at 5 GeV/c. (*D2*) $d\sigma/dt$; and (*D3*) Δ^{++} density matrix elements for $K^+p \to K^0\Delta^{++}$ at 2.5 GeV c (205). (*D4*) Comparison of reaction cross sections for various line-reversed reactions. (Data is unpublished compilation of G. C. Fox.)

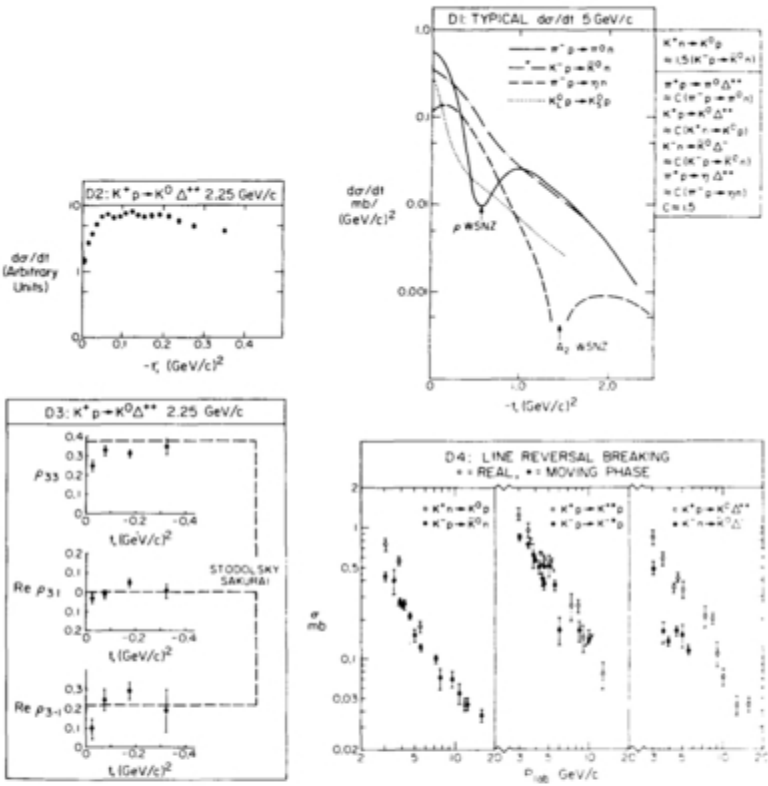

5E *Hypercharge and Natural Parity Exchange*

(*i*) We have discussed reactions E1, E2 under amplitude analyses (sections 4E and 4F). The latter are still uncertain and require both R and A measurements (section 3) and clarification of line reversal systematics [see (*r*)] e.g. careful measurement of $K^- p \to \Sigma^+$ and $\pi^+ p \to K^+ \Sigma^+$ with no relative normalization error. The most reasonable amplitude analyses suggest a surprising nonperipheral tensor (K^{**}) exchange (71, 134 Figure 19(c).

(*ii*) As expected theoretically [SU(3)], reactions E1 E3 are mainly nonflip (cf.

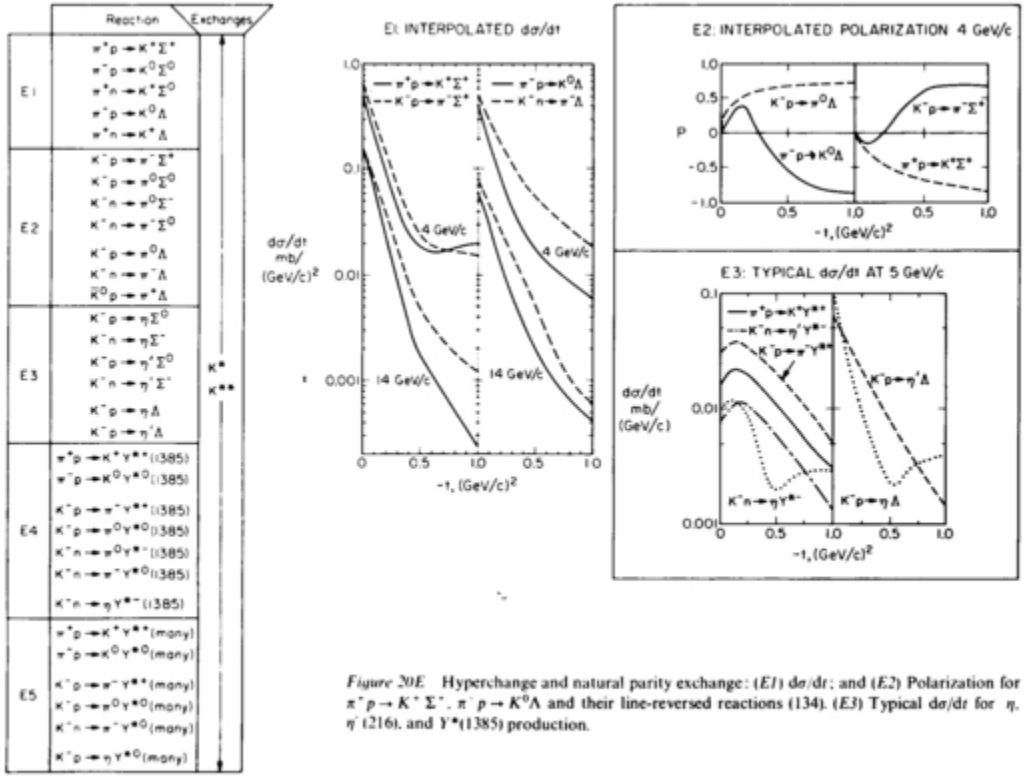

Figure 20E Hyperchange and natural parity exchange: (*E1*) $d\sigma/dt$; and (*E2*) Polarization for $\pi^+ p \to K^+ \Sigma^+$, $\pi^- p \to K^0 \Lambda$ and their line-reversed reactions (134). (*E3*) Typical $d\sigma/dt$ for η, η' (216), and $Y^*(1385)$ production.

Figures 20 E1, E2) and so, like $K_L^0 p \to K_S^0 p$, should exhibit more deviations from Regge theory than reactions D1, D3. Comparison of Λ and Σ $d\sigma/dt$ at $t = 0$ (e.g. $\pi^- p \to K^0 \Lambda$ vs $\pi^- p \to K^- \Sigma^+$) gives directly a D F value for the relevant K^* and K^{**} exchanges in the nonflip amplitude (10, 131, 133, 134). Although this qualitatively agrees with that obtained from σ_{tot}, there is a tendency for the Σ data to be higher than expected. The spinflip amplitude can only be bounded by polarization data (134) and extracted explicitly in models. This amplitude is also consistent with SU(3) and the D F values discussed in section 5D. The polarization observed in "real" reactions $K^- n \to \pi^- \Lambda$, etc., is sizable (Figure 20E2). This suggests that K^* and K^{**} do not have the equal imaginary parts in nonflip amplitude N demanded by EXD. In the amplitude analyses of section 4F, these amplitudes indeed differed but by huge factors (Figure 17) as we discussed there, this appears to violate SU(3) at $t = 0$.

There is an interesting dip at $t \approx -0.4$ (GeV c)^2 in $K^- p \to \eta \Lambda$ (Figure 20E3) it is probably related to K^* WSNZ (in the spinflip amplitude?) for SU(3) predicts a suppression of K^{**} in this reaction (216).

The Y^* channel (reactions E4) is, like its SU(3) friends in reaction group D3, mainly spinflip (Figure 20E3). The expected dip in $K^- n \to \eta Y^{*-}$ has not yet been seen experimentally.

(*iii*) One can extract the $\eta - \eta'$ mixing angle by combining reactions in E3 with $\pi N \to (\eta, \eta')N$ (reactions D1). The analysis is more complicated than in $\pi N \to \eta\Delta$, $\eta'\Delta$ because of the different nonflip and spinflip D F values at the NN vertex. However, the data are better and one can avoid the assumption of no "disconnected quark graphs" [this would also be possible for the Δ data if you also used $\pi N \to \pi\Delta$ and $KN \to K\Delta$ and did a full SU(3) analysis]. The analysis of (216) gives a mixing angle of -11° in agreement with a quadratic mass formula.

(*iv*) The energy dependence of the data is odd. The best measured channel, $\pi^- p \to K^- \Sigma^+$, falls with an $\alpha_{eff}(0) \approx 0.7$ (0.35 expected) although it does exhibit canonical shrinkage. In particular, the break at $t \approx -0.4$ (GeV c) disappears rapidly with energy (cf. Figure 20E1).

(*v*) The experimental information on line reversal breaking is inconsistent. It appears that the "real" reaction ($K^- p \to \pi^- \Sigma^+$, $K^- p \to \pi^0 \Lambda$, $K^- p \to \pi^- Y^{*+}$) is generally larger than its "moving phase" counterpart ($\pi^+ p \to K^+ \Sigma^+$, $\pi^- p \to K^0 \Lambda$, $\pi^- p \to K^+ Y^{*-}$) but there are differences between Λ and Σ data (Figure 20E1), and it is not clear if the breaking vanishes at high energy (as it did for $K^- p \to \bar{K}^0 n$ vs $K^+ n \to K^0 p$ Figure 20D4).

Lai & Louie (209) first systematized these differences but since then the situation has been confused by fresh and contradictory data. The current Y^* data are summarized in Figure 18 while Figure 20E1 reproduces the interpolation (134) of Λ and Σ processes. New data of reliable normalization are urgently needed. We emphasize that current data does *not* support the idea (71, 134) that line reversal breaking is smaller in spinflip than in nonflip reactions (compare Figures 18 and 20E1).

(*vi*) The reactions E4 are related by SU(3) to D3 ($\pi^- p \to K^+ Y^{*-}$ to $K^- n \to \bar{K}^0 \Delta^-$,

FULLY FLEDGED π $(1/(1-m_\pi^2)^2)$

	Reaction	Exchanges
F1	$\pi^+p \to \rho^0\Delta^{++}$ $\pi^-n \to \rho^0\Delta^-$ $\pi^-n \to \rho^-\Delta^0$ $\pi^-p \to \rho^0\Delta^0$ $\pi^+n \to \rho^0\Delta^+$ $\pi^-p \to \rho^-\Delta^+$ $\pi^+n \to \rho^+\Delta^0$	A_2 π
F2	$\pi^+p \to f^0\Delta^{++}$ $\pi^+p \to g^0\Delta^{++}$	A_2, π
	$\pi^-p \to (\pi^-\pi^-)\Delta^{++}$	π
F3	$K^+p \to K^{*0}(890)\Delta^{++}$ $K^-n \to \bar{K}^{*0}(890)\Delta^-$ $\bar{K}^0p \to K^{*-}(890)\Delta^{++}$ $K^+p \to K^{*+}(890)\Delta^+$ $K^-n \to K^{*-}(890)\Delta^0$ $K^-p \to K^{*-}(890)\Delta^+$ $K^-p \to K^{*0}(890)\Delta^0$	A_2, ρ π, B
F4	$K^+p \to K^{*0}(1420)\Delta^{++}$ $K^-n \to \bar{K}^{*0}(1420)\Delta^-$ $K^+p \to K^{*+}(1420)\Delta^+$ $K^-p \to K^{*-}(1420)\Delta^+$	A_2, ρ π, B
	$K^-p \to (K^-\pi^+)\Delta^{++}$ $K^+n \to (K^+\pi^+)\Delta^-$	π, B
F5	$\pi N \to (\pi\pi)N^*(\text{many})$	A_2, π
	$KN \to (K\pi)N^*(\text{many})$	A_2, ρ π, B
F6	$\bar{p}p \to (\bar{\Delta}^{++})\Delta^{++}$ $\bar{p}n \to (\bar{\Delta}^{++})\Delta^{+}$ $\bar{p}n \to (\bar{\Delta}^{0})\Delta^{-}$ $\bar{p}p \to (\bar{\Delta}^{0})\Delta^{0}$ $pp \to \Delta^0\Delta^{++}$ $pn \to \Delta^{++}\Delta^-$ $pn \to \Delta^+\Delta^0$	A_2, ρ π, B
F7	$N\bar{N} \to N^*(\text{many})N^*(\text{many})$ $\bar{N}N \to \bar{N}^*(\text{many})N^*(\text{many})$	A_2, ρ π, B
F8	$\Delta p \to Y^{*-}(1385)\Delta^{++}$	A_2, ρ π, B
F9	$\gamma p \to \rho^-\Delta^{++}$ $\gamma p \to \rho^0\Delta^+$ $\gamma p \to \rho^+\Delta^0$	A_2, ρ π, B

GENERAL π EXCHANGE FIGURES

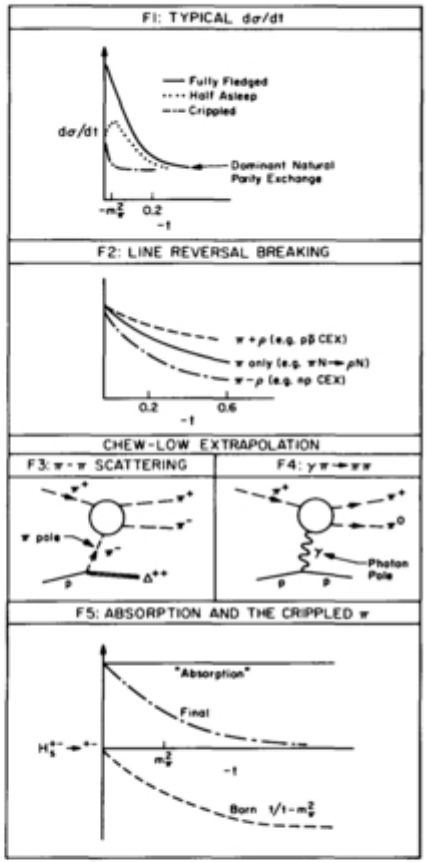

Figure 20F Fully fledged π exchange reactions: Figures *F1–F5* are relevant for all π exchange reactions. (*F1*) Typical $d\sigma/dt$ from π exchange [section 5F(*i*)]. (*F2*) Typical line reversal breaking [section 5F(*iii*)]. (*F3*) Chew-Low extrapolation for π exchange [section 5F(*iv*)]. (*F4*) Chew-Low extrapolation for photon exchange [section 5F(*v*)]. (*F5*) Role of absorption for crippled π exchange amplitudes [section 5H(*xi*)].

G: HALF ASLEEP $\pi \left(-t/(t-m_\pi^2)^2\right)$

	Reaction	Exchanges
G1	$\pi^+p \to \rho^+p$	ω, A_2
	$\pi^-p \to \rho^-p$	π, h
	$\pi^-p \to \rho^0n$	π, A_2
	$\pi^+n \to \rho^0p$	
G2	$\pi^-p \to f^0n$	π, A_2
	$\pi^+n \to f^0p$	
G3	$\pi^+p \to q^+p$	ω, A_2
	$\pi^-p \to q^-p$	π, h
	$\pi^-p \to q^0n$	π, A_2
	$\pi^+n \to q^0p$	
G4	$\pi^+n \to (\pi^0\pi^0)p$	π
	$\pi^-p \to (\pi^0\pi^0)n$	
	$\pi^+p \to (\pi^+\pi^+)n$	
	$\pi^-n \to (\pi^-\pi^-)p$	
G5	$K^+p \to K^{*+}(890)p$	ρ', ω
	$K^+n \to K^{*+}(890)n$	A_2, ρ
	$K^-n \to K^{*-}(890)n$	π, B
	$K^-p \to K^{*-}(890)p$	η, h
	$K^+n \to K^{*0}(890)p$	A_2, ρ
	$K^-p \to \bar{K}^{*0}(890)n$	π, B
G6	$K^+p \to K^{*+}(1420)p$	ρ', ω
	$K^+n \to K^{*+}(1420)n$	A_2, ρ
	$K^-n \to K^{*-}(1420)n$	π, B
	$K^-p \to K^{*-}(1420)p$	η, h
	$K^+n \to K^{*0}(1420)p$	A_2, ρ
	$K^-p \to \bar{K}^{*0}(1420)n$	π, B
G7	$K^+p \to (K^+\pi^+)n$	
	$K^-n \to (K^-\pi^-)p$	π, B
G8	$\pi N \to (\pi\pi)N$	ω, A_2
		π, h
	$KN \to (K\pi)N$	ρ', ω
		A_2, ρ
		π, B
		η, h
G9	$pp \to n\,\Delta^{++}$	A_2, ρ
	$\bar{p}p \to (\bar{\Delta}^{--})n$	π, B
	$\bar{p}p \to (\bar{\Delta}^0)n$	
	$pp \to p\,\Delta^+$	ρ', ω
	$pn \to p\,\Delta^0$	A_2, ρ
	$\bar{p}p \to (\bar{\Delta}^+)p$	π, B
		η, h

	Reaction	Exchanges
G10	$NN \to N^*(\text{many})$	P', ω
	$\bar{N}N \to \bar{N}^*(\text{many})N$	A_2, ρ
	$\bar{N}N \to \bar{N}N^*(\text{many})$	π, B
		η, h
G11	$Ap \to \Sigma^-\Delta^{++}$	A_2, ρ
		π, B
G12	$\gamma p \to \rho^+n$	A_2, ρ
	$\gamma n \to \rho^-p$	π, B
	$\gamma p \to \omega p$	P
		P', A_2
		π, η
G13	$\gamma p \to \pi^-\Delta^{++}$	A_2, ρ
	$\gamma p \to \pi^+\Delta^0$	π, B
	$\gamma n \to \pi^+\Delta^-$	
	$\gamma n \to \pi^-\Delta^+$	
G14	$\gamma p \to A_1^+n$	A_2, ρ
	$\gamma p \to A_2^+n$	π, B
	$\gamma p \to B^0p$	P', A_2
		π, η

H: CRIPPLED $\pi \left(t^2/(t-m_\pi^2)^2\right)$

H1	$np \to pn$	A_2, ρ
	$\bar{p}p \to \bar{n}n$	π, B
H2	$Ap \to \Sigma^0p$	A_2, ρ
	$Ap \to \Sigma^+n$	π, B
	$\Sigma^-p \to An$	
	$\Sigma^-p \to \Sigma^0n$	
H3	$\gamma p \to \pi^+n$	A_2, ρ
	$\gamma n \to \pi^-p$	π, B

Figure 20G, H G: Half-asleep π exchange reactions. H: Crippled π exchange reactions.

etc). The simple relation fails but this can be accounted for by the different Regge intercepts in $(s\ s_0)^\alpha$ with $s_0 \approx 1$ (GeV c)^2. A similar effect lowers reactions E1–E3 in the direct comparison with D1–D2. An unorthodox explanation of this suppression in terms of direct channel thresholds was advanced by Trilling (217).

The correctness of a low energy $s_0 \approx 1$ scale factor in this case suggests that in Figure 21*a* we should use the low energy value $D/F \approx -0.2$ value and not $D/F \approx 0$ suggested by the Serpukhov data (151).

(*viii*) The Y^* decays into π and Λ and the observed Λ polarization gives more information on the Y^* density matrix elements than the simple $\pi\Lambda$ decay angular distribution. This allows more stringent tests of the quark model predictions [section 5D(*i*), Figure 20D3] and seems to show some clear if small violations (218).

5F, G, H General π Exchange

(*i*) All π exchange processes are described at small t [$-t$ is $O(m_\pi^2)$] by the Poor Man's Absorption Model (PMA). The reader is referred to (67) for a full treatment – here we just note that PMA specifies that each s-channel helicity amplitude have the minimum t-dependence expected from analyticity [$(t_\wedge - t)^n$ with n the amount of spinflip] and the known residue at the π pole. Although this is a simple and successful prescription, it has never been understood theoretically. In the Regge pole language it corresponds to a complicated lack of factorization [conspiracy (219)] of the π Regge pole. Classical absorption models (50) have similar qualitative predictions to PMA but they never have been able naturally to get as precise a fit as the PMA. The model predicts that a reaction should be classified by the t-dependence of its Born term. This is the motivation for the three subdivisions F, G, and H (Figure 20F1).

(*ii*) Before specializing to the three divisions, note that almost all π exchange processes also allow natural parity exchange. Experimentally the natural parity exchange is observed to dominate the cross section for $-t \gtrsim 0.2$ (GeV/c)^2 (Figure 22). Theoretically the attribution of this to A_2 exchange is questionable because the PMA modifications of π exchange also produce a (large) natural parity component.

Experimentally the energy dependence of the data gives further information. The unnatural parity exchange component appears to shrink (220, 221) just as one expects for a π Regge pole of canonical slope ≈ 1 (GeV/c)$^{-2}$ (Figure 23*a–c*). Unfortunately, this conclusion is only statistically convincing if you use data below 5 GeV/c and there all processes known to man shrink (9, 16). (Simply because they are flat at threshold and peaked at higher energy!?) To be unambiguously identified with a Regge effect, the shrinkage must be confirmed in better data at higher energies. To further confuse the issue, some surprising effective π trajectories were reported (222) from studies of $KN \to K^*\Delta$, $NN \to \Delta\Delta$, and $\pi N \to \rho\Delta$.

The natural parity component exhibits little shrinkage up to large $-t \approx 3$ (GeV/c)^2 (Figure 23*d–f*). This contrasts with the reactions of groups A, D, and E which exhibit dramatic shrinkage at large $-t$. This difference is not understood theoretically. Note that this energy dependence implies that natural parity exchange dominance (hinted at) in Figure 22 will become more dominant as energy increases

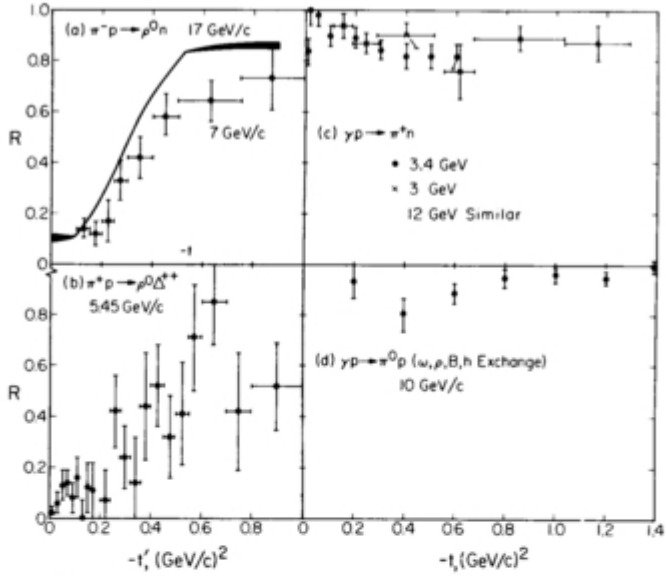

Figure 22 Fraction R of natural parity exchange discussed in section 5F(*iii*). The unnatural parity exchange is essentially π exchange for (*a*), (*c*) and B exchange for (*d*). The data come from (*a*) (315, 316), (*b*) (317), (*c*) (223, 224, 318), and (*d*) (319).

(*iii*) There is also a universal structure of the line reversal breaking (67). This is generated from the interference between a π exchange which vanishes at $t = 0$ and the natural parity component of the PMA π (Figure 20F2). The effect is large because both exchanges are dominantly in the same flip-flip ($m = 0, 2$) amplitudes. The sign of interference is correctly predicted by the quark model in all reactions. The interference is destructive, giving a very sharp $d\sigma/dt$ and a reduced natural parity component in np charge exchange (CEX), $\gamma n \to \pi^- p$, $\gamma p \to \pi^- \Delta^{++}$, $K^+ n \to K^{*0} p$, $K^+ p \to K^{0*} \Delta^{++}$, $pp \to n\Delta^{++}$, $p n \to \Delta^{++} \Delta^-$. The interference is constructive in $\bar{p}p$ CEX, $\gamma p \to \pi^+ n$, $\gamma p \to \pi^+ \Delta^0$, $K^- p \to \bar{K}^{0*} n$, $K^- n \to \bar{K}^{0*} \Delta^-$, $\bar{p}n \to (\overline{\Delta^{++}})p$, $\bar{p}p \to (\overline{\Delta^{++}})\Delta^{++}$; these show a flat $d\sigma/dt$ (Figure 24) and an increased natural parity exchange. Thus this effect will alter the natural parity component at large $-t$ discussed in (*ii*) and reduce it in $\gamma n \to \pi^- p$ and $\gamma p \to \pi^- \Delta^{++}$. [This is in fact seen experimentally (223, 224).]

Note in particular that the effect is especially dramatic in np CEX where the

ρ exchange is three times bigger than in $\gamma n \to \pi^- p$ which has already a very sharp $d\sigma/dt$. It follows that the very sharp np CEX $d\sigma/dt$, which has evinced much interest, is an accidental combination of a π pole with a large destructive ρ exchange. Similarly the flat $d\sigma/dt$ for $p\bar{p}$ CEX (where ρ is constructive) is of no special significance.

The equality of $\gamma n \to \pi^- p$ and $\gamma p \to \pi^+ n$ at $t = 0$ is particularly interesting as direct evidence that, in accordance with factorization, ρ exchange truly vanishes at $t = 0$. [In an ancient language (219), the ρ is evasive or $M = 0$.] $p\bar{p}$ CEX and np CEX are also almost equal at $t = 0$; however, at low energies ($\lesssim 5$ GeV/c), the

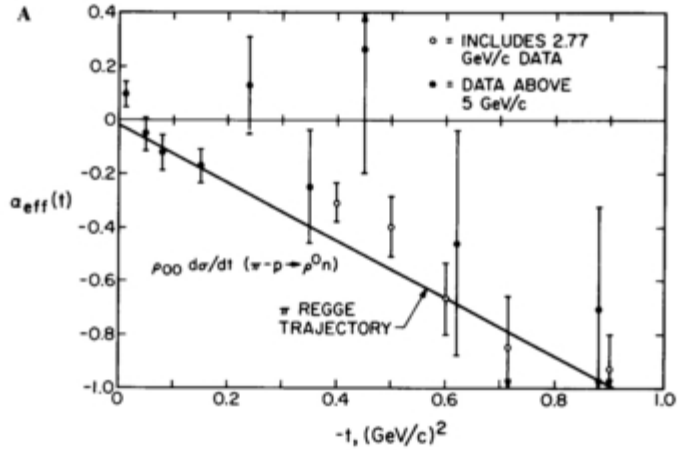

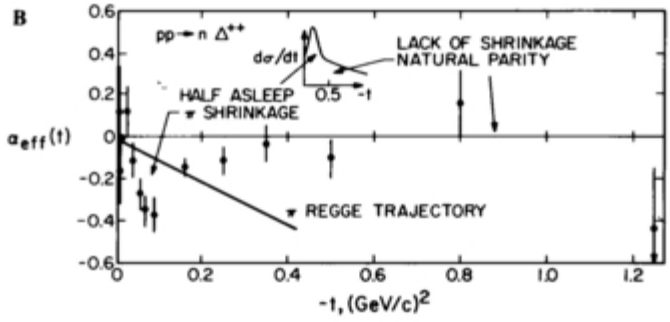

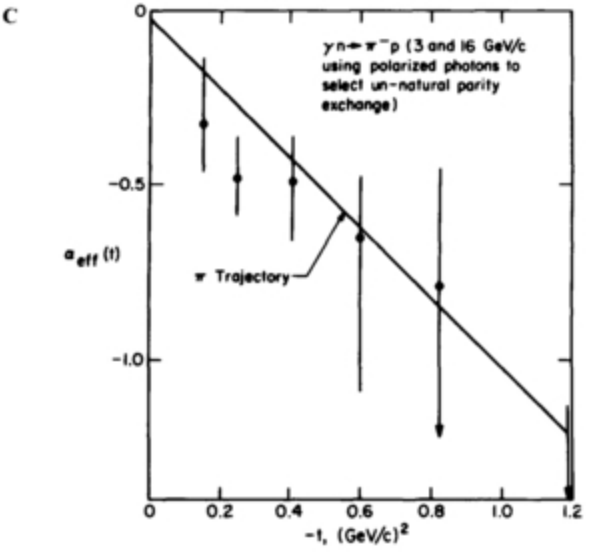

Figures 23a–c Shrinkage? Energy dependence of processes with large π-exchange discussed in section 5F(*ii*). Precisely (*a*) (data from 221) and (*c*) (220) select pure π exchange. Meanwhile, (*b*) (320) is π at small $-t$ and natural parity exchange at large $-t$.

resonance reactions (Figure 24*d–g*) differ at $t = 0$ (225, 227). This inequality is not understood but maybe it disappears at higher energies.

For the resonance reaction this ρ interference effect occurs in the $I = 1$ "crippled π" $\rho_{11}\, d\sigma/dt$ amplitudes which in fact dominate at large $-t$ in the processes listed. One can also examine line reversal breaking in the other amplitudes contributing to resonance production. For instance, for $I = 0$ natural parity exchange seen in $(\rho_{11} + \rho_{1-1})d\sigma/dt$ for $K^+ p \to K^{*+} p$, we have a single $n = 1$ spinflip amplitude and as explained in section 5D(*iv*), this exhibits the well-known "real" greater than "moving phase" systematic (Figure 20D4). The same systematic is also probably exhibited by the pure π exchange $\rho_{00}\, d\sigma\, dt$ for the vector meson production processes; it has not been as carefully studied.

(*iv*) The reactions F1 to F7, G1 to G10 can be used to study $\pi\pi$, $K\pi$, and πN (this as a check on the technique) elastic scattering by Chew-Low extrapolation (Figure 20F3).

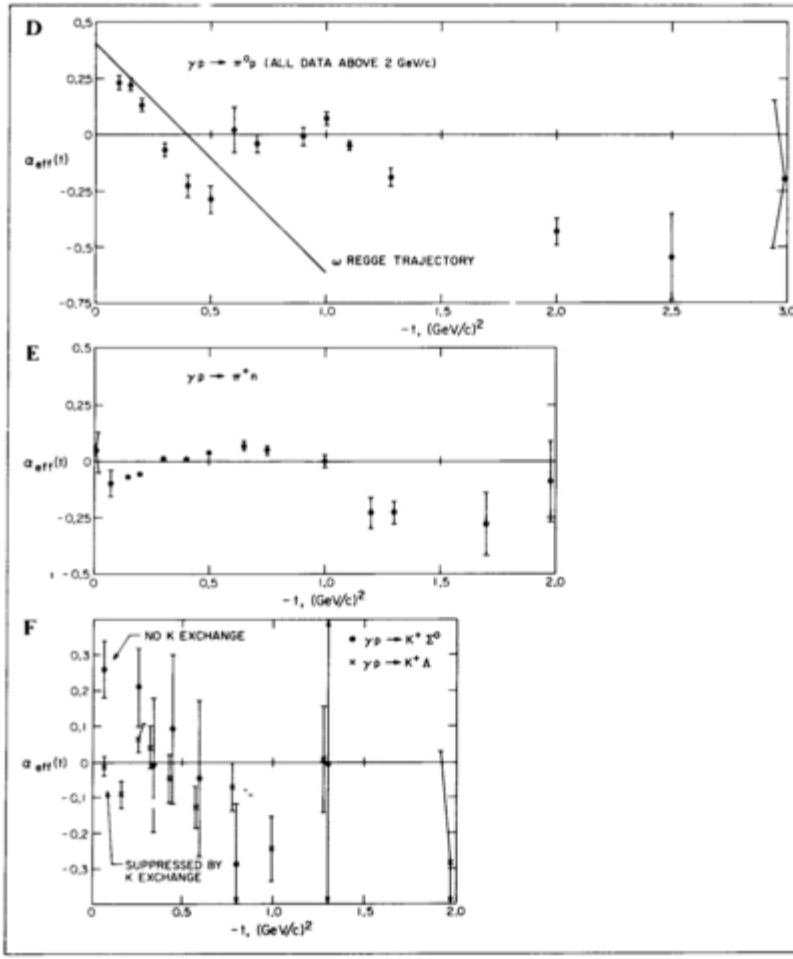

Figures 23d f Shrinkage? Energy dependence of some dominantly natural parity exchange reactions. The graphs are updated from (14) and discussed in section 5F(*ii*).

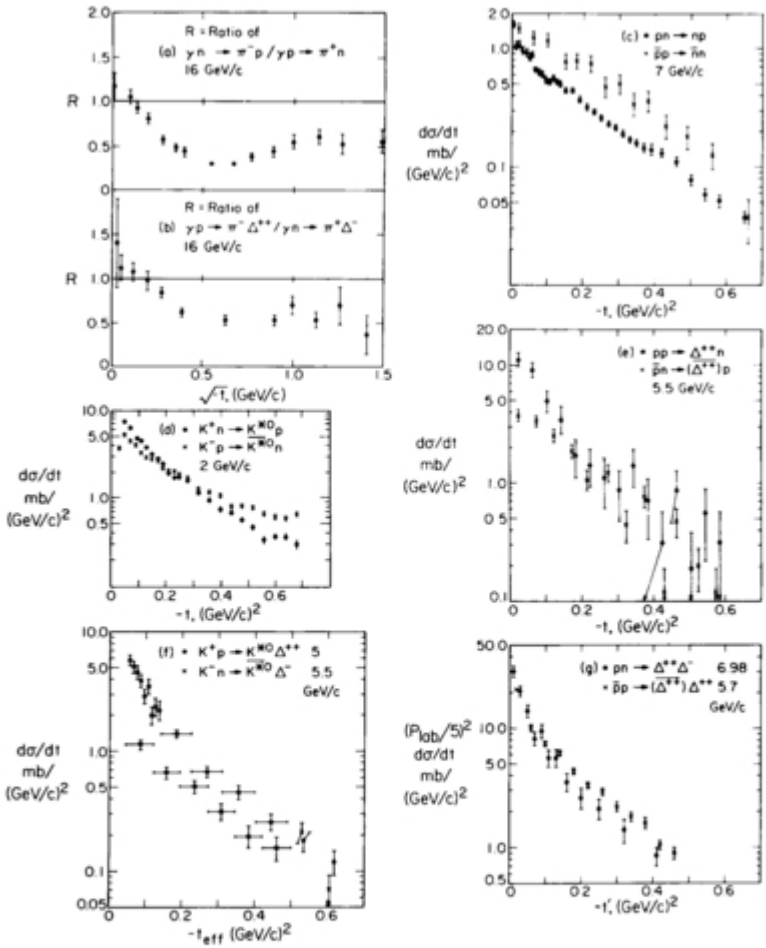

Figure 24 Line reversal breaking discussed in π exchange processes in section 5F(iii). The data are from (*a*) (321), (*b*) (243), (*c*) (322, 323), (*d*) (226), (*e*) (324, 325) similar but less dramatic differences are seen in the 2.8-GeV c data of (326), (*f*) (327, 328), and (*g*) (329, 330).

This has been generally very successful although it has been obscured at times by over-extravagant claims as to the reliability of the method. In principle, the fully fledged reactions F are best because the t in the Born Term (cf. Figure 20F1) suppresses the π exchange in group G reactions and renders it hard to distinguish from other (A_2, ρ) exchanges. However, this advantage (F vs G) can only be realized at high energies because the physical region boundary ($\propto 1/s$ in F, $1/s^2$ in G) keeps one away from the π pole. For instance, to study the spin 2 $[f^0, K^*(1420)]$ region well, one needs lab momentum of 50 GeV/c for group F but only 8 GeV/c for group G. So for established accelerators the latter are preferable (67).

It is important to note that the background (A_2, ρ) exchange *decreases* relative to π exchange as $(K\pi, \pi\pi)$ mass *increases*. This was demonstrated phenomenologically (213) for the 2^- region (cf. ρ, B exchange $\pi^+p \to A_2^0\Delta^{++}$ in reaction group I1) and has been qualitatively explained theoretically in terms of duality and properties of the triple Regge coupling (228). It follows that increasing the energy in group F reaction *will* isolate π exchange by reducing t_{min} and *not* drown it by increasing the A_2 exchange with its higher intercept and hence asymptotic dominance over π exchange (Figure 17 of Ref. 213).

(*r*) It is convenient to mention here that a similar study of $\gamma\pi$ and γK scattering may be possible at high energy in reactions like $\pi^+p \to (\pi^+\pi^0)p$ and $K^+p \to (K^0\pi^+)p$ by "Chew-Low" extrapolation to the photon pole at $t = 0$ (Figure 20F4). The latter dominates at very high energies because its cross section is constant with energy while π exchange falls like $1/p_{lab}^2$ and ω exchange like $1/p_{lab}$ (229). Estimates suggest that the integrated photon exchange contribution to $\pi^+p \to \rho^+p$ will catch up with the strong interaction cross section at $p_{lab} = 200$ GeV/c. Further the photon cross section can be increased by using nuclear targets (230).

5F *Fully fledged* π

(*ri*) The reactions F1 and F3 and $\pi^+p \to \omega^0\Delta^{++}$ (reaction I1) have the imposing total of 20 independent observables to describe the simultaneous decay of the spin 1^- and $3/2^+$ particles. The quark model (34) relates the twelve independent (complex) amplitudes for such a reaction to only five amplitudes. This implies many relations between observables which are strikingly successful (16, 231). More generally, one need only supplement the experimental information by three extra assumptions (the quark model gives many more than this) to do an amplitude analysis for these reactions. This has been attempted (232, 233) but current data do not allow very precise conclusions. For instance, the simple Regge interpretation of (232) must be wrong because of the conspiracy necessary to give the nonzero amplitudes at $t = 0$ seen in the data and predicted by PMA (234). Similar quark tests are successful for the sparse data for F6 (233).

5G *Half-asleep* π

(*rii*) Particularly neat phenomenology of half-asleep reactions was the use of data on $\pi^+p \to \rho^+p$, $\pi^-p \to \rho^0n$ at the *same* energy to isolate the separate contributions of $I = 0$ (h, ω) and $I = 1$ $[\pi, A_2, A_1\ (?)]$ exchanges plus their interference. Use of the

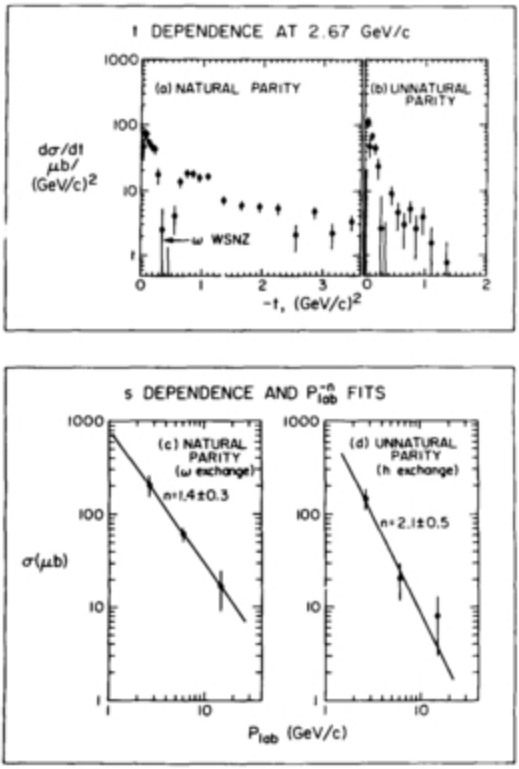

Figure 25 $I = 0$ exchange in $\pi N \to \rho N$ described in section 5G(iii). (*a*), (*b*) t-dependence of natural and unnatural parity exchange at 2.67 GeV c (236). (*c*), (*d*) s-dependence of integrated cross sections (238). To be exact, (*b*) only shows $\rho^1_{00}\, d\sigma\, dt$, not the full $(\rho_{00} + \rho_{11} - \rho_{1-1})d\sigma/dt$ used in (*d*).

ρ density matrix elements (section 3B) allows further separation of each isospin channel into natural and unnatural parity exchange. This analysis (235–239) shows (Figure 25) the following:

(*a*) A break occurs in $\rho^H_{00}\, d\sigma/dt$ for $I = 1$ unnatural parity (π) exchange at

$t \approx -0.4$ (GeV/c)^2—not too far from the canonical spinflip dip of the absorption model. This break is a dip in $\pi^- p \to \rho^- p$ at low energies (235).

(*b*) A dip occurs in $(\rho_{11} + \rho_{1-1})d\sigma/dt$ at $t \approx -0.4$ (GeV/c)^2 for $I = 0$ natural parity (ω) exchange which has already been mentioned in section 5D(*iii*) and is interpreted as an ω WSNZ just as in the related reaction $\gamma p \to \pi^0 p$.

(*c*) The presence of $I = 0$ unnatural parity (h) exchange. The h is the SU(3) partner of the B and so the h amplitude in $\pi N \to \rho N$ can be related to that of the B in $\pi N \to \omega N$. For instance, in terms of the D/F ratio for $(B, h)\, N\bar{N}$ couplings

$$\frac{h \text{ part of } \pi^- p \to \rho^- p}{B \text{ part of } \pi^- p \to \omega^0 n} = \frac{(3F-D)^2}{2(F+D)^2} = 0.18 \qquad 5.3.$$

which is calculated for the accepted value $D/(F+D) = 0.6$ for π couplings. (The ratio for B should be the same by EXD.) At 2.7 GeV/c the experimental ratio is $(140 \pm 30)\,\mu$b/$(500 \pm 50)\,\mu$b which is in fair agreement with equation 5.3. In fact, the latter assumed magic mixing for the B nonet—as suggested by duality (240). On the other hand, if we had used an unmixed B nonet, similar to the π nonet, 0.18 would be replaced by 0.06 with consequent *dis*agreement with experiment. Further, the energy dependence of h exchange (238) is comparable to that of B (241)—as one would expect for a magically mixed nonet. (Both are p_{lab}^{-2} to $p_{lab}^{-2.5}$.)

It would be nice to have a similar analysis for the K^* reactions; partial results have been reported in (242).

(*viii*) The reactions G4, G7, and $\pi^- p \to (\pi^- \pi^-)\Delta^{++}$ are pure π exchange (to the extent that the S-wave dominates low mass $\pi\pi$, $K\pi$ scattering) and so provide a good place to examine it without confusion by natural parity exchange.

(*ix*) As pointed out in (213), reactions G14 are very favorable for meson spectroscopy of the 1^+ nonets because the π exchange should give much cleaner and (relatively) larger cross sections than the usual natural parity exchange (reaction group J).

5H *Crippled* π

(*x*) We did not list in H the many crippled amplitudes (e.g. $2\rho_{11}^H\, d\sigma/dt$ for $\pi^- p \to \rho^0 n$) that can be isolated from half-asleep and fully fledged reactions. Also reactions H2 are only of the standard type if one neglects the $\Sigma - \Lambda$ mass difference (a similar proviso holds for G11).

(*xi*) For these reactions, the Born Term vanishes at $t = 0$; any absorption model will add an additional slowly varying and destructive amplitude to produce the resultant sharp forward peak seen in the data. This is sketched in Figures 20F1 and F5; the PMA model specifies the size of the absorption amplitude exactly; this value agrees with current data to around 10% (67).

(*xii*) It is appropriate to notice here that the reasonably successful vector dominance (VDM) relation between $\gamma N \to \pi N$ (reactions H3) and $\pi N \to \rho N$ (G1) can be understood in terms of the validity of VDM at the π pole and the universal dynamics of π exchange expressed through PMA (122). Similarly its *failure* to relate G13 to F1 correctly at current energies is a simple t_{min} effect which will disappear at higher energies (234, 243).

(*xiii*) The polarization in np CEX has been measured rather well (244, 245); it shows little energy dependence and is large ($\gtrsim 50\%$) at $-t = 0.5$ (GeV/c)^2. It is of philosophical importance because the reaction is truly exotic and so EXD predicts all amplitudes to be real. Thus there can be no polarization. $K^- n \to \pi^- \Lambda$ is also exotic and sizable polarization is observed [see section 5E(*iii*)]; however, this reaction requires SU(3) to prove exoticity. Again $K^+ p \to pK^+$ is an exotic channel (not to be confused with exotic exchange) and polarization is in fact small (246); however, here, the measurements are nowhere near as detailed as in np CEX. Unfortunately, the many amplitudes discourage theoretical interpretation of the np CEX polarization. First, we need some hints from the polarization measurements in the simpler exotic reaction $K^+ n \to K^0 p$.

51 *B and Natural Parity Exchange*

(*i*) Universal acclaim and rightful recognition was first enjoyed by the B meson upon discovery of the $\rho - \omega$ interference effect (201, 247, 248), illustrated in Figure 2011) for the reaction $\pi^+ p \to \rho^0 \Delta^{++}$ where it was first seen convincingly (249). According to standard mass mixing theory (251), the effect depends on $\delta A(\omega)/A(\rho)$ where δ is the off-diagonal element of the ω, ρ electromagnetic mass matrix while $A(\omega), A(\rho)$ are the ω, ρ production amplitudes. δ is best determined from the electromagnetic processes $e^+ e^- \to \pi^+ \pi^-$ which gives $\delta = 4 \pm 1$ MeV (250) or somewhat less reliably theoretically $\gamma A \to (\pi^+ \pi^-) A$ which gives $\delta = 1.8 \pm 0.2$ MeV [R. Marshall cited in (201)]. Figure 2012 illustrates the various $\pi^+ \pi^-$ mass shapes possible with $\delta A(\omega)/A(\rho)$ of modulus 2 MeV and various phases β. The observed dip in $\pi^+ p \to \rho^0 \Delta^{++}$ indicated both $\beta \approx 90^\circ$ and that ρ and ω production amplitudes were rather coherent. This phase is correctly predicted (251) by EXD between π and B, although the magnitude of the B amplitude is underestimated by a factor of 1.5 to 2 by the EXD argument (252).

EXD also makes precise predictions for $\pi^- p \to \rho^0 n$ ($\beta = 270^\circ$ with a bump—see Figure 2012) which is confirmed by data from 2 to 5 GeV/c (248, 253). At the higher energy of 13 GeV/c (254), interference is still seen but it is no longer simply explained by EXD. This failure is probably due to the increasing importance of other exchanges (ρ, A_2). This is not a disaster because the relative phases are all known from EXD while the overall sign of π, B compared with ρ, A_2 is known from the data discussed in section 5F(*iii*). Such an analysis even agrees with the 13-GeV/c experiment but precise statements require use of the density matrix elements of the produced ρ^0 meson to isolate definite exchanges (section 3B); this was attempted in (255) but limited statistics defeated the effort.

The $\rho - \omega$ interference phenomenon provides a unique opportunity to study strong interaction phases and will repay deeper investigation. Further good reactions with different theoretical phases β (e.g. $K^- p \to \rho^0 \Lambda$) where one can study the interference are discussed in (251).

(*ii*) One can also use EXD to relate B exchange in $\pi^+ p \to A_2^0 \Delta^{++}$, $\pi^+ n \to A_2^0 p$, $\pi^+ n \to \phi_s^0(1680) p$, and $\pi^- p \to \pi_s^-(980) p$ to π exchange in $\pi^+ p \to f^0 \Delta^{++}$, $\pi^+ n \to f^0 p$, $\pi^+ n \to g^0 p$, and $\pi^- p \to \varepsilon(\approx 700) n$, respectively. These relations are all good to within a factor of 2 in cross section (213). Reaction 12 ($\pi^- p \to \pi_s^- p$) is particularly

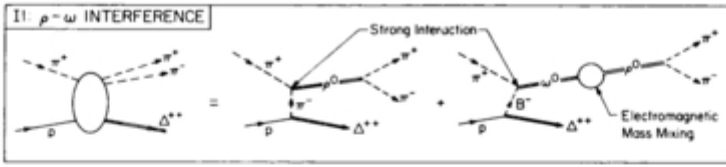

	Reaction	Exchanges
I1	$\pi^+p \to \omega^0\Delta^{++}$	ρ, B
	$\pi^-p \to \omega^0\Delta^0$	
	$\pi^+p \to A_2^0\Delta^{++}$	
	$\pi^-p \to \omega n$	
	$\pi^+n \to \omega p$	
	$\pi^+p \to A_2^+p$	P', ρ
	$\pi^-p \to A_2^-p$	η, B
	$\pi^+n \to A_2^0p$	ρ, B
	$\pi^+n \to \phi_N^0(1680)p$	ρ, B
I2	$\pi^-p \to \pi_N^-(980)p$	B, η
I3	$\gamma p \to \pi^0 p$	ω, ρ
	$\gamma n \to \pi^0 n$	h, B
	$\gamma p \to \eta p$	
	$\gamma p \to \eta' p$	
I4	$\pi^-p \to \omega N^{*0}(\text{many})$	ρ, B
	$\pi^-n \to (\rho\pi)^-p$	

I2: $\rho^0 \to \pi^+\pi^-$ Mass Spectrum (β is Relative Phase of ω and ρ Production)

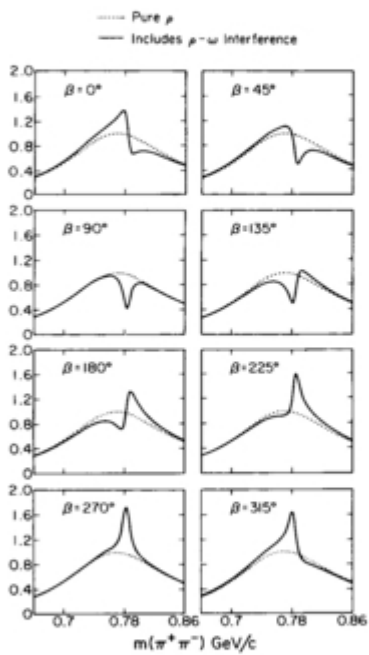

Figure 201 B and natural parity exchange: (*I1*) $\rho-\omega$ interference diagram. (*I2*) Shape of $\pi^+\pi^-$ mass spectrum in the ρ region for various relative phases β for ω and ρ production [section 5II(i)].

interesting because it has no additional natural parity exchange (as π_V is spin 0^+).

(*iii*) We have already remarked in section 5F(*ii*) that the π A_2 exchange ratio increases as we move from $1^-(\rho)$ to $2^+(f^0)$ production. By EXD, the same is true for the B/ρ ratio; correspondingly, $\pi^+ p \to A_2^0 \Delta^{++}$ and $\pi^+ n \to A_2^0 p$ are dominantly unnatural parity exchange (213).

(*iv*) B exchange, studied in $\rho_{00}\, d\sigma/dt$ for $\pi^+ n \to \omega^0 p$, has been shown to decrease with an $\alpha_{\text{eff}} \approx 0$ to -0.3 at $t = 0$ (241). This is not unreasonable for a B Regge trajectory either with canonical slope 0.9 [$\alpha(0) \approx -0.35$] or passing through the $\pi[\alpha(0) \approx 0, \alpha'(0) \approx 0.65]$. This was discussed further in section 5G(*vii*).

(*v*) The data on reaction 13 are particularly good. ω exchange dominates (due to Clebsch-Gordon factors) $\gamma N \to \pi^0 N$ and has already been mentioned [section 5D(*iii*)]. According to naive expectation, this ω exchange reaction should be very similar to the ρ exchange reaction $\pi^- p \to \pi^0 n$. Both have a dip around $t \approx -0.5$ $(\text{GeV/c})^2$; however, although $\gamma N \to \pi^0 N$ has some shrinkage, it is nowhere near as much as in $\pi^- p \to \pi^0 n$ especially for $-t > 1$ $(\text{GeV/c})^2$. [See Figure 23*d*.] This difference cannot be explained in current theories (14, 123). In fact, the major theoretical difficulty with all photoproduction processes [see (256) for the latest review on this] is that although they show more or less canonical shrinkage for $-t \gtrsim 0.5$ $(\text{GeV/c})^2$ (cf. Figure 23*d*–*f*) where two natural parity dominated reactions $\gamma p \to \pi^0 p$, $\gamma p \to K^+ \Sigma^0$, both shrink for small t; this disappears at large $-t$ where a "universal" $e^{bt} P_{\text{lab}}^{-2}$ behavior sets in. This contrasts (16, 67) with strong interactions which shrink at all t values.

$\gamma p \to (\eta, \eta')p$ are, on the other hand, dominantly ρ and B exchange. They are kinematically very similar to $\rho_{11}\, d\sigma/dt$ for $\pi N \to \omega N$; like the latter reaction they show no ρ WSNZ at $t \approx -0.6$ $(\text{GeV/c})^2$ even if the natural parity component is extracted. According to folklore, this lack of a WSNZ [also seen in the nonequality of $\gamma n \to \pi^- p$ and $\gamma p \to \pi^+ n$ at $t \approx -0.6$ $(\text{GeV/c})^2$] follows because ρ is dominantly in the non-Regge $n = 0$ and 2 amplitudes. There is some evidence that the usual P_{lab}^{-2} behavior does not apply to $\gamma N \to \eta N$ (256, 257).

(*vi*) Just as in $\pi N \to \rho N$ [section 5G(*viii*)], one can use data on $\pi^- p \to A_2^- p$, $\pi^+ n \to A_2^0 p$ to isolate the separate $I = 0$ and 1 exchanges (92). As described in section 5I(*ii*), $I = 1$ exchange is dominantly unnatural parity B. For $I = 0$, we have a reversal of roles; unnatural parity (η) exchange is still lost in the sea of statistical errors while a virile f^0 exchange dominates the reaction. At least that's what one would have thought: f^0 exchange lives in our fairyland spinflip amplitude [section 5D(*iii*)] where all Regge dreams come true. Indeed at 5 GeV c, the $I = 0$ $\pi N \to A_2 N$ cross section has just the right size and shape for f^0 exchange (213); however, the energy dependence of the data is wrong and is suggestive of Pomeron dominance at higher energies (11, 92).

(*vii*) Finally we recall that it may be possible to study $f^0 - A_2$ interference in their mutual $K\bar{K}$ decay (258–260). The dominance of unnatural parity exchange in, say, $\pi^+ n \to (A_2^0, f^0)p$ and EXD should lead to even *more* amplitude coherence than seen in $\rho - \omega$ interference.

5J *Natural and Unnatural Parity Exchange without π, K Poles*

These reactions are characterized by allowing both parities to be exchanged but not a 0^- particle. Thus unnatural parity exchange is both suppressed and in a segment of which we have essentially no theoretical understanding. The whole subject was reviewed very recently in (182) and (213), and we refer the reader there for more details and explicit references.

(*i*) There are good data on $\pi^+ p \to B^+ p$ and these show a surprisingly small natural parity exchange cross section. Both the size and shape (it looks like a spinflip not the expected nonflip amplitude) are consistent with an extra t factor in the other-

	Reaction	Exchanges
J1	$\pi^+ p \to B^+ p$	ω, A_2
	$\pi^- p \to B^- p$	π, h
J2	$\pi^+ n \to D^0(1285)\, p$	π, A_2
	$\pi^- p \to D^0(1285)\, n$	
	$\pi^+ p \to D^0(1285)\, \Delta^{++}$	
	$\pi^- p \to Q^0 \Lambda$	K^*, K^{**}
	$K^- n \to B^- \Lambda$	K, Q
	$K^- n \to A_1^- \Lambda$	
	$K^- p \to D^0(1285)\, \Lambda$	
J3	$K^- p \to L^0 n$	A_2, ρ π, B
J4	$\pi, KN \to$ ($1^+, 2^-$ ..meson) N, Y, Δ, Y*	· · ·

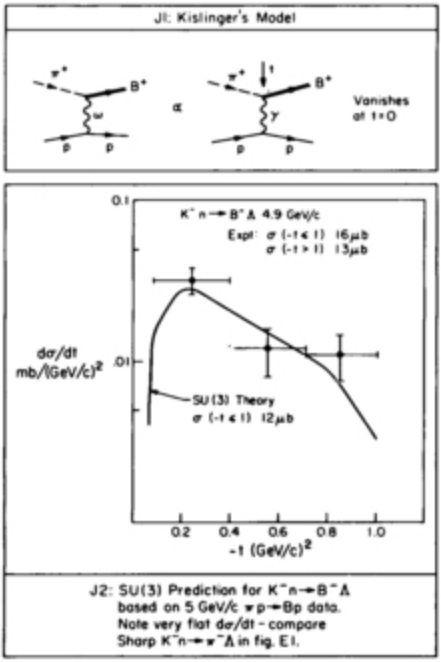

Figure 20J Natural parity exchange plus unnatural parity with no π, K poles: (*J1*) Kislinger's Model (261). (*J2*) Typical successful SU(3) prediction (213) for $K^- n \to B^- \Lambda$ from $\pi^+ p \to B^+ p$ data at same energy.

wise dominant nonflip amplitude. This factor is predicted in Kislinger's (261) generalization of the photon-vector meson exchange model (Figure 20J1).

(*ii*) There are many SU(3) relations between reactions in J1 and J2 which work quite reasonably (Figure 20J2). However, many of the predicted values (in particular, those involving the elusive nondiffractive A_1 production) are too small to be reliably identified in existing experiments. The data and hence our knowledge of 1^- meson spectroscopy should improve quite soon. The hypercharge exchange $\pi N \to QA$, $KN \to (A, B, D, h)(\Lambda, \Sigma)$ reactions are probably best for such studies as there is little background from competing channels with larger cross sections.

5K *Nondiffractive Coherent Deuteron Reactions*

This is a quiet backwater of conceptually beautiful reactions that limited statistics have prevented from telling us anything really new about reaction mechanisms. $I = 0$ exchange (ω, f^0, h, η) exchange is picked out and accordingly natural parity exchange dominates. The cross section is thus a curious combination of a t factor from the spinflip PV coupling and the sharp (e^{20t}) falloff of the deuteron wave function [see Figure 20K1 from (262)]. Best studied is $Kd \to K^{*-}(890)d$ which shows (263) an overall energy dependence, $\alpha_{\text{eff}}(0) \approx 0.33 \pm 0.04$ in agreement with $\omega - f^0$ exchange, plus a bit of unnatural parity exchange whose energy dependence cannot be studied with present statistics. The latter is presumably the h exchange we studied earlier in section 5G(*iii*) from $\pi N \to \rho N$ data. The latter study has

	Reaction	Exchanges
K1	$\pi^+ d \to \rho^+ d$	ω, h
	$\pi^+ d \to A_2^+ d$	P', η
	$K^+ d \to K^{*+}(890) d$	P', ω
	$K^- d \to K^{-*}(890) d$	η, h
	$K^- d \to K^{-*}(1420) d$	
	$\gamma d \to \pi^0 d$	ω, h

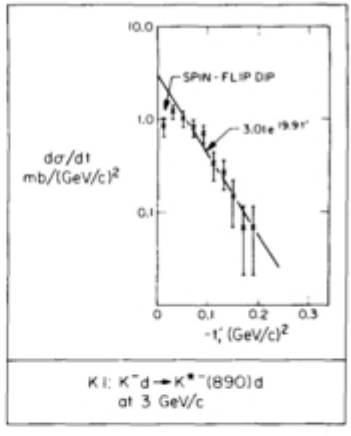

Figure 20K Coherent nondiffractive deuteron reactions: (*K1*) $d\sigma/dt$ for $K^- d \to K^{*-}(890) d$ at 3 GeV/c (262).

intrinsic difficulties coming from the necessity of subtracting cross sections to isolate $I = 0$ exchange. The deuteron data are far cleaner but higher statistics are required to isolate the object of major theoretical interest, i.e. the energy dependence where possibilities range from P_{lab}^{-2} (as for π exchange) to a slope one trajectory through B mass which is $P_{lab}^{-2.8}$. h exchange can be isolated from density matrix elements of the vector meson in $\pi^{\pm}d \to \rho^{\pm}d$, $K^{\pm}d \to K^{*\pm}d$ (section 3B) or using polarized photons in $\gamma d \to \pi^0 d$.

The deuteron data can be successfully predicted (264) from proton and neutron data using standard (Glauber) theory.

5L. *Natural and Unnatural Parity Exchange in Hypercharge Exchange Reactions*

(*i*) A melting pot of sundry poorly measured processes which we should first categorize. Consider reactions L1–L9, which are arranged in order of decreasing importance of natural parity exchange. The reader can find the coupling structure using factorization; at small t, L1 is nonflip, L2–L5 single flip, and L6–L9 double flip; the increasing number of $\sqrt{-t}$ factors thereby decreasing the size of the natural parity exchange.

(*ii*) On the other hand, the importance of unnatural parity exchange increases as we move through the list. The rules governing K (and its EXD friend Q) exchange are:

(*a*) SU(3) implies a very small $p\bar{\Sigma}$ coupling. However, the $p\bar{\Lambda}$ and $p\bar{Y}^*$ couplings are both large. The suppression of unnatural parity exchange for Σ reactions agrees with experiment (265, 266, Figure 20L1).

(*b*) For reactions involving a $p\bar{Y}^*$ vertex, the unnatural parity exchange is particularly apparent because of $\sqrt{-t}$ suppression of the spinflip $p\bar{Y}^*$ natural parity coupling.

(*c*) As discussed in sections 5F(*iv*) and 5I(*iii*), unnatural parity exchange is additionally enhanced over natural parity for 2^- nonet (reactions L10–L12) production.

(*d*) The reactions in L13 have *no* natural parity exchange. SU(3) and EXD relate the processes – successfully but with large errors (213) – to $\pi^- p \to \varepsilon^0(700)n$ [cf. section 5I(*ii*)].

(*e*) It is also possible to exchange the strange partner Q_{A_1} of the A_1 and its EXD friend. However, the quark model (has this ever been badly wrong?) predicts such an exchange to have the same D/F ratio as nonflip V, T exchange, i.e. such an exchange would have similar $\bar{p}\Sigma$ and $\bar{p}\Lambda$ couplings. To the extent that there is no evidence for unnatural parity exchange in any Σ reaction, it follows that there is also no evidence for A_1 nonet exchange in these reactions. This can be compared with studies (267) of $\pi^- p \to \pi^+ \pi^- n$ near $t = 0$ which showed no A_1 exchange and with polarization (268) in $\pi^- p \to (\pi^0\pi^0)n$ which indicated some. The latter data deserves confirmation. Theoretical fits (269, 270) to reactions L2, L3 needed Q_{A_1} exchange but the expected D/F was not enforced; it is possible that the Q_{A_1} in these analyses just reflects an oversimplified parameterization of $K-Q$ exchange.

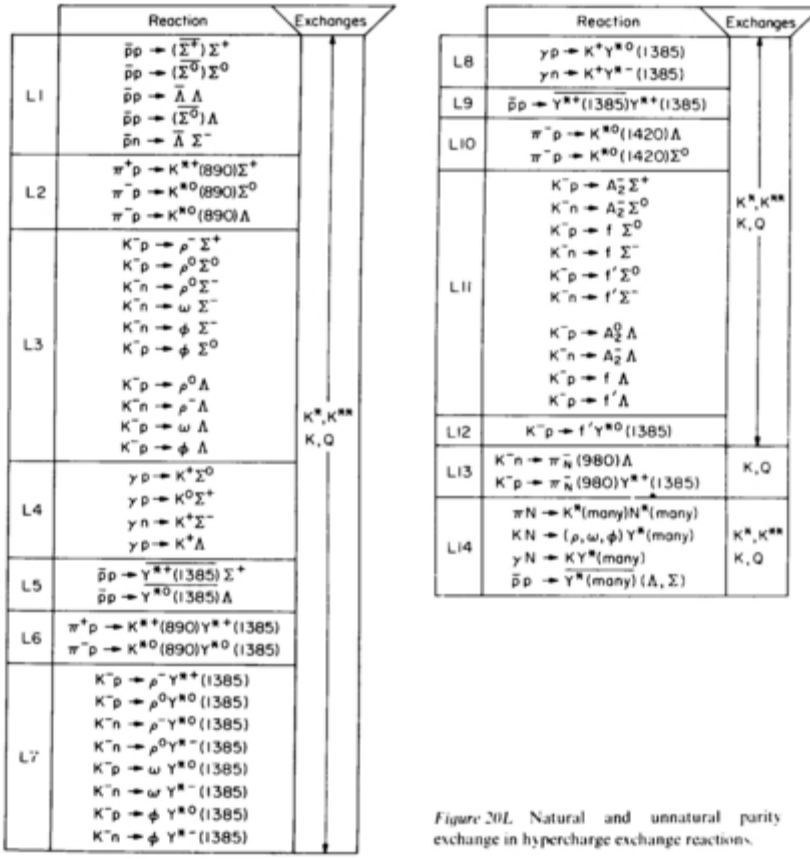

Figure 20L Natural and unnatural parity exchange in hypercharge exchange reactions.

For instance, the observed Λ polarization in $K^-p \to \omega\Lambda$, after unnatural parity exchange has been selected using ω density matrix elements, only implies Q_A exchange if SU(3) is used (neglect $p-\Lambda$ splitting) to restrict $K-Q_B$ exchange to a single $\bar{p}\Lambda$ helicity state. Perhaps this is not reliable.

Experimentally it would be nice to study unnatural parity exchange in Σ reactions particularly in the enhanced reaction L10–L12. Again it would be important to

confirm the small unnatural parity exchange in $\pi^- p \to K^{*0}\Sigma^0$ which is in fact seen in the first bin of Figure 20L1.

(*iii*) There are polarization and even correlation data for the $\bar{p}$ reactions L1, L5, L9. However, the complicated amplitude structure and pauce data have discouraged

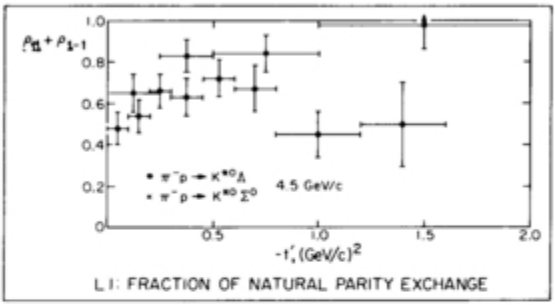

L1: FRACTION OF NATURAL PARITY EXCHANGE

L2: AMPLITUDE ANALYSIS

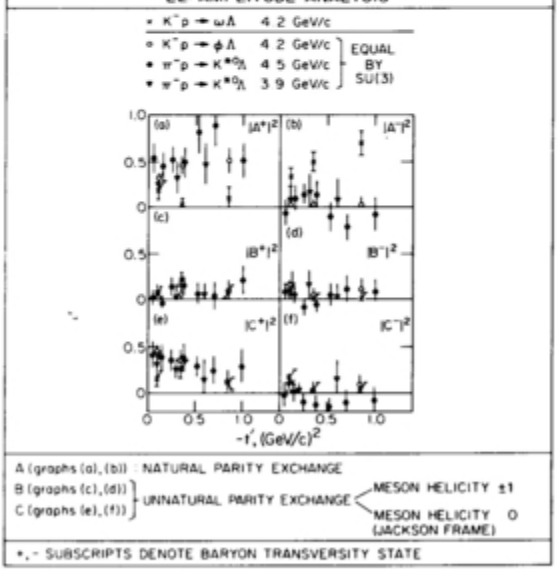

A (graphs (a), (b)) : NATURAL PARITY EXCHANGE

B (graphs (c), (d)) } UNNATURAL PARITY EXCHANGE — MESON HELICITY ±1

C (graphs (e), (f)) } UNNATURAL PARITY EXCHANGE — MESON HELICITY 0 (JACKSON FRAME)

+, − SUBSCRIPTS DENOTE BARYON TRANSVERSITY STATE

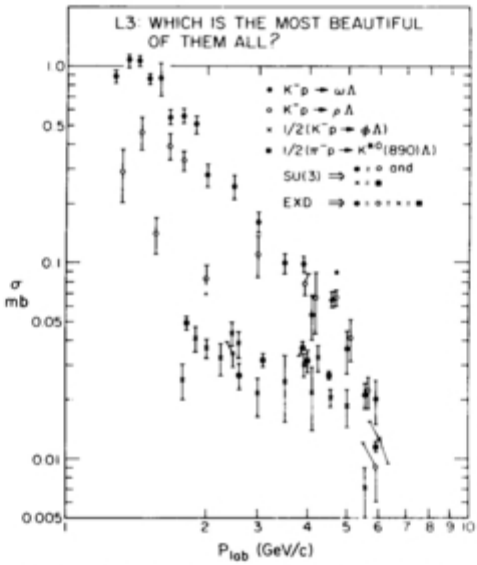

Figure 20L 1-3 Natural and unnatural parity exchange in hypercharge exchange reactions: (*L1*) Fraction of natural parity exchange in $\pi^- p \to K^{*0}(890)\,(\Lambda, \Sigma^0)$ at 4.5 GeV/c (266) discussed in section 5L(*ii*). (*L2*) Amplitude analysis (271) for $\pi^- p \to K^{*0}(890)\,\Lambda$, $K^- p \to (\omega, \phi)\,\Lambda$ discussed in section 5L(*iv*). (*L3*) Comparison of reaction cross sections for $K^- p \to (\rho, \omega, \phi)\,\Lambda$, $\pi^- p \to K^{*0}(890)\,\Lambda$ discussed in sections 5L(*iv*) and (*v*) with data from (265, 266, 272, 297).

authoritative theoretical statements. An attempt to relate Λ polarization in $\pi^- p \to K^0\Lambda$ and $\bar{p}p \to \bar{\Lambda}\Lambda$ was given by Michael (11). Michael also suggests qualitative relations between, say, polarization in $\pi^- p \to K^{*0}\Lambda$ and $\pi^- p \to K^0\Lambda$ by assuming that natural parity exchanges have the same modifications of the Regge phase in each reaction. These predictions disagree with experiment but offhand this is not surprising as the basic assumption isn't valid in any absorption model. The situation is muddied somewhat as the assumption *does* give a correct relation between $\pi^- p \to \pi^0 n$ and $\gamma p \to \pi^0 p$ polarization (11).

(*iv*) Observation of the joint decay distribution is possible in reactions L2, L3 using the weak decay of the hyperon. This gives all but one of a complete set of observables. The work of Field and collaborators (271) is very encouraging. SU(3) predicts the equality $K^- p \to \phi\Lambda = \pi^- p \to K^{*0}\Lambda$ while EXD further states that both are equal to

$2(K^- p \to \omega\Lambda)$. The amplitude analysis shown in Figure 20L2 showed that the first equality is valid amplitude by amplitude; the last equality is, however, badly violated not only in magnitude, $d\sigma/dt$, but also in amplitude structure. This argues that the EXD violations seen [sections 4E, 4F, 5E(*ri*)] in hypercharge exchange reactions are not simply due to SU(3) violations (e.g. to predict $K^- n \to \pi^- \Lambda$ to be real needs SU(3)+EXD; the observed polarization is then a consequence of EXD not SU(3) violation). This is spectacularly illustrated in Figure 20L3. Supplementing the experimental observables by additional assumptions, they were able (271) to find the individual amplitudes; in particular, they suggest that the $n = 2$ amplitude in $K^- p \to \omega\Lambda$ is indeed real and so suffered little absorption. This important conclusion [natural in most models (2) except the dual absorption model (31)] deserves confirmation by higher statistics data. It is apparent from Figure 20L2 that the most difference between $K^- p \to \omega\Lambda$ and $\phi\Lambda$ occurs in the natural parity exchange segment; this is also a bit surprising as one would have expected it and not the low-lying (in J plane) unnatural parity exchange to agree best with theoretical expectations (EXD).

(*r*) In fact, the reader will by now be bored to hear that these reactions exhibit exactly the same systematic in line reversal breaking; "real" reactions $[K^- p \to (\omega, \rho)\Lambda]$ are greater than "moving phase" $(K^- p \to \phi\Lambda,\ \pi^- p \to K^{*0}\Lambda)$ reactions as found in section 5D(*ir*). The production cross section comparison is summarized in Figure 20L3; if you select definite exchange, then just as in $K^- p \to K^{-*} p$ [see section 5D(*ir*)], one finds more breaking for natural than unnatural parity exchange (213). We can note again, just as in Figure 18, that the suppressed reactions $(\phi\Lambda, K^{*0}\Lambda)$ have a higher threshold than $\omega\Lambda$, $\rho\Lambda$ and so must be lower at low energy. Perhaps the observed violation at 4 GeV/c is connected with this.[25]

(*ri*) It is possible to use SU(3) and vector dominance $\gamma = \rho + \omega/3 - \sqrt{2}\phi/3$ to predict the amplitudes for $\gamma p \to K^+(\Lambda, \Sigma)$ from those for vector meson production $K^- p \to (\omega, \phi)(\Lambda, \Sigma)$; this unfortunately predicts the photon data to be a mixture of real and rotating phases and one can only say that the sign of the polarization and the size of $d\sigma/dt$ for $\gamma p \to K^+(\Lambda, \Sigma^0)$ are in reasonable accord with expectations (11). Note that K exchange is important at small t in $\gamma p \to K^+\Lambda$ but its effect falls with energy compared with the dominant K^*, K^{**} exchange. This produces a noticeable effect on $\alpha_{eff}(t \approx 0)$ for the two processes, i.e. that for Λ lies lower than that for Σ^0 (see Figure 23*f*).

(*rii*) There are of course many quark model relations (34) for the class L reactions. First, we have the double correlation relations for $\bar{p}p \to \bar{Y}^* Y^*$, $K^- p \to \rho Y^*$, etc.; the SU(3) analogs of those for $\bar{p}p \to \bar{\Delta}^{++}\Delta^{++}$ and $\pi^+ p \to \rho^0 \Delta^{++}$. Current data do not provide stringent tests, but the nice data of (272) showed pleasing agreement between theory and experiment.

Secondly, there are the quark model relations following from the equality of the

[25] Such ideas cannot directly explain difference between $K^+ n \to K^0 p$ and $K^- p \to \bar{K}^0 n$ which have the same threshold. Nevertheless, there is a lot of difference between low energy $K^- p$ and $K^+ n$ scattering, i.e. in unitarity effects.

PV (e.g. πK^*), $B\bar{B}$ spinflip (e.g. $N\bar{\Lambda}$), and $B\bar{D}$ (e.g. $P\bar{\Upsilon}^*$) vertices. These only worked to a factor of 1.5 to 2 for the similar $B\bar{B}$ to $B\bar{D}$ nonstrange exchange (ρ, A_2) relation coupling [section 5D(*ii*)]. A similarly precise statement has not been extracted from the hypercharge exchange data.

Thirdly, there are simple predictions of the quark model D/F values. That for unnatural parity exchange is OK experimentally (i.e. the coupling is roughly zero in Σ reactions as in section 5L(*iia*). There are two D/Fs for natural parity exchange and so it is not possible to relate Λ to Σ reactions directly. However, adding the spinflip $B\bar{B}$ to $B\bar{D}$ relation enables one to write the sum rule (273, 274).

$$\sigma(AN \to B\Lambda) = 3(\sigma(AN \to B\Sigma) + \sigma(AN \to BY^*[1385])) \qquad 5.4$$

for nucleon N and any hadrons A, B.

This is a cavalier approach because it is sensitive to kinematic factors and breaking of the $B\bar{B}$ to $B\bar{D}$ relation. Anyhow, however you do it, the Σ data is much larger than expected (272, 273). The reason for this is twofold. First, the nonflip $B\bar{B}$ amplitude has a $D/F \approx -0.2$ which does enhance the Σ reactions compared with the quark $D/F = 0$ (265, 275). Secondly, the quark model predicts Σ to have essentially zero t-channel spinflip coupling at $t = 0$ (taking, for definiteness, the t-channel as the additivity frame). Rotating this prediction, it corresponds to comparable Σ and Λ s-channel spinflip amplitudes [section 5D(*ii*)]. Folklore suggests that it is sensible to take the ratio of s-channel (and *not* t-channel) amplitudes at $t = 0$ as a measure of their ratio away from $t = 0$ (i.e. we assume s-channel amplitudes have a universal shape). This simple dynamical effect completely invalidates the application of equation 5.4 away from $t = 0$; nearly all claimed violations of equation 5.4 come from comparing it with data integrated over t and so are irrelevant. An alternate view on the violation of equation 5.4 was given in (274).

The application of equation 5.2, exactly at $t = 0$, is extremely interesting because all amplitudes for reactions L2–L13 vanish there for factorizable Regge poles. So examination of the quark relations at $t = 0$ then enables one to check if they are more general than the pole approximation or if they are just symmetries of pole residues. This point is best studied in $\gamma p \to K^+(\Lambda, \Sigma^0)$ where the data (276, 277) are good and t_{min} effects small. The Σ^0/Λ ratio does decrease towards $t = 0$ but, *miserabile dictu*, it is not enough for the quark model. Rather it is in rough agreement with absorption calculations[26] based on poles whose residues obey quark relations.

5M *Exotic Exchange*

(*i*) In this category, we can place all reactions whose quantum numbers forbid the exchange of all known single particle states. As anticipated in section 2, the cross sections are indeed small and fall fast with energy. A representative sample of the data (266, 278–280) is shown in Figures 20M2–M5. First consider the energy dependence of the data: below 2 GeV/c, there is a rapid ($\propto s^{-10}$) fall which is in fact shared by many processes – exotic and nonexotic. Figure 20M2 shows the

[26] G. C. Fox, Unpublished fits and (275).

similarity of K^+p backward scattering at low energy. From 2 to 5 GeV/c, the rate of fall slows—s^{-5} seems typical while there is at present no data above this energy. Now consider the t-dependence: at low energy, we found the Odorico zeros [Figure 8, (45); see also (281) for $K^-p \to \pi^+\Sigma^-$]. These have not been reported above 2 GeV/c. Rather, around 5 GeV/c, the data exhibit a definite peak with a rather flat (e^{4t}) behavior. It is worth noting explicitly that although $K^-p \to K^-p$ has a backward peak at 5 GeV/c (280 and Figure 20M2), it has a backward dip below 2.5 GeV/c (282).

(*ii*) Theoretical models (Figure 20M1) include double scattering or equivalently Regge-Regge cuts (64, 65, 283–289), exotic exchange, s-channel effects (290), and reflection mechanism (291).

(*iii*) The Regge-Regge cut model naturally reproduces the t-dependence observed at 5 GeV/c: it predicts energy dependence[27] $\sigma \propto s^{2\alpha-2}$ where Quigg (65) finds $\alpha \approx \alpha_{\text{cut}} - \frac{1}{2}$ where $\alpha_{\text{cut}}(0) = \alpha_1(0) + \alpha_2(0) - 1$, for exchange of trajectories α_1 and α_2, is the tip of the cut. It is clear from Figures 20M3 and 20M4 that data below 5 GeV/c must be due to some other mechanism. It is worth noting that (even at 5 GeV/c) $\pi^+p \to K^+\Sigma^+$, $K^-p \to K^-p$, $\bar{p}p \to \bar{p}p$, and $\bar{p}p \to K^+K^-$ all have similar size exotic peaks. This equality is rather surprising theoretically. For instance, one naively expects

$$\frac{\sigma(\bar{p}p \to p\bar{p})}{\sigma(\pi^-p \to K^-\Sigma^+)} \approx \frac{\sigma(\bar{p}p \to \pi^0\pi^0)^2}{\sigma(\pi^-p \to \pi^0 n) \times \sigma(\pi^0 n \to K^+\Sigma^-)} \ll 1$$

References (65) and (289) emphasize that this argument ignores important spin effects. However, Figure 20M4 shows that the model is unable to account for the experimental difference between $K^-p \to \pi^+\Sigma^-$ and $\pi^-p \to K^+\Sigma^-$.

(*iv*) The resonance reactions M5 exhibit large exotic exchange. $\pi^-p \to \pi^+\Delta^-$ is ≈ 45 μb at 4 GeV/c (292) and $\pi^-p \to K^+Y^{*-}$ (1385) roughly $\frac{1}{2}$ μb at 5 GeV/c (266). These large values may be due to a reflection mechanism proposed by Berger (291, 293) and calculated in the latter case by Sivers & Von Hippel (294). Note that if one includes final state interactions (between π^- and n in Figure 20M1) the reflection model becomes equivalent to the double scattering model plus the remark that cross sections involving π exchange are particularly large.

(*v*) Figure 20M3 indicates that the statistical calculation of Frautschi (290) qualitatively reproduces backward K^-p scattering. It cannot explain the similarity of K^+p at low energy because K^+p is predicted to be zero as there are no resonances.

(*vi*) Exotic exchange can also be found by comparing values of nonexotic reactions (295). For instance, the difference between 2 ($\pi^-p \to K^0\Sigma^0$) and $\pi^+p \to K^+\Sigma^+$ (reactions E1) measures an $I = 1/2, 3/2$ interference. In principle this is more sensitive than the direct measurement of the $I = 3/2$ amplitude squared in $\pi^-p \to K^+\Sigma^-$. It is more difficult, however, because of normalization and systematic errors in

[27] Such a power law energy dependence with s also given by exchange of an exotic trajectory $\alpha(t)$.

the cross sections being compared. The comparison method, outlined above, used for $\gamma p \to \pi^- \Delta^0$ vs $\gamma n \to \pi^- \Delta^-$ (reactions G13) (243) and $\gamma p \to K^- \Sigma^0$ vs $\gamma n \to K^- \Sigma^-$ (reactions L4) (277) gave a large (10%) of nonexotic) exotic exchange amplitude at 11–16 GeV/c. The SLAC group checked that their extraction of neutron cross sections from deuterium was correct by comparison of $\gamma p \to K^+ \Lambda$ and $\gamma p \to \pi^+ n$ for free protons and those in deuterium.

M1	$K^- p \to p K^-$ $\bar{p} p \to p \bar{p}$ $\bar{p} p \to K^+ K^-$
M2	$\pi^+ n \to \phi p$ $\pi^- p \to \phi n$ $\pi^+ p \to \phi \Delta^{++}$ $\pi^+ n \to f' p$
M3	$\pi^+ n \to \pi^- \Delta^{++}$ $\pi^- p \to \pi^+ \Delta^-$
M4	$\pi^- p \to K^+ \Sigma^-$ $\pi^+ n \to K^0 \Sigma^+$ $K^- p \to \pi^+ \Sigma^-$ $\bar{p} p \to (\bar{\Sigma}^{*0}) \Sigma^-$ $\pi^- p \to K^{*+}(890) \Sigma^-$ $K^- p \to \rho^+ \Sigma^-$ $\pi^- p \to K^+ Y^{*-}(1385)$ $K^- p \to \pi^+ Y^{*-}(1385)$ $\bar{p} p \to \overline{Y^{*-}}(1385) \Sigma^-$ $K^- p \to \pi^+ Y^{*-}$(many) $\pi^- p \to K^{*+}(890) Y^{*-}(1385)$ $K^- p \to \rho^+ Y^{*-}(1385)$ $\bar{p} p \to \overline{Y^{*-}}(1385) Y^{*-}(1385)$
M5	$\bar{K} N \to (K, K^*)(\Xi, \Xi^*)$ $\bar{p} p \to (\Xi, \bar{\Xi}^*)(\Xi, \Xi^*)$

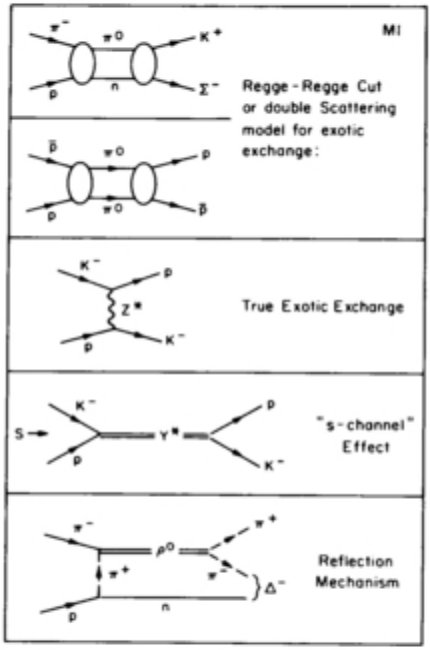

Figures 20M, 20M1 Exotic exchange: (*M1*) Theories for exotic exchange discussed in section 5M(*iii*). (*M2*) Elastic differential cross sections over the whole angular range at 5 GeV/c (280). (*M3*) Comparison of energy dependence for $K^- p$ backward scattering (280) with Regge cut (64) and statistical model (290) calculations for $K^- p$. The latter is calculated at $\theta_{cms} = 180°$ not $u = 0$ like the data but this is not a large effect. (*M4*) Comparison of Regge-cut calculations (65) with $d\sigma/dt$ data on $K^- p \to \pi^- \Sigma^+$ and $\pi^- p \to K^- \Sigma^+$ at $t = 0$. (*M5*) Compilation (279) of cross sections σ for some exotic reactions with results of $\sigma \propto P_{lab}^{\alpha}$ fits.

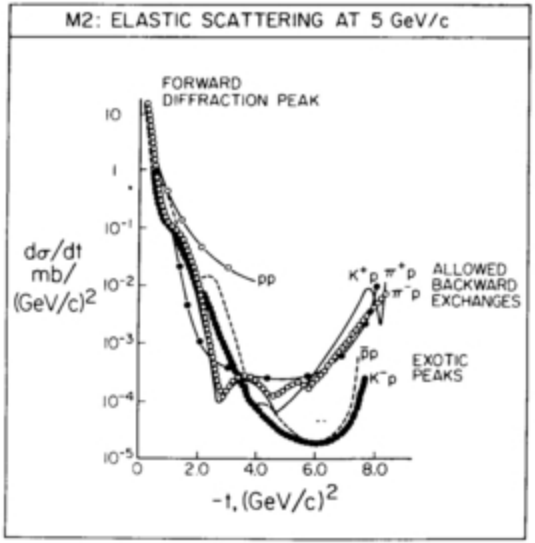
M2: ELASTIC SCATTERING AT 5 GeV/c
FORWARD
DIFFRACTION PEAK
dσ/dt
mb/
(GeV/c)²
pp
K⁺p π⁺p
K⁻p π⁻p
ALLOWED
BACKWARD
EXCHANGES
p̄p
K⁻p
EXOTIC
PEAKS
-t, (GeV/c)²

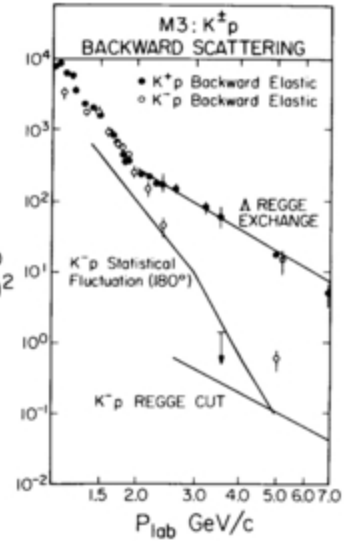
M3: K±p
BACKWARD SCATTERING
K⁺p Backward Elastic
K⁻p Backward Elastic
Δ REGGE
EXCHANGE
K⁻p Statistical
Fluctuation (180°)
K⁻p REGGE CUT
dσ/du|u=0
μb/(GeV/c)²
Plab GeV/c

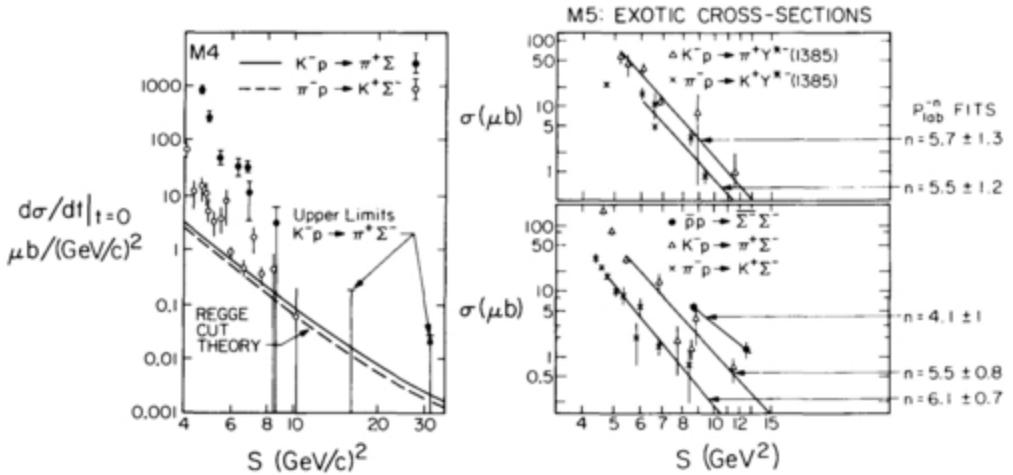

Figures 20M 2–5 Exotic exchange (see legend to Figures 20M, 20M1).

(*vii*) Reactions M2 are only exotic for canonical quark rules (34). A current limit (214) is

$$\frac{\sigma(\pi^+ p \to \phi^0 \Delta^{++})}{\sigma(\pi^+ p \to \omega^0 \Delta^{++})} \leqq 1/330$$

at 3.7 GeV/c.

6 KEY CONCEPTS AND INTRIGUING EXPERIMENTS

The spellbound reader of section 5 will have gained the impression (through repetition) that a number of theoretical ideas stand out as especially important organizers of the experimental systematics. We describe them briefly again, for the particular benefit of the nonspecialist who has not waded through the details of sections 3–5. In addition, we point the way to a modest number of future experiments at intermediate energies which may be expected to clarify several of the questions raised in section 5.

6A Particularly Useful Ideas

As is our custom, we shall neglect to mention Regge theory in our catalog of constructs because acceptance of Reggeism is *sine qua non* for trying to make sense of two-body scattering. Therefore the schemes we outline here are some which are useful adjuncts to the basic Regge pole hypothesis.

Predictive power is what is lacking in the unadorned Regge pole framework. We are rarely able to compute anything from what we might hope to call "first principles," but we can, with great success, relate amplitudes for one reaction to amplitudes for another by invoking internal symmetries, specifically SU(3) and its more detailed incarnation, the quark model. There are no important violations of the conjecture that Regge residues satisfy SU(3) symmetry. The source of the $\approx 20\%$ violations which are common has never been traced satisfactorily. For resonance decays, all deviations of partial widths from the predictions of SU(3) are understood in terms of kinematic effects. (In other words, apart from mass splittings within SU(3) multiplets, there are no sizable deviations from SU(3) symmetric behavior.) Attempts to make similar kinematic excuses for the deviations from SU(3) for scattering amplitudes have been too casual to settle the issue. The quark model has no qualitative failures, neither for the hadron spectrum nor for selection rules, nor indeed for the relative magnitudes of couplings. At the same level, predictions for the spin structure of amplitudes deduced from the quark model are successful as well. The quark model thus poses a two-pronged challenge; it cries out for experimental obstacles and for theoretical understanding.

Exchange degeneracy provides line reversal relations, predictions for t-dependence of cross sections (by the occurrence of nonsense wrong signature zeros), and, especially when coupled with the quark model in duality diagrams, predictions for relative and absolute phases of scattering amplitudes. In most cases line reversal predictions are roughly satisfied and in the pair of reactions for which the data seem most credible (KN charge exchange), line reversal symmetry seems well-

satisfied above 10 GeV/c. Nonsense dips seem to occur, as prescribed, in all but (s-channel) nonflip amplitudes. The phase predictions are in general successful: the amplitude for $K^- n \to K^0 p$ does seem to be real, π exchange and B exchange are 90° out of phase in $\pi N \to (\rho, \omega)\Delta$, the polarization in $K^- p$ elastic scattering suggests a Regge pole contribution to the flip amplitude proportional to $\exp[-i\pi\alpha_\rho(t)]$, etc. Much less successful are predictions of the absence of polarization in inelastic reactions which are based on the requirement that all spin amplitudes should have exactly the same phase. (Inability to account for polarization naturally in the archetypal Regge reaction, $\pi^- p \to \pi^0 n$, was a chink in the Regge armor long before exchange degeneracy was invoked.)

The physical basis of absorption models seems almost unimpeachable, and examples exist (see section 4B,F; section 5F,G,H) of strong circumstantial evidence for absorptive effects, but there is no successful quantitative implementation of the absorption scheme. Four years ago, absorptive corrections were heralded as solutions to all the woes of Regge phenomenology. The early enthusiasm has gone unrewarded by spectacular results, but the idea on which hopes were based retains its appeal. In fact, there has been renewed theoretical interest[28] in calculating Regge cuts (absorption effects) using the triple Regge techniques[29] developed to study inclusive reactions. So far the only practical application has been to the evaluation of the Glauber correction (198), but one can anticipate that the union of the Gribov calculus[28] with triple Regge phenomenology will lead to a better understanding of cuts.

The study of inclusive reactions as a function of s and x may be likened to total cross section phenomenology.[29] In the same analogy, triple Regge studies correspond to $d\sigma/dt$, density matrix, and polarization. Independent of theoretical breakthroughs, we must expect the triple Regge couplings, extracted from detailed analysis of inclusive data, to exhibit the same wealth of structure section 5 detailed for two-body scattering.

6B Experiments of Future Interest

Although we display the obligatory reviewer's hubris by enumerating our favorite list of essentially impossible experiments which will tell us everything we need to know,[30] we shall keep the shopping list mercifully short. Many specific suggestions will be found midst the flood of information in sections 4 and 5, so here we concentrate on slightly bizarre experiments which lie just beyond present-day experimental capabilities.

Let us contemplate the possibilities for experiments with a polarized HD target.[31]

[28] There is no comprehensive review: see the many talks at the 1972 Batavia Conference (296).

[29] For the nonexpert, we remark that the triple Regge coupling is that between three Regge poles whereas two-to-two scattering processes are analyzed in terms of couplings of one Regge pole and two particles.

[30] Or at least everything we know we need to know.

[31] Such targets exist in the low-temperature lab (E. Graf, Private communication) and will someday soon (we hope) find their way onto the accelerator floor.

Beyond improving polarization measurements for the two-body reactions already studied (by improving the dilution factor), targets free of complex nuclei open new experimental vistas. For example, the information to be gained from now impractical two-body reactions such as[32] forward

$$n + \vec{p} \to n + p \qquad 6.1.$$

could be extracted from

$$p + \vec{d} \to p + n + p_s \qquad 6.2.$$

One can also hope to make precise measurements of the polarization in reactions for which, according to duality diagrams, the scattering amplitudes should be purely real, such as

$$K^+ \vec{n} \to K^0 p \qquad 6.3.$$

In the absence of complex target nuclei, it will also be possible to study (107) quasi two-body or authentic multibody final states, among which

$$\pi^- \vec{p} \to \pi^0 \pi^0 n \qquad 6.4.$$

and

$$\pi^- \vec{p} \to \rho^0 n \qquad 6.5.$$

can clarify the role of A_1 exchange. In reactions such as

$$\pi \vec{N} \to K Y^* \qquad 6.6.$$
$$\hookrightarrow \pi Y$$
$$\hookrightarrow \pi N$$

one can go far toward measuring directly *all* of the participating amplitudes.

Recently constructed hyperon beams may be used to perform diffraction dissociation experiments in which background problems are substantially reduced. Good signal-to-background ratios seem to make these experiments appealing in spite of the relatively low flux of hyperons. Since Σ^- beams exist at Brookhaven and CERN, we will give examples appropriate to them, but it will be obvious that a Λ beam, for example, would serve equally well.

The reactions

$$\Sigma^- p \to Y_1^{*-} p \qquad 6.7.$$

are SU(3) analogs of the already studied reactions

$$pp \to N^{*+} p \qquad 6.8.$$

Corresponding to the prominent N^* peaks

$N^*(1518)$ $3/2^-$ $\Gamma \approx 105$ to 150 MeV
$N^*(1688)$ $5/2^+$ $\Gamma \approx 105$ to 180 MeV

[32] We denote polarized particles by a superior arrow.

in reactions 6.8, reaction 6.7 should exhibit

$\Sigma(1670)$ $3/2^-$ $\Gamma \approx 50$ MeV
$\Sigma(1915)$ $5/2^+$ $\Gamma \approx 70$ MeV

which should be relatively easier to establish, due to their narrower widths. Even in a missing mass experiment, therefore, it may be possible to obtain more reliable production angular distributions for equation 6.7 than for equation 6.8. The important potential advantage of channel (6.7) lies in the measurement of decay angular distributions of the Y^*s. Both Y^*s (probably) decay appreciably into $\bar{K}N$, as well as into the $\pi\Lambda$, $\pi\Sigma$, and $\pi\pi\Sigma$ channels which are likely to be complicated by Deck background. In particular, the sequence

$$\begin{array}{l} \Sigma^- p \to Y_1^{*-} p \\ \qquad\quad \hookrightarrow \pi^- \Lambda \\ \qquad\qquad\quad \hookrightarrow p\pi^- \end{array} \qquad 6.9.$$

which, for narrow Y_1^{*-}, should be distinguishable from nonresonant (Deck) background, contains very detailed information about the Y_1^* decay angular distribution which in turn has much to say about the diffractive production process. If reaction 6.9 is feasible, it should be an exceptionally clean experiment by which to elucidate the detailed dynamics of diffraction dissociation.

How large will the cross sections be? If the Pomeranchuk trajectory were a pure SU(3) singlet, we would have

$$(d\sigma/dt)[\Sigma^- p \to \Sigma(1670)p]_{\text{Pomeranchuk}} = (d\sigma/dt)[pp \to N(1518)p]_{\text{Pomeranchuk}}$$

and

$$(d\sigma/dt)[\Sigma^- p \to \Sigma(1915)p]_{\text{Pomeranchuk}} = (d\sigma/dt)[pp \to N(1688)p]_{\text{Pomeranchuk}}$$

Similar remarks apply to the meson (e.g. ω) exchange contributions. These crude estimates suggest that at 10 GeV c the forward differential cross section for equation 6.7 should be comparable to those (189) for the corresponding N^* reactions [0.5–5 mb/(GeV/c)^2].

7 OUTLOOK

We see no immediate danger that two-body reaction mechanisms will become completely understood and relegated to a Handbuch on a dusty shelf. Developments of the past three years convince us that a description of two-body reactions at intermediate energies is unlikely to be simple in detail, however neat the broad outlines of a future theory seem. More than a sign of resignation, amplitude analysis is a recognition that nature is less simple (and perhaps more intricately fascinating) than had been hoped in earlier days. Progress is therefore likely to follow detailed and difficult experiments which map out amplitude structure and present us with (we can only hope) more systematic systematics.

Looking ahead to studies of two-body reactions at the higher energies of the Serpukhov and Batavia machines, we anticipate the disappearance of canonical

Regge behavior. J-plane singularities more complicated than Regge poles must surely exist, and some of these ineluctably will resemble absorptive Regge cuts. Although these may be weak, they lie higher in the J-plane than the poles which generate them, and give rise to amplitudes with milder energy dependence than those corresponding to Regge pole exchange. At some point Regge cuts will have to dominate the reaction mechanisms, and we guess on the basis of model fits that they will do so by 100 GeV/c.

Finally, we deem it unlikely that new facts discovered at higher energies will invalidate the basic picture of two-body reactions that we hold today. The framework we described in section 2 is simply too firmly grounded in experimental results for us to get off so easily. The elementary facts are in our possession; the challenge is to build a theory from them.

ACKNOWLEDGMENTS

We would like to thank Nancy Clark and Pat Lee for their excellent and cheerful job of typing and drawing our herculean effort.

Literature Cited

1. Jackson, J. D. 1972. *Particle Physics*, ed. M. Bander, G. L. Shaw, D. Y. Wong, p. 164. New York: Am. Inst. Phys.
2. Chiu, C. B. 1972. *Ann. Rev. Nucl. Sci.* 22:255
3. Barger, V., Cline, D. B. 1969. *Phenomenological Theories of High Energy Scattering*. New York: Benjamin
4. Jacob, M. 1968. *Resonances and Exchange Processes*. Presented at L'Ecole Int. Phys. Particules Elem., *Herceg-Novi, Yugoslavia*
5. Collins, P. D. B., Squires, E. J. 1968. *Springer Tracts in Modern Physics*. Vol. 45. Berlin: Springer-Verlag
6. Jackson, J. D. 1970. *Rev. Mod. Phys.* 42:12
7. Harari, H. 1969. *Theories of Strong Interactions at High Energies*, ed. R. F. Peierls, p. 385. *Brookhaven Nat. Lab. Rep. BNL50212*
8. Schmid, C. 1971. *Proceedings of the Amsterdam International Conference on Elementary Particles*, ed. A. G. Tenner, M. J. G. Veltman, p. 275. Amsterdam: North-Holland
9. Schmid, C. 1971. *Phenomenology in Particle Physics*, ed. C. B. Chiu, G. C. Fox, A. J. G. Hey, p. 629. Pasadena: Caltech
10. Michael, C. 1972. *Proc. Fourth Int. Conf. High Energy Collisions*, ed. J. R. Smith. *Rutherford Lab. Rep. RHEL-72-001*
11. Michael, C. 1972. *Proc. XVI Int. Conf. High Energy Physics, Batavia*
12. Giacomelli, G. 1972. *Proc. XVI Int. Conf. High Energy Physics, Batavia*
13. Leith, D. W. G. S. 1972. *Proc. XVI Int. Conf. High Energy Physics, Batavia*
14. Fox, G. C. 1970. *High Energy Collisions*, ed. C. N. Yang et al, p. 367. New York: Gordon and Breach
15. Lovelace, C. 1971. *Phenomenology in Particle Physics*, ed. C. B. Chiu, G. C. Fox, A. J. G. Hey, p. 668. Pasadena: Caltech
16. Fox, G. C. 1971. *Phenomenology in Particle Physics*, ed. C. B. Chiu, G. C. Fox, A. J. G. Hey, p. 703. Pasadena: Caltech
17. Chiu, C. B. 1971. *Proc. Workshop Particle Physics at Intermediate Energies*, ed. R. D. Field, Jr., p. 396. *Lawrence Radiation Lab. Rep. UCRL-20655*
18. Guisan, O. 1971. *High Energy Phenomenology*, ed. J. Tran Thanh Van, p. 105. Paris: Société Polygraphique Mang.
19. Harari, H. 1971. *Proc. Int. Conf. Duality and Symmetry in Hadron Physics*, ed. E. Gotsman, p. 148. Jerusalem: Weizmann Sci.
20. Phillips, R. J. N. 1971. *Proceedings of the Amsterdam International Conference on Elementary Particles*, ed. A. G. Tenner, M. J. G. Veltman, p. 110.

Amsterdam: North-Holland
21. Lovelace, C. 1971. *Proceedings of the Amsterdam International Conference on Elementary Particles*, ed. A. G. Tenner, M. J. G. Veltman, p. 141. Amsterdam: North-Holland
22. Phillips, R. J. N., Ringland, G. A. 1972. *High Energy Physics*, ed. E. H. S. Burhop, 5: 187. New York: Academic
23. Joachain, C. J., Quigg, C. 1972. *Nat. Accelerator Lab. Rep. NAL-THY-99; Rev. Mod. Phys.* In press
24. Sonderegger, P. 1972. *Two-Body Collisions*, ed. J. Tran Thanh Van, p. 518. Paris: Société Polygraphique Mang.
25. Quigg, C. 1971. *Particles and Fields, 1971*, ed. A. C. Melissinos, P. F. Slattery, p. 40. New York: Am. Inst. Phys.
26. Chan, Hong-Mo. 1972. *Proc. Fourth Int. Conf. High Energy Collisions*, ed. J. R. Smith. *Rutherford High Energy Lab. Rep. RHEL-72-001*
27. Mueller, A. H. 1972. *Proc. XVI Int. Conf. High Energy Physics, Batavia*
28. Abarbanel, H. D. I. 1971. *Phys. Lett. B* 34: 69
29. Chan, Hong-Mo, Hsue, C. S., Quigg, C., Wang, J.-M. 1971. *Phys. Rev. Lett.* 26: 672
30. Mueller, A. H. 1970. *Phys. Rev. D* 2: 2963
31. Harari, H. 1971. *Phys. Rev. Lett.* 26: 1400
32. Barger, V., Geer, K., Halzen, F. 1972. *Nucl. Phys. B* 49: 302
33. Martin, A., Stevens, P. R. 1972. *Tensor Meson Exchange Amplitudes*. Preprint
34. Bialas, A., Zalewski, K. 1968. *Nucl. Phys. B* 6: 449, 465, 478, 483
35. Evans, R. D. 1955. *The Atomic Nucleus*. New York: McGraw
36. Benecke, J., Chou, T. T., Yang, C. N., Yen, E. 1969. *Phys. Rev.* 188: 2159
37. Jackson, J. D. 1966. *Proceedings of the XIII International Conference on High Energy Physics*, ed. M. Alston-Garnjost, p. 148. Berkeley: Univ. Calif.
38. Hearn, A. C., Drell, S. D. 1967. *High Energy Physics*, ed. E. H. S. Burhop, 2: 219. New York: Academic
39. Kokkedee, J. J. J. 1969. *The Quark Model*. New York: Benjamin
40. Chew, G. F. 1966. *The Analytic S-Matrix*. New York: Benjamin
41. Sivers, D., Yellin, J. 1971. *Rev. Mod. Phys.* 43: 125
42. Arnold, R. C. 1965. *Phys. Rev. Lett.* 14: 657
43. Dolen, R., Horn, D., Schmid, C. 1968. *Phys. Rev.* 166: 1768
44. Veneziano, G. 1968. *Nuovo Cimento A* 57: 190
45. Odorico, R. 1971. *Phys. Lett. B* 34: 65
46. Berger, E. L. 1971. *Phenomenology in Particle Physics*, ed. C. B. Chiu, G. C. Fox, A. J. G. Hey, p. 83. Pasadena: Caltech
47. Finkelstein, J. 1969. *Phys. Rev. Lett.* 22: 362
48. Freund, P. G. O. 1968. *Phys. Rev. Lett.* 21: 1375
49. Chen, M.-S. et al 1971. *Phys. Rev. Lett.* 26: 1585
50. Ross, M., Henyey, F. S., Kane, G. L. 1970. *Nucl. Phys. B* 23: 269
51. Dar, A., Kugler, M., Dothan, Y., Nussinov, S. 1964. *Phys. Rev. Lett.* 12: 82
52. Roy, D. P. 1971. *High Energy Phenomenology*, ed. J. Tran Thanh Van, p. 309. Paris: Société Polygraphique Mang.
53. Tran Thanh Van, J. 1972. *Two Body Collisions*, ed. J. Tran Thanh Van, p. 1. Paris: Société Polygraphique Mang.
54. Martin, A., Stevens, P. R. 1972. *Phys. Rev. D* 5: 147
55. Martin, A., Stevens, P. R. 1972. *Comparative Evaluation of Absorption Models for ρ Exchange*. Preprint
56. Ross, M. 1972. *Phys. Lett. B* 38: 321
57. Johnson, R. C. 1972. *Phys. Lett. B* 38: 325
58. Ringland, G. A., Roberts, R. G., Roy, D. P., Tran Thanh Van, J. 1972. *Nucl. Phys. B* 44: 395
59. Hartley, B. J., Kane, G. L. 1972. *Phys. Lett. B* 39: 531
60. Hartley, B. J., Kane, G. L. 1973. *Towards a General Description of Two-Body Hadron Reactions*. Preprint
61. Worden, R. 1972. *Duality and Regge Absorption Models*. Michigan preprint
62. Finkelstein, J. 1971. *Nuovo Cimento A* 5: 413
63. Worden, R. 1972. *Phys. Lett. B* 40: 260
64. Michael, C. 1969. *Phys. Lett. B* 29: 230; *Nucl. Phys. B* 13: 644
65. Quigg, C. 1971. *Nucl. Phys. B* 34: 77
66. Williams, P. K. 1970. *Phys. Rev. D* 1: 1312
67. Fox, G. C. 1972. *π-Exchange*. In *ANL HEP 7208*, Vol. II
68. Gottfried, K., Jackson, J. D. 1964. *Nuovo Cimento* 34: 735
69. Harari, H. 1969. *Phys. Rev. Lett.* 22: 562
70. Rosner, J. L. 1969. *Phys. Rev. Lett.* 22: 689
71. Chiu, C. B., Ugaz, E. 1973. *Phys. Lett. B* 43: 327
72. Fox, G. C., Rosenfeld, A. H. 1971. Unpublished Particle Data Group Memo
73. Jacob, M., Wick, G. C. 1959. *Ann.*

Phys. New York 7:404
74. Trueman, T. L., Wick, G. C. 1964. *Ann. Phys. New York* 26:322
75. Wolfenstein, L. 1956. *Ann. Rev. Nucl. Sci.* 6:43
76. Cronin, J. W., Overseth, O. E. 1963. *Phys. Rev.* 129:1795
77. Gottfried, K., Jackson, J. D. 1964. *Phys. Lett.* 8:144
78. Gottfried, K., Jackson, J. D. 1964. *Nuovo Cimento* 33:309
79. Jackson, J. D. 1964. *Nuovo Cimento* 34:1644
80. Jackson, J. D. 1965. *High Energy Physics*, ed. C. DeWitt, M. Jacob, p. 325. New York: Gordon and Breach
81. Berman, S. M., Jacob, M. 1965. *Phys. Rev. B* 139:1023
82. Pilkuhn, H., Svensson, B. E. Y. 1965. *Nuovo Cimento* 38:518
83. Kotanski, A. 1966. *Acta Phys. Pol.* 29: 699; 30:629
84. Barger, V., Phillips, R. J. N. 1972. *Phys. Lett. B* 42:479
85. de Lesquen, A. et al 1972. *Phys. Lett. B* 40:277
86. von Hippel, F., Quigg, C. 1972. *Phys. Rev. D* 5:624
87. Eberhard, P., Pripstein, M. 1963. *Phys. Rev. Lett.* 10:351
88. Wolters, G. F. 1968. *Kinematics and Multiparticle Systems*, ed. M. Nikolić, p. 129. New York: Gordon and Breach
89. Jongejans, B. 1969. *Methods in Subnuclear Physics*, ed. M. Nikolić, 4:349. New York: Gordon and Breach
90. Brau, J. E., Dao, F. T., Hodous, M. F., Pless, I. A., Singer, R. A. 1971. *Phys. Rev. Lett.* 27:1481
91. Ascoli, G. 1972. *Experimental Meson Spectroscopy-1972*, ed. A. H. Rosenfeld, K.-W. Lai, p. 185. New York: Am. Inst. Phys.
92. Ascoli, G. 1972. *Summary of the Experimental Situation Regarding A_1, A_2, A_3 Production*. Submitted to *XVI Int. Conf. High Energy Physics, Batavia*
93. Berger, E. L., Fox, G. C. 1970. *Phys. Rev. Lett.* 25:1783
94. Halzen, F., Michael, C. 1971. *Phys. Lett. B* 36:367 [Erratum in footnote 2 of Ref. (10)]
95. Kelly, R. L. 1972. *Phys. Lett. B* 39:635
96. Cozzika, G. et al 1972. *Phys. Lett. B* 40:281
97. Johnson, P., Lassila, K. E., Koehler, P., Miller, R., Yokosawa, A. 1973. *Phys. Rev. Lett.* 30:242
98. Barger, V., Phillips, R. J. N. 1969. *Phys. Rev.* 187:2210
99. McClure, J. A., Pitts, L. E. 1972. *Phys. Rev. D* 5:109
100. Höhler, G., Jakob, H. P. 1971. *Nuovo Cimento Lett.* 2:485
101. Hill, D. et al 1973. *Phys. Rev. Lett.* 30:239
102. Bonamy, P. et al 1973. *Nucl. Phys. B* 52:392
103. Ambats, I. et al 1972. *Phys. Rev. Lett.* 29:1415
104. Pietarinen, E. 1972. *Nucl. Phys. B* 49: 315
105. Elvekjaer, F., Pietarinen, E. 1973. *Optimized FESR Applied to πN Charge Exchange Amplitudes (Preprint RPP/T/36)*
106. Lovelace, C. 1972. *XVI Int. Conf. High Energy Physics, Batavia*
107. Fox, G. C. 1971. *Proceedings of the II International Conference on Polarized Targets*, ed. G. Shapiro. Berkeley: Lawrence Berkeley Laboratory
108. Högaasen, H., Michael, C. 1972. *Nucl. Phys. B* 44:214
109. Barger, V., Halzen, F. 1972. *Phys. Rev. D* 6:1918
110. Gilman, F. J., Pumplin, J., Schwimmer, A., Stodolsky, L. 1970. *Phys. Lett. B* 31:387
111. Zarmi, Y. 1971. *Phys. Rev. D* 4:3455
112. Dronkers, J., Kroll, P. 1972. *Nucl. Phys. B* 47:291
113. Jakob, H. P., Kroll, P. 1972. *The Slope of the πN Charge Exchange Amplitude at $t = 0$ (Preprint TKP 20/72)*
114. Alcock, J. W., Cottingham, W. N. 1971. *Nucl. Phys. B* 31:445
115. Shirkov, D. V., Serebryakov, V. V., Mescheryakov, V. A. 1969. *Dispersion Theories of Strong Interactions at Low Energy*. New York: Wiley Interscience
116. Donnachie, A., Kirsopp, R., Lovelace, C. 1968. *Phys. Lett. B* 26:161
117. Ayed, R. et al 1972. *Zero Strangeness Baryon States Below 2.5 GeV Mass*, Saclay preprint
118. Almehed, S., Lovelace, C. 1972. *Nucl. Phys. B* 40:157
119. Höhler, G., Strauss, R. 1970. *Z. Phys.* 232:205
120. Barger, V., Phillips, R. J. N. 1971. *Nucl. Phys. B* 32:93
121. Jackson, J. D., Quigg, C. 1969. *Phys. Lett. B* 29:236; Ibid. 1970. *Nucl. Phys. B* 22:301
122. Cho, C. F., Sakurai, J. J. 1970. *Phys. Rev. D* 2:517
123. Worden, R. 1972. *Nucl. Phys. B* 37:253
124. Dass, G. V., Michael, C. 1968. *Phys. Rev.* 175:1774
125. Berger, E. L., Fox, G. C. 1969. *Phys. Rev.* 188:2120
126. Harari, H. 1968. *Phys. Rev. Lett.* 20: 1395

127. Freund, P. G. O. 1968. *Phys. Rev. Lett.* 20:235
128. Harari, H., Zarmi, Y. 1969. *Phys. Rev.* 187:2230
129. Fukugita, M., Inami, T. 1972. *Impact Parameter Analysis of KN and πN Scattering in the Intermediate Energy Region (Preprint Rutherford Lab. RPP/T/32)*
130. Irving, A. C., Martin, A. D., Michael, C. 1971. *Nucl. Phys. B* 32:1
131. Michael, C., Odorico, R. 1971. *Phys. Lett. B* 34:422
132. Field, R. D., Jackson, J. D. 1971. *Phys. Rev. D* 4:693
133. Martin, A. D., Michael, C., Phillips, R. J. N. 1972. *Nucl. Phys. B* 43:13
134. Irving, A. C., Martin, A. D., Barger, V. 1972. *Analysis of Data for Hypercharge Exchange Reactions (Preprint CERN TH-1585)*
135. Loos, J. S., Matthews, J. A. J. 1972. *Phys. Rev. D* 6:2463
136. Bashian, A. et al 1972. *Phys. Rev. D* 4:2667
137. Mott, J. 1969. *Nucl. Phys. B* 13:565
138. Davier, M., Harari, H. 1971. *Phys. Lett. B* 35:239
139. Barger, V., Geer, K., Halzen, F. 1972. *Nucl. Phys. B* 44:214
140. Dikmen, F. N. 1969. *Phys. Rev. Lett.* 22:622
141. Barger, V., Halzen, F. 1972. *Nucl. Phys. B* 43:62
142. Davier, M. 1972. *Phys. Lett. B* 40:369
143. Austin, D. M., Greiman, W. H., Rarita, W. 1970. *Phys. Rev. D* 2:2613; Ibid. 1971. *Phys. Rev. D* 4:3507
144. Drobnis, D. D. et al 1968. *Phys. Rev. Lett.* 20:274
145. Bonamy, P. et al 1970. *Nucl. Phys. B* 16:335
146. Morrison, D. R. O. 1968. *Phys. Rev.* 165:1699
147. Johnson, K., Treiman, S. B. 1965. *Phys. Rev. Lett.* 14:189
148. Lipkin, H. J., Scheck, F. 1966. *Phys. Rev. Lett.* 16:71
149. Levinson, C. A., Wall, N. S., Lipkin, H. J. 1966. *Phys. Rev. Lett.* 17:1122
150. Wolf, G. 1971. *Proceedings of the 1971 International Symposium on Electron and Photon Interactions at High Energies*, ed. N. Mistry. Ithaca: Cornell
151. Denisov, S. P. et al 1972. *Differences of Total Cross Sections for Momenta up to 65 GeV c.* Submitted to *XVI Int. Conf. High Energy Physics, Batavia*
152. Gjesdal, S. et al 1972. *Phys. Lett. B* 40:152
153. Badier, J. et al 1972. *Phys. Lett. B* 41:387
154. Kadyk, J. A., Hauptman, J. M., Trilling, G. H. 1972. *Ap Interactions in the Momentum Range 0.5 → 8 GeV c (Preprint LBL-1064)*
155. Lipkin, H. J. 1971. *Quark Model Predictions for Reactions with Hyperon Beams (Preprint NAL-THY-81)*
156. Denisov, S. P. et al 1971. *Phys. Lett. B* 36:415

156a. Amaldi, U. et al 1973. *Phys. Lett. B* 44:112; Amendolia, S. R. et al 1973. *Phys. Lett. B* 44:119

157. Soloviev, L. D., Shelkacher, A. V. 1972. *XVI Int. Conf. High Energy Physics, Batavia*
158. Bolotov, V. N. et al 1972. *A Study of $\pi^- p \to \pi^0 n$ Charge Exchange in the Momentum Range 20 to 50 GeV c.* Preprint submitted to *XVI Int. Conf. High Energy Physics, Batavia*
159. Foley, K. J. et al 1969. *Phys. Rev.* 181:1775
160. Beznogikh, G. G. et al 1972. *Phys. Lett. B* 39:411
161. Alvensleben, H. et al 1973. *Phys. Rev. Lett.* 30:328
162. Barger, V., Halzen, F., Lutke, J. 1972. *Phys. Lett. B* 42:428
163. Chou, T. T., Yang, C. N. 1968. *Phys. Rev. Lett.* 20:1213
164. Durand, L., Lipes, R. 1968. *Phys. Rev. Lett.* 20:637
165. White, J. N. J. 1973. *Nucl. Phys. B* 51:23
166. Carrigan, R. A. 1970. *Phys. Rev. Lett.* 24:168
167. Dzierba, A. R. et al 1973. *Phys. Rev. D* 7:725
168. Antipov, Yu. M. et al 1972. *Elastic Scattering of π^- p, K$^-$ p and pp at 25 and 40 GeV c.* Submitted to *XVI Int. Conf. High Energy Physics, Batavia*
169. Höhler, G., Staudenmaier, H. M. 1972. *Is There a Break in the π^- p Diffraction Peak? (Preprint TK 19 72)*
170. Anselm, A. A., Gribov, V. N. 1972. *Phys. Lett. B* 40:487
171. Barshay, S., Chao, Y.-A. 1972. *Structure in Diffraction Scattering Inside $|t| \sim 4m_\pi^2$.* Preprint submitted to *XVI Int. Conf. High Energy Physics, Batavia*
172. Gunion, J. F., Brodsky, S. J., Blankenbecler, R. 1972. *Phys. Lett. B* 39:649
173. Theis, W. R. 1972. *Phys. Lett. B* 42:246
174. Horn, D., Moshe, M. 1972. *Nucl. Phys. B* 48:557
175. Phillips, R. J. N., Ringland, G. A. 1971. *Nucl Phys. B* 32:131
176. Borghini, M. et al 1971. *Phys. Lett. B* 36:501

177. Odorico, R. 1973. *Nucl. Phys. B* 52: 248
178. Bloom, E. D., Gilman, F. J. 1971. *Phys. Rev. D* 4: 2901
179. Harari, H. 1972. *Proceedings of the 1971 International Symposium on Electron and Photon Interactions at High Energies*, ed. N. B. Mistry. Ithaca: Cornell
180. Morrison, D. R. O. 1970. *Proc. XV Int. Conf. High Energy Physics, Kiev*
181. Zachariasen, F. 1971. *Phys. Rep. C* 2: 1
182. Fox, G. C. 1972. *Experimental Meson Spectroscopy-1972*, ed. A. H. Rosenfeld, K.-W. Lai. New York: Am. Inst. Phys.
183. Berger, E. L. 1969. Review talk at Irvine (*Preprint ANL/HEP 6927*)
184. Oh, Y. T. et al 1972. *Phys. Lett. B* 42: 497
185. Lissauer, D. et al 1972. *Phys. Rev. D* 6: 1852
186. Wang, J. M., Wang, L.-L. 1971. *Phys. Rev. Lett.* 26: 1287
187. Einhorn, M. B. et al 1973. *Phys. Rev. D* 7: 102
188. Ljung, S. 1972. *Diffraction Dissociation in the Reaction* $pp \to pp\pi^+\pi^-\pi^0$ *at 19 GeV/c*. Preprint submitted to *XVI Int. Conf. High Energy Physics, Batavia*
189. Allaby, J. V. et al 1973. *Nucl. Phys. B* 52: 316
190. Ravndal, F. 1971. *Phys. Lett. B* 37: 300
191. Brandenburg, G. et al 1972. *Nucl. Phys. B* 45: 397
192. Anderson, R. L. et al 1973. *Phys. Rev. Lett.* 30: 149
193. Bingham, H. H. et al 1972. *Phys. Lett. B* 41: 635
194. Beusch, W. 1971. *Production of Particles and Resonances on Nuclei, Dubna Conf.*
195. Lubatti, H. J. 1971. *Hadron Nucleus Interactions – An Experimental Study*. Preprint
196. Binon, F. 1971. *Pion-Nucleus Scattering: Experiment*. Rapporteur's Talk at *Int. Seminar π-Meson Nucleus Interactions, Strasbourg*
197. Bingham, H. H. 1970. *Review of Coherent Multiparticle Production Reactions from Nuclei* (*Preprint CERN/PHYS 70-60*)
198. Quigg, C., Wang, L.-L. 1973. *Phys. Lett. B* 43: 314
199. Sidhu, D. P., Quigg, C. 1973. *Phys. Rev. D* 7: 755
200. Firestone, A., Goldhaber, G., Lissauer, D., Trilling, G. H. 1972. *Phys. Rev. D* 5: 505
201. Gottfried, K. 1972. *Proceedings of the 1971 International Symposium on Electron and Photon Interactions at High Energies*, ed. N. B. Mistry. Ithaca: Cornell
202. Heynen, V. et al 1972. *Total Photoproduction Cross Section for Hadrons on Carbon and Copper at 6 GeV/c*. Preprint submitted to *XVI Int. Conf. on High Energy Physics, Batavia*
203. Vander Velde, J. C. et al 1972. *Nucl. Phys. B* 45: 1
204. Goldhaber, A. S. 1973. *Phys. Rev. D* 7: 765
205. Neuhofer, G. et al 1972. *Phys. Lett. B* 39: 271
206. Brockett, W. S. et al 1971. *Phys. Rev. Lett.* 26: 527
207. Cronillon, P. et al 1973. *Phys. Rev. Lett.* 30: 403
208. Chiu, C. B. 1971. *Nucl. Phys. B* 30: 477
209. Lai, K. W., Louie, J. 1970. *Nucl. Phys. B* 19: 205
210. Brody, A. D. et al 1970. *Preprint SLAC-PUB-823*. Unpublished
211. Carney, J. N. et al 1972. *Phys. Lett. B* 42: 124
212. Brody, A. D. et al 1971. *Phys. Rev. Lett.* 26: 1050
213. Fox, G. C., Hey, A. J. G. 1972. *Non-diffraction Production of Meson Resonances* (*Preprint CALT-68-373*)
214. Butler, W. R. 1970. *UCRL-19845*. Ph.D. thesis. Univ. Calif., Berkeley. Unpublished; Butler, W. R. et al 1969. Contribution to the *Lund Int. Conf. on Elementary Particles* (*UCRL-19225*); Abrams, G. S. et al 1970. Contribution to *XV Int. Conf. High Energy Physics, Kiev*
215. Bloodworth, I. J., Jackson, W. C., Prentice, J. D., Yoon, T. S. 1972. *Nucl. Phys. B* 39: 525
216. Martin, A. D., Michael, C. 1971. *Phys. Lett. B* 37: 513
217. Trilling, G. H. 1972. *Nucl. Phys. B* 40: 13
218. Aguilar-Benitez, M., Chung, S. U., Eisner, R. L., Field, R. D. 1972. *Phys. Rev. Lett.* 29: 749, 1201
219. Leader, E. 1968. *Phys. Rev.* 166: 1599
220. Sherden, D. J. et al 1973. *Asymmetries in Charged Pion Photoproduction on Nucleons by 16 GeV Polarized Photons* (*Preprint SLAC-PUB-1206*)
221. Estabrooks, P., Martin, A. D. 1972. *Phys. Lett. B* 42: 229
222. Firestone, A., Colton, E. 1972. *Determination of the Effective Trajectory in Δ(1238)-Producing Reactions* (*Preprint CALT-68-353*)
223. Schwitters, R. F. et al 1971. *Phys. Rev. Lett.* 27: 120
224. Bar-Yam, Z. et al 1970. *Phys. Rev. Lett.* 25: 1053
225. Fox, G. C. et al 1971. *Phys. Rev. D* 4: 2647

226. Poster, R. et al 1971. *Comparison of $K^+n \to K^{*0}p$ and $K^-p \to K^{*0}n$ at 2 GeV/c.* Submitted to *1971 Amsterdam Conf.* Preprint
227. Alexander, G., Fridman, A., Gotsman, E. 1972. *Nucl. Phys. B* 40:1
228. Hoyer, P., Roberts, R. G., Roy, D. P. 1973. *New Relations for Two-Body Reactions from Inclusive Finite Mass Sum Rules (Preprint Rutherford Lab. RPP/T/35)*
229. Dar, A. 1971. *High Energy Phenomenology*, ed. J. Tran Thanh Van, p. 17. Paris: Société Polygraphique Mang.
230. Stodolsky, L. 1971. *Phys. Rev. Lett.* 26:404
231. Abrams, G. S., Barnham, K. W. J. 1972. *Quark Model Comparisons with $\rho^0\Delta^{++}$ and $\omega^0\Delta^{++}$ Data at 3.7 GeV/c (Preprint LBL-961)*; Barnham, K. W. J. 1972. *Two Body Collisions*, ed. J. Tran Thanh Van, p. 459. Paris: Société Polygraphique Mang.
232. Barnham, K. W. J. et al 1972. *$\rho^0\Delta^{++}$ and $\omega\Delta^{++}$ Joint Decay Correlations at 3.7 GeV/c (Preprint LBL-960)*
233. Kotanski, A., Zalewski, K. 1969. *Nucl. Phys. B* 13:119
234. Carnegie, R. K. et al 1972. *Study of Reactions $\pi^+p \to \pi^+\pi^-\Delta^0$ and $\pi^+p \to \pi^+\pi^-\Delta^{++}$ at 15 GeV/c.* Preprint submitted to *XVI Int. Conf. High Energy Physics, Batavia*
235. Williamson, Y. et al 1972. *Dip Structures in $\pi^+p \to \rho^+\rho$ at 1.55–1.84 GeV/c.* Preprint submitted to *XVI Int. Conf. High Energy Physics, Batavia*
236. Michael, W., Gidal, G. 1972. *Phys. Rev. Lett.* 28:1475
237. Crennell, D. J. et al 1971. *Phys. Rev. Lett.* 27:1674; Scarr, J. M., Lai, K.-W. 1972. *Phys. Rev. Lett.* 29:310
238. Pratt, J. C. et al 1972. *Phys. Lett. B* 41:383; Ibid. *Isolation of Isovector Exchange in $\pi^-p \to \rho^0p$ at 15 GeV/c.* SLAC preprint
239. A-B-B-C-C-H-W collaboration. 1972. *Nucl. Phys. B* 46:46
240. Mandula, J., Weyers, J., Zweig, G. 1970. *Ann. Rev. Nucl. Sci.* 20:289
241. Holloway, L. E. et al 1971. *Phys. Rev. Lett.* 27:1671
242. Aguilar-Benitez, M., Eisner, R. L., Kinson, J. B., Samios, N. P., Scarr, J. M. 1971. *Observation of Structure in Production and Decay of K^* (890) (Preprint BNL-15707).* Unpublished
243. Boyarski, A. M. et al 1970. *Phys. Rev. Lett.* 25:695
244. Robrish, P. R. et al 1970. *Phys. Lett. B* 31:617
245. Abolins, M. A. et al 1972. Quoted by A. Diddens in *Proc. 4th Int. Conf. High Energy Collisions*, ed. J. R. Smith. *Rutherford Lab. Report RHEL 72-001*
246. Yokosawa, A. 1971. *Phenomenology in Particle Physics*, ed. C. B. Chiu, G. C. Fox, A. J. G. Hey. Pasadena: Caltech
247. Donnachie, A., Gabathuler, E., Eds. 1970. *Vector Meson Production and $\omega-\rho$ Interference, Daresbury Study Weekend No. 1*
248. *Goldhaber, G.* 1970. *Experimental Meson Spectroscopy*, ed. C. Baltay, A. H. Rosenfeld. New York: Columbia
249. Goldhaber, G. et al 1969. *Phys. Rev. Lett.* 23:1351
250. Le Francois, J. 1972. *Proceedings of the 1971 International Symposium on Electron and Photon Interactions at High Energies*, ed. N. B. Mistry. Ithaca: Cornell
251. Goldhaber, A. S., Fox, G. C., Quigg, C. 1969. *Phys. Lett. B* 30:249
252. Abrams, G. S., Maor, U. 1970. *Phys. Rev. Lett.* 25:617
253. Hagopian, S. et al 1970. *Phys. Rev. Lett.* 25:1050
254. Ratcliff, B. N. et al 1972. *Phys. Lett. B* 38:345
255. Bloodworth, I. J. et al 1971. *Nucl. Phys. B* 35:133
256. Wiik, B. 1971. *Proceedings of the 1971 International Symposium on Electron and Photon Interactions at High Energies*, ed. N. B. Mistry. Ithaca: Cornell
257. De Wire, J. et al 1971. *Photoproduction of η Mesons from Hydrogen (Preprint CLNS-170)*
258. Rosner, J. L. 1971. *Phenomenology in Particle Physics*, ed. C. B. Chiu, G. C. Fox, A. J. G. Hey. Pasadena: Caltech
259. Michael, C., Ruuskanen, P. V. 1971. *Phys. Lett. B* 35:65
260. Biswas, N. N. et al 1972. *Phys. Rev. D* 5:1564
261. Kislinger, M. 1971. *Vector, Tensor and Pomeron Regge Couplings (Preprint Caltech CALT-68-341).* Unpublished
262. Hoogland, W. et al 1969. *Nucl. Phys. B* 11:309
263. Firestone, A. et al 1973. *Nucl Phys. B* 52:403
264. Harrison, D. et al 1972. *Phys. Rev. D* 5:2730
265. Abramovich, M. et al 1972. *Nucl. Phys. B* 39:189
266. Crennell, D. J., Gordon, H. A., Lai, K.-W., Scarr, J. M. 1972. *Phys. Rev. D* 6:1220
267. Estabrooks, P., Martin, A. D. 1972. *Phys. Lett. B* 41:350
268. Sonderegger, P., Bonamy, P. 1969. Sub-

mitted to *1969 Lund Conf.*, Preprint. Results quoted in (24)
269. Field, R. D. et al 1972. *Phys. Rev. D* 6:1863
270. Abramovich, M., Irving, A. C., Martin, A. D., Michael, C. 1972. *Phys. Lett. B* 39:353
271. Field, R. D., Eisner, R. L., Chung, S. U., Aguilar-Benitez, M. 1972. *Transversity Amplitude Analysis of the Reactions* $K^- p \to (\omega, \phi)\Lambda$. Brookhaven preprint
272. Aguilar-Benitez, M., Chung, S. U., Eisner, R. L., Samios, N. P. 1972. *Phys. Rev. D* 6:29
273. Hirsch, E. et al 1971. *Phys. Lett. B* 36:139
274. Hirsch, E., Karshon, U., Lipkin, H. J. 1971. *Phys. Lett. B* 36:385
275. Michael, C., Odorico, R. 1971. *Phys. Lett. B* 34:422
276. Boyarski, A. M. et al 1969. *Phys. Rev. Lett.* 22:1131
277. Boyarski, A. M. et al 1971. *Phys. Lett. B* 34:547
278. Akerlof, C. W. 1970. *Double Charge Exchange Reactions*, Michigan preprint
279. Atherton, H. W. et al 1972. *Phys. Lett. B* 42:522
280. Chabaud, V. et al 1972. *Phys. Lett. B* 38:441, 445, 449
281. Langbein, W., Wagner, F. 1972. *Nucl. Phys. B* 47:477
282. Carroll, A. S. et al 1969. *Phys. Rev. Lett.* 23:887
283. Rivers, R. J. 1968. *Nuovo Cimento A* 57:174
284. Dean, N. 1968. *Nucl. Phys. B* 7:311
285. Chiu, C. B., Finkelstein, J. 1969. *Nuovo Cimento A* 59:92
286. Quigg, C. 1970. PhD thesis. Univ. Calif., Berkeley; *Preprint UCRL-20032*
287. Quigg, C. 1971. *Nucl. Phys. B* 29:67
288. Harari, H. 1971. *Phys. Rev. Lett.* 26:1079
289. Henyey, F. S., Kane, G. L., Scanio, J. J. G. 1971. *Phys. Rev. Lett.* 27:350
290. Frautschi, S. 1972. *Ericson Fluctuations and the Bohr Model in Hadron Physics* (*Preprint CERN-TH-1463*)
291. Berger, E. L. 1969. *Phys. Rev. Lett.* 23:1139
292. Dauber, P. M. et al 1969. *Phys. Lett. B* 29:609
293. Berger, E. L., Morrow, R. A. 1970. *Phys. Rev. Lett.* 25:1136
294. Sivers, D., von Hippel, F. 1972. *Phys. Rev. D* 6:874
295. Halzen, F., Mandula, J., Weyers, J., Zweig, G. 1971. *Tests of the Absence of Exotic Exchanges* (*CERN-TH-1371*)
296. Gribov, V. N., Low, F. E. 1972. *Proc. XVI Int. Conf. High Energy Physics, Batavia*
297. Bracci, E., Droulez, J. P., Flaminio, E., Hansen, J. D., Morrison, D. R. O. 1972. *CERN/HERA 72-1*
298. Carroll, A. S. et al 1966. *Phys. Rev. Lett.* 16:289
299. Yvert, M. 1969. PhD thesis, Orsay. Unpublished
300. Schneider, J. et al 1969. *Phys. Rev. Lett.* 23:1068
301. Litchfield, P. J. et al 1971. *Nucl. Phys. B* 30:125
302. Lovelace, C., Wagner, F. 1971. *Nucl. Phys. B* 28:141
303. Cutkosky, R. E. et al 1973. $K^+ p$ *Phase-shift Analysis Using the Accelerated Convergence Expansion*, Preprint
304. Davies, A. 1971. *Nucl. Phys. B* 21:359
305. Flaminio, E., Hansen, J. D., Morrison, D. R. O., Tovey, N. 1970. *CERN/HERA 70-7*
306. Birnbaum, D. et al 1970. *Phys. Lett. B* 31:484
307. Bradamante, F. et al 1970. *Phys. Lett. B* 31:87
308. Abrams, R. J. et al 1970. *Phys. Rev. D* 1:1917
309. Galbraith, W. et al 1965. *Phys. Rev. B* 138:913
310. Citron, A. et al 1966. *Phys. Rev. B* 144:1101
311. Foley, K. J. et al 1967. *Phys. Rev. Lett.* 19:330
312. Bugg, D. V. et al 1966. *Phys. Rev.* 146:980
313. Foley, K. J. et al 1967. *Phys. Rev. Lett.* 19:857
314. Jones, L. W. et al 1971. *Phys. Lett.* 36:509
315. Matthews, J. A. J. et al 1971. *Nucl. Phys. B* 32:366
316. Grayer, G. 1972. *Nucl. Phys. B* 50:29
317. Bloodworth, I. J., Jackson, W. C., Prentice, J. D., Yoon, T. S. 1971. *Nucl. Phys. B* 35:79
318. Geweniger, C. et al 1969. *Phys. Lett. B* 29:41
319. Anderson, R. L. et al 1971. *Phys. Rev. D* 4:1937
320. Grayer, G. et al 1972. *Measurement of* $pp \to (p\pi^+)n$ *at 12.5 and 16.9 GeV/c*. Preprint submitted to *XVI Int. Conf. High Energy Physics, Batavia*
321. Boyarski, A. M. et al 1968. *Phys. Rev. Lett.* 21:1767
322. Astbury, P. et al 1966. *Phys. Lett. B* 23:160
323. Miller, E. L. et al 1971. *Phys. Rev. Lett.* 26:984
324. Braun, H. et al 1970. *Phys. Rev. D* 2:488

325. Alexander, G. et al 1967. *Phys. Rev. B* 154: 1284
326. Bacon, T. C. et al 1966. *Phys. Rev.* 162: 1320
327. Werner, B. et al 1970. *Nucl. Phys. B* 23: 37
328. De Baere, W. et al 1969. *Nuovo Cimento A* 61: 397
329. Atherton, H. W. et al 1972. *Preliminary Results on* $\bar{p}p \to \bar{\Delta}^{--}\Delta^{++}$ *at 5.7 GeV/c.* Preprint submitted to *XVI Int. Conf. High Energy Physics, Batavia*
330. Shapira, A. et al 1970. *Nucl. Phys. B* 23: 583